CR-114686

VARIABLE CONDUCTANCE

HEAT PIPE

TECHNOLOGY

Research Report No. 4

DECEMBER 1973

Prepared by

B.D. MARCUS
D.K. EDWARDS
W.T. ANDERSON

TRW
SYSTEMS GROUP

TABLE OF CONTENTS

FIGURES

TABLES

1.0   INTRODUCTION

For the last several years TRW Systems Group, under contract
to NASA-ARC, has performed an extensive research and development
program in variable conductance heat pipe technology. The treatment
has been comprehensive, involving theoretical and/or experimental
studies in hydrostatics, hydrodynamics, heat transfer into and out of
the pipe, fluid selection, and materials compatibility, in addition to
the principal subject of variable conductance control techniques.

Efforts were not limited to analytical work and laboratory
experimentation, but extended to the development, fabrication and
test of spacecraft hardware, culminating in the successful flight of
the Ames Heat Pipe Experiment on the OAO-C spacecraft.

Most of the program's accomplishments have been previously
documented in a series of reports and publications. Early theoretical
and design developments appear in References [1, 2, 3 4, 5]. Later
fundamental work was published in References [6,7]. Hardware develop-
ment and application efforts were documented in References [8, 9, 10],
and a computer program for designing and predicting performance of gas
loaded heat pipes was presented in Reference [11].

This document represents the fourth research report issued
on this program. It deals with further analytical, experimental and
developmental studies pertinent to variable conductance heat pipe
technology.

The particular studies which are covered in this report fall
into three areas, as follows:

1) An analysis was performed on the influence of the
    noncondensible gas on the operation of arteries in
    gas loaded heat pipes. Analytical models were
    derived to a) examine the degree to which dissolved
    gas in the liquid increases the propensity for nucleation
    of a gas bubble within an artery (Section 2.0) and
    b) explore the stability of large pre-existing gas
    bubbles within an artery (Section 3.0).

2) An analytical and experimental study was performed
   to explore the feasibility of establishing gas
   generation scaling laws for accelerated life testing
   of heat pipes. (Section 4.0).

3) A design study was carried out on the use of extensible
   containers (e.g. bellows, bladders) to provide variable
   conductance control usin_ either the vapor flow modulation
   or excess fluid condenser flooding techniques. A vapor
   flow modulation prototype heat pipe was fabricated
   and tested. (Section 5.0).

2.0   ANALYSIS OF THE GROWTH OR COLLAPSE OF SMALL BUBBLES IN
        GAS LOADED HEAT PIPE ARTERIES

In heat pipes containing gas in the condenser, arterial liquid
acts as a solvent and carries dissolved gas with it into nigher temper-
ature, lower liquid pressure regions. The dissolved gas may come out of
solution at these higher temperatures and lower pressures permitting gas
and vapor bubbles larger than a certain critical size to grow. Such
growth will cause a heat pipe artery to deprime and the heat pipe to
fail to carry its design load.

In what follows there is an examination of the axial variation
of the tendency for bubbles to form in the bulk of the fluid flowing in
the adiabatic section of a heat pipe having a circular artery of uniform
cross-section. There is first a review of the laws for the behavior at
the interface of ideal gas-liquid solutions, Eqs. (2-1)-(2-3). Then
the gas fraction in the evaporator vapor is found, not from thermostatics,
but from simple conservation of mass in the steady-state, Eq. (2-5).
There then follows a very quick review of fluid mechanics and the bubble
growth (or collapse) criterion for a pre-existing bubble nucleus. Counter-
current heat and mass exchanger analysis is then applied, and two numer-
ical examples are presented and discussed. It will be shown that the
presence of gas would cause a gas/vapor bubble smaller than the pumping
pore size to grow, if one were present in the adiabatic section.

2.1   Analysis:

2.1.1   Henry's, Dalton's and Raoult's Laws:

The partial pressure of gas P_g in thermodynamic equilibrium with
a mixture of liquid and dissolved gas is described by Henry's Law for
dilute solutions of gas in the liquid,

$$P_g = C\,x_g \tag{2-1}$$

where C is Henry's constant, having units of pressure and being tem-
perature dependent, and x_g is the molar fraction of the gas in the gas-

3

liquid mixture.

The total pressure P is given by Dalton's Law,

$$P = P_v + P_g \tag{2-2}$$

where P_v and P_g are the partial pressures of the vapor and gas respectively.

Raoult's Law gives P_v. For a binary mixture of dissolved gas in a liquid,

$$P_v = P_{sat} x_v = P_{sat} (1-x_g) \tag{2-3}$$

where P_{sat} is the saturation pressure (vapor pressure) in thermodynamic equilibrium with the pure liquid.

Typical values of Henry's constant for dilute aqueous solutions are as shown in Table 2-1. Note the large differences depending upon the gas species, and note that C doubles approximately over the range of temperatures from 60°F to 150°F. A large value of Henry's constant denotes a relatively insoluble gas and vice versa.

2.1.2 Steady-State Dynamic Conditions at an Interface:

The preceeding relations hold for a static condition at the interface. In a dynamic situation such as exists in a heat pipe evaporator where liquid evaporates at an interface, and the vapor sweeps gas away, conservation of species dictates that,

$$c_\ell v_\ell^* x_g - c_\ell \mathcal{D}_\ell \frac{\partial x_g}{\partial r} = cv^* y_g - c \mathcal{D} \frac{\partial y_g}{\partial r} \tag{2-4}$$

where c is the molar concentration (density divided by molecular weight), v^* the mole average velocity normal to the interface, $\mathcal{D}$ the diffusivity of the gas in the liquid or vapor, x_g the mole fraction of the g species on the liquid side, y_g the mole fraction on the vapor side, and r the coordinate normal

4

TABLE 2-1

HENRY'S CONSTANT FOR AQUEOUS SOLUTIONS

SOLUTE	HENRY'S CONSTANT, ATMOSPHERES					
	60°F	80°F	100°F	120°F	140°F	160°F
NH_3	26.0	30.2				
SO_2	290	440	620	840	1090	1370
Cl_2	480	620	770	880	950	980
CO_2	1260	1710	2220	2790	3500	
O_2	37000	45500	53000	59000	63000	67000
Air	61000	74000	86000	96000	104000	111000
H_2	66000	72000	76000	77000	77000	77000
N_2	74000	89000	104000			

to the interface in question. The subscript ℓ denotes the $\ldots$ phase. The above equation holds at any pair of values of r, one value on the liquid side for the left term and the other on the gas side. Thus each side is equal to the same constant, namely the molar flux of gas normal to the interface.

The solution to Eq. (2-4) shows that, on the liquid side very near the interface, a boundary layer is established of exponential decay thickness $\mathscr{D}_\ell/v_\ell^*$. This thickness is rather small; for example, for N_2 dissolved in liquid H_2O at 140°F, $\mathscr{D}_\ell = 4.29 \times 10^{-8}$ ft^2/sec., and for an evaporation rate corresponding to 20.0 watts/in^2, $v_\ell = 0.436 \times 10^{-4}$ ft/sec; the boundary layer thickness Δr is then 0.012 inches. At a distance of a few such thicknesses removed from the interface x_g is constant at the bulk value so that the diffusion term drops. On the gas side y_g is constant so that the diffusion term likewise drops. Since $c_\ell v_\ell^* \doteq cv^*$, because the moles of species are conserved,

$$x_g = y_g \qquad (2-5)$$

where x_g is now understood to be the bulk value a few boundary layer thicknesses from the interface.

The pressures under dynamic conditions are then NOT given by Eqs. (2-1)-(2-3), when x_g is understood to be the bulk value. The equations still hold, of course, when the surface value of x_g, $x_{g,s}$ is employed. Hence,

$$P = C\, x_{g,s} + P_{sat}\, (1-x_{g,s})$$

and

$$y_g = y_{g,s} = P_{g,s}/P = C\, x_{g,s}/P = x_g, \qquad P = C\, x_{g,s}/x_g$$

Substituting into the preceding relation yields

$$C\, x_{g,s}/x_g = C\, x_{g,s} + P_{sat}\, (1-x_{g,s})$$

$$x_{g,s} = \frac{P_{sat}}{C/x_g - C + P_{sat}}$$

6

Since y_g and P are constant in the gas phase

$$P_g = P_{g,s} = C \, x_{g,s} = \frac{P_{sat}}{\frac{1}{x_g} - 1 + \frac{P_{sat}}{C}}$$

$$P_g = \frac{x_g \, P_{sat}}{1 - x_g \, (1-P_{sat}/C)} \doteq x_g \, P_{sat} \left[1 + x_g \, (1-P_{sat}/C) \right] \qquad (2\text{-}6)$$

$$P_v = P_{sat} \, (1-x_{g,s}) \doteq P_{sat} \left[1 - x_g \, \frac{P_{sat}}{C} \right] \qquad (2\text{-}7)$$

where terms x_g^2 and smaller have been neglected, compared to unity.

2.1.3   Pressure in the Artery of an Adiabatic Section:

Let the conditions at the end of an evaporator on of heat pipe adjoining the beginning of an adiabatic section ? oted by a subscript e. Let the distance down the adiabatic section (in the direction of the vapor flow) be z. Then the pressure in the liquid inside a uniform artery is:

$$P_\ell \, (z) = P_{\ell,e} + (dP_\ell/dz) \, z \qquad (2\text{-}8)$$

where for laminar flow in an artery of diameter D

$$\frac{dP_\ell}{dz} = \frac{32 \, \mu_\ell V}{D^2} = \frac{128}{\pi} \, \frac{\mu_\ell}{D^4} \, \frac{\dot{Q}}{\rho_\ell \, \lambda} \qquad (2\text{-}9)$$

where μ_ℓ is liquid viscosity, $\dot{Q}$ heat flow, ρ_ℓ liquid density, and λ latent heat. Note that dP_ℓ /dz is constant in an adiabatic section.

The pressure $P_{\ell,e}$ is in turn related to the total (gas plus vapor) pressure and radius of curvature of the menisci in the wick at that point.

$$P_{\ell,e} = P_e - \frac{2 \sigma_e}{r_e} \qquad (2\text{-}10)$$

Since P_e is equal to the sum of Eqs. (2-6) and (2-7), from Eq. (2-10), we can write

$$P_{\ell,e} = P_{sat,e} \left[1 - x_{g,e} \frac{P_{sat,e}}{C_e} + x_{g,e} + \cdots \right] - \frac{2 \sigma_e}{r_e} \qquad (2\text{-}11)$$

where again terms of order $x_{g,e}^2$ have been neglected. Eq. (2-8) becomes

$$P_{\ell}(z) = P_{sat,e} \left[1 + x_{g,e} \left(1 - \frac{P_{sat,e}}{C_e} \right) \right] + \frac{dP_{\ell}}{dz} \cdot z - \frac{2 \sigma_e}{r_e} \qquad (2\text{-}12)$$

2.1.4 Criterion for Bubble Growth:

The critical bubble size is related to the surface tension and the pressure difference between the gas-vapor mixture and liquid.

$$\frac{2 \sigma}{r_{cr}} = P - P_{\ell} \qquad (2\text{-}13)$$

Substituting Eqs. (2-1)-(2-3), (valid for the static conditions presumed at the bubble interface) and Eq. (2-12) into (2-13) gives

$$\frac{2 \sigma}{r_{cr}} - \frac{2 \sigma_e}{r_e} = - \left(\frac{dP_{\ell}}{dz} \right) z - P_{sat,e} \left[1 + x_{g,e} \left(1 - \frac{P_{sat,e}}{C_e} \right) \right]$$

$$+ C x_g + P_{sat}(1 - x_g)$$

$$\frac{2}{r_{cr}} - \frac{2}{r_e} = -\left(\frac{dP}{dz}\right) z - \left(P_{sat,e} - P_{sat}\right)$$

$$+ (C - P_{sat}) \, x_g - x_{g,e} \, P_{sat,e} \left(1 - \frac{P_{sat,e}}{C_e}\right) \tag{2-14}$$

The terms on the right hand side may be identified as follows:

1. $-\left(\frac{dP}{dz}\right) z$, the liquid pressure rise effect, good.

2. $-\left(P_{sat,e} - P_{sat}\right)$, the liquid subcooling effect, good.

3. $(C - P_{sat}) \, x_g$, the dissolved gas effect, bad.

4. $-x_{g,e} \, P_{sat,e} \left(1 - \frac{P_{sat,e}}{C_e}\right)$, the effect of dissolved gas on total pressure, good but small.

It remains to determine x_g and T as functions of z.

2.1.5   Counter-Current Exchanger Relationships:

At the junction of the adiabatic section and condenser $z = L$, the liquid in the artery may be somewhat subcooled at bulk temperature T_L and is gas-rich at mole fraction $x_{g,L}$. The liquid then flows down the artery counter-current to vapor sweeping up the artery. The liquid warms rather quickly due to a small amount of condensation on the artery outer surface and is stripped of gas by the counter-flowing stream of nearly pure vapor. The governing differential equation for the bulk temperature is:

$$-\dot{m} \, c_p \, \frac{dT}{dz} = U \mathcal{P} \, (T_s - T) \tag{2-15}$$

where $\dot{m}$ is mass flow, c_p specific heat of the liquid, $\mathcal{P}$ perimeter, and

$$U = h = \frac{k}{D} \, Nu \tag{2-16}$$

9

For established laminar flow in a circular artery $Nu = 3.65$ and $\mathscr{P} = \pi D$. Similarly, the governing differential equations for bulk mole fraction in the liquid and vapor streams are, respectively,

$$- (\dot{m}/M) \ \frac{d\,x_g}{dz} = K_\ell \ \mathscr{P} \ (x_{g,s} - x_g) \tag{2-17}$$

$$+ (\dot{m}/M) \ \frac{d\,y_g}{dz} = K_g \mathscr{P} \ (y_{g,s} - y_g) \tag{2-18}$$

where M is molecular weight of the working fluid, and K is mass transfer coefficient.

The interfacial conditions are determined by continuity of gas flow across the interface,

$$K_\ell \ \mathscr{P} \ (x_{g,s} - x_g) = K_g \ \mathscr{P} \ (y_g - y_{g,s}) \tag{2-19}$$

and Henry's and Dalton's Laws

$$y_{g,s} = \frac{C}{P_e - \left(\frac{dP}{dz}\right)_g z} \cdot x_{g,s} \tag{2-20}$$

where $(dP/dz)_g$ is given by an expression similar to Eq. (2-9) for laminar vapor flow on the gas side. The mass transfer coefficients are:

$$K_g = \frac{\rho_g \mathscr{D}_g}{M_g \ D_g} \ Nu_{m,g} \tag{2-21}$$

$$K_\ell = \frac{\rho_\ell \mathscr{D}_\ell}{M_\ell \ D} \ Nu_{m,\ell} \tag{2-22}$$

A number of realistic simplifications can be made. For negligible $(dP/dz)_g$ Eq. (2-20) reduces to:

$$y_{g,s} = H \ x_{g,s}; \ H = C/P_e \tag{2-23}$$

Henry number H is always quite large for cases of interest. Whether H is large or not, Eqs. (2-19) and (2-23) can be found to result in:

$$K_\lambda \mathcal{P} (x_{g,s} - x_g) = K_g \mathcal{P} (y_g - y_{g,s}) = K_{oa,\lambda} \mathcal{P} (y_g/H - x_g) \qquad (2-24)$$

where

$$K_{oa,\lambda} = \cfrac{1}{\cfrac{1}{\overline{H}K_g} + \cfrac{1}{K_\lambda}} \qquad (2-25)$$

But because H is large and because $\mathcal{D}_g \gg \mathcal{D}_\lambda$, we have $HK_g \gg K_\lambda$

$$K_{oa,\lambda} \doteq K_\lambda = \frac{\dot{\nu}_\lambda \mathcal{D}_\lambda}{M_\lambda D} Nu_{m,\lambda} \qquad (2-26)$$

The right hand equality is based upon negligible resistance to mass transfer through the artery wall; i.e., a thin porous artery wall.

An additional simplication is, because of large H, and because $\dot{m}_g = \dot{m}_\lambda$, and $y_g = x_g$ is small,

$$\frac{y_g}{H} - x_g \doteq -x_g$$

For these reasons Eq. (2-18) is of no interest, and Eq. (2-17) becomes

$$\left(\frac{\dot{m}}{M}\right) \frac{d x_g}{dz} \doteq K_\ell \mathcal{P} x_g \qquad (2-27)$$

Eqs. (2-15) and (2-27) are in identical form, and the solutions are, assuming constant Nusselt numbers,

$$T_s - T = (T_s - T_L) e^{-N_{tu,h} (L-z)/L} \qquad (2-28)$$

11

$$x_g = x_{g,L} \, e^{-N_{tu,m} \, (L-z)/L} \tag{2-29}$$

where N_{tu} is the number of transfer units with the subscripts h for heat transfer and m for mass transfer,

$$N_{tu,h} = \frac{U \mathscr{P} L}{\dot{m} \, c_p} \tag{2-30}$$

$$N_{tu,m} = \frac{K_{oa} \mathscr{P} L}{\dot{m}/M} \tag{2-31}$$

Note that

$$\frac{N_{tu,h}}{N_{tu,m}} = \frac{K/c_p}{\rho_\ell \mathscr{D}_\ell} = \frac{Sc}{Pr} \tag{2-32}$$

For gases dissolved in water, the following values pertain:

TABLE 2-2

PROPERTIES FOR DILUTE AQUEOUS
SOLUTIONS OF NITROGEN

T °F	ν ft^2/sec	Pr	$Sc/Sc_{528°R}$	Sc_{N_2}	Sc_{N_2}/Pr	$\mathscr{D}_{N_2}$ ft^2/hr
68	1.03×10^{-5}	7.02	1.00	613	87.3	$.605 \times 10^{-4}$
100	$.741 \times 10^{-5}$	4.53	.436	257	56.7	1.04×10^{-4}
120	$.615 \times 10^{-5}$	3.64	.290	178	48.9	1.24×10^{-4}
140	$.513 \times 10^{-5}$	3.01	.195	120	39.9	1.54×10^{-4}
160	$.442 \times 10^{-5}$	2.53	.140	85.8	33.9	1.86×10^{-4}
180	$.388 \times 10^{-5}$	2.16	.104	64.1	29.7	2.18×10^{-4}
200	$.392 \times 10^{-5}$	1.90	.079	48.4	25.5	2.54×10^{-4}

TABLE 2-3

SCHMIDT NUMBER AT 68°F
FOR SOME AQUEOUS SOLUTIONS

Species	NH_3	Cl_2	CO_2	O_2	H_2	N_2
Schmidt No.	570	834	559	558	196	613

Unfortunately, Schmidt number exceeds Prandtl number. For example, at $T = 140°F$ $Sc_{N_2}/Pr = 39.9$, and the N_{tu} for heat transfer is nearly forty times larger than the N_{tu} for mass transfer. The effect is that the region in which the liquid is heated is forty times shorter in length than the region in which the liquid is stripped of gas. Hence the beneficial effect of subcooling is lost before the effect of gas stripping can be fully realized.

2.1.6   The Most Critical Axial Position:

The final solution for the danger of bubble growth is given by Eq. (2-14) combined with Eqs. (2-28) and (2-29). Let,

$$\xi = \frac{\dfrac{2\sigma}{r_{cr}} - \dfrac{2\sigma_e}{r_e}}{\dfrac{2\sigma_e}{r_e}} = \frac{r_e}{r_{cr}} - 1 \tag{2-33}$$

and

$$\zeta_{se} = \frac{r_e P_{sat,e}}{2\sigma_e} \ , \quad \zeta_\ell = \frac{r_e}{2\sigma_e}\left(\frac{128\ \nu_\ell\ \dot{Q}\ L}{\pi\ D^4\ \lambda}\right), \quad H_{se} = \frac{C}{P_{sat,e}} \tag{2-34}$$

Then

$$\xi = -\zeta_\ell \frac{z}{L} - \zeta_{se}\left(1 - \frac{P_{sat}}{P_{sat,e}}\right) - \zeta_{se}\ x_L\left(1 - \frac{1}{H_{se}}\right) e^{-N_{tu,m}}$$

$$+ \zeta_{se}\ x_L\left(H_{se} - \frac{P_{sat}}{P_{sat,e}}\right) e^{-N_{tu,m}\ (1 - \frac{z}{L})} \tag{2-35}$$

13

The quantity ξ is a measure of the danger of bubble growth, and it may be plotted versus z/L to find the most critical axial position.

We have noted that $N_{tu,h}$ tends to be many times larger than $N_{tu,m}$. Because of this fact, T will rapidly approach T_e, and, for z sufficiently smaller than L, the term $\zeta_{se} (1-P_{sat}/P_{sat,e})$ may be approximated by

$$\zeta_{se} \left(1 - \frac{P_{sat}}{P_{sat,e}} \right) \doteq \zeta_{se} \frac{1}{P_{sat,e}} \frac{dP_{sat,e}}{dT_e} (T_e - T_L) e^{-N_{tu,h} (1-\frac{z}{L})} \qquad (2-36)$$

With the Clausius-Clapeyron approximation

$$\zeta_{se} \left(1 - \frac{P_{sat}}{P_{sat,e}} \right) \doteq \zeta_{se} \left(\frac{\lambda M}{R_u T_e} \right) \frac{T_e - T_L}{T_e} e^{-N_{tu,h} (1-\frac{z}{L})} \qquad (2-36a)$$

If $N_{tu,h}$ is large enough this term may be negligible.

If, in addition to a large $N_{tu,h}$, the parameter S is small compared to ζ_ℓ, where

$$S = (H_{se} - 1) x_L N_{tu,m} \frac{\zeta_{se}}{\zeta_\ell} \leq 1, \qquad (2-36b)$$

the most critical spot may be found from Eq. (2-35) to be at the junction of the evaporator and adiabatic section at $z = 0$. At this location, under the conditions above, and neglecting $1/H_{se}^2$ compared to unity, there results

$$\xi_0 = \zeta_{se} x_L H_{se} e^{-N_{tu,m}} \qquad (2-37)$$

This result is seen to be quite simple. It shows that the controlling factors are x_L, the fraction of gas picked up in the condensate and the $e^{-N_{tu,m}}$, the measure of the effectiveness of the adiabatic section as a mass exchanger. However, as will be seen in Section 2.2, the parameter S is large for aqueous solutions, and this simple result is not pertinent to them.

14

2.1.7 The Determination of x_L and T_L:

The TRW GASPIPE computer program [11] predicts fairly accurately the temperature in the condenser wall and the vapor wick interface temperature as a function of z and the vapor and total pressures. Hence the molar fraction of gas y as a function of z is known reasonably accurately. With somewhat less accuracy the program also predicts condensate flow rate $\dot{m}$ as a function of z.

Under the assumption that the condensate condenses in a saturated state and loses negligible gas by back diffusion as long as the condensation rate is high, one can calculate x (z) from:

$$\frac{d}{dz} (x\dot{m}) = x_{sat} \frac{d\dot{m}}{dz} = \frac{y(z)}{H} \frac{d\dot{m}}{dz}$$

$$x_L = \frac{1}{\dot{m}_L} \int_L^{L+L_c} \left(\frac{y(z)}{H} \right) \left(\frac{d\dot{m}}{dz} \right) dz \qquad (2\text{-}38)$$

where L_c is the length of the condenser and L retains its meaning for now as the length of the adiabatic section, more explicitly L_a.

By the same reasoning and neglecting heat transfer to or from the condensate after it condenses (which may or may not be justified, depending on the condenser wick configuration)

$$\frac{d}{dz} (T\dot{m}) = T_{sat} \frac{d\dot{m}}{dz}$$

$$T_{\dot{e}} - T_L = \frac{1}{\dot{m}_L} \int_L^{L+L_c} \left(T_e - T_{sat} \right) \left(\frac{d\dot{m}}{dz} \right) dz \qquad (2\text{-}39)$$

Eqs. (2-38) and (2-39) conclude the analysis in Section 2 of this report. The results are summarized and two numerical examples are presented in the remainder of the section.

2.1.8   Summary of Analytical Results:

Eqs. (2-35) together with (2-36a) describe the bubble growth para-
meter ξ versus distance in an adiabatic section. Eqs. (2-38) and (2-39)
together with GASPIPE results for $T_e - T_{sat}$ and y versus z serve to fix
x_L and T_L needed for Eqs. (2-35) and (2-36a). If the ζ_L term in Eq.
(2-35) is large, then Eq. (2-37) may hold. The inequality shown above
Eq. (2-37) determines whether or not ζ_L is large enough.

2.2   Two Numerical Examples:

Consider a water heat pipe with a 2 foot long adiabatic section
having an 0.060 inch diameter pedestal artery. Two operating conditions
are considered:

1)   Low Power: $\dot{Q}$ = 24.6 Btu/hr, T_e = 637.6°R

2)   High Power: $\dot{Q}$ = 249.4 Btu/hr, T_e = 740°R

The remaining assumed conditions are taken to be those shown in
Table 6-2 and Figure 6-22 of Reference [3].

Under the assumption of constant H_c values of y_L were obtained
as indicated by Eq. (2-38):

$$y_L = \frac{1}{\dot{m}_L} \int_{L}^{l_c+L} y(z) \frac{d\dot{m}}{dz} dz$$

For case (1)

$$y_L = \frac{1}{.02786} (6.74 \times 10^{-4}) = 0.0242$$

While for case (2)

$$y_L = \frac{1}{.2825} (1.028 \times 10^{-2}) = 0.0364$$

(These results are obtained from GASPIPE [11]).

16

Assuming a pumping pore of 1/200 inches gives ζ_{se}. For case (1)

$$\zeta_{se} = \frac{r_{se}P_{se}}{2\sigma_e} = \frac{(1/2400)(7.19 \times 144)}{(2)(.00427)} = 50.5$$

For case (2)

$$\zeta_{se} = \frac{(1/2400)(49.2 \times 144)}{(2)(.00340)} = 434$$

Henry number was not found for the higher temperatures. It is therefore possible only to estimate H_{se}/H_{sc} for case (1). In this case:

$$\frac{H_{se}}{H_{sc}} = \frac{C_e/P_{sc}}{C_c/P_{se}} = \frac{C_e}{C_c} = \frac{120,000}{110,000} = 1.09$$

The $N_{tu,m}$ value is then obtained from Eq. (2-31). For case (1)

$$N_{tu,m} = 3.65 \; \frac{\rho_\ell \mathscr{D}_\ell}{D} \; \frac{\mathscr{P}_L}{\dot{m}} = 3.65 \; \frac{\rho_\ell \mathscr{D}_\ell}{D} \; \frac{\pi D L}{\dot{m}}$$

$$= 3.65 \; \frac{(61)(2.2 \times 10^{-4})(3.14)(2)}{.02786} = 11.1$$

For case (2)

$$N_{tu,m} = 3.65 \; \frac{(59)(4.6 \times 10^{-4})(3.14)(2)}{.2825} = 2.2$$

The remaining parameter in Eq. (2-35) is ζ_ℓ. From Eq. (2-34),

$$\zeta_\ell = \frac{r_e}{2\sigma_e} \left(\frac{128 \; \nu_\ell \; \dot{Q}L}{\pi D^4 \lambda} \right) = \frac{\zeta_{se}}{P_{se}} \left(\frac{128 \; \nu_\ell \; \dot{m}L}{\pi D^4} \right)$$

17

For case (1)

$$\zeta_\ell = \left(\frac{50.4}{1037}\right)\left(\frac{128(.388 \times 10^{-5})(.02786/(32.2 \times 3600))(2)}{3.14(0.060/12)^4}\right) = 5.91 \times 10^{-3}$$

For case (2)

$$\zeta_\ell = \left(\frac{434}{7090}\right)\left(\frac{128(.234 \times 10^{-5})(.2825/(32.2 \times 3600))(2)}{3.14(0.060/12)^4}\right) = 4.55 \times 10^{-2}$$

To see whether or not Eq. (2-37) is applicable, we compute:

$$S = (H_{se} - 1) \, x_L \, N_{tu,m} \, \frac{\zeta_{se}}{\zeta_\ell} = \left(\frac{H_{se}}{H_c} - \frac{1}{H_c}\right) y_L \, N_{tu,m} \, \frac{\zeta_{se}}{\zeta_\ell}$$

For case (1)

$$S = (1.09)(0.0242)(11.1)(50.5/5.91 \times 10^{-3}) = 2500$$

For case (2)

$$S = (1.09)(0.0364)(2.2)(434/4.55 \times 10^{-2}) = 833$$

Both are much larger than unity, and Eq. (2-37) is not applicable.
Table 2-4 summarizes the above results, and Figure 2-1 shows a plot of
Eq. (2-35).

2.2.1   Discussion:

The figure shows that the subcooling effect predominates the
dissolved gas effect at 1- z/L = 0 (where the liquid condensate enters
the adiabatic section). In both cases ξ is negative, which indicates
that a bubble the size of the pumping pore would collapse completely.

In case (1) the heat flow and resulting velocities are small so
that the N_{tu} for both heat and mass transfer are large. In this case

TABLE 2-4

SUMMARY OF PARAMETERS: NUMERICAL EXAMPLES

PARAMETER	CASE 1	CASE 2
$\dot{Q}$ (Btu/hr)	24.6	249.4
$\dot{m}_L$ (lb_m/hr)	0.02786	0.2825
y_L	0.0242	0.0364
T_e, (°R)	637.6	740
$T_{c,avg}$, (°R)	620	620
$P_{sat,e}$ (lb_f/ft^2)	1037	7090
H_{sc}	225,000	33000
H_{se}/H_{sc}	1.09	~1.2
ζ_{se}	50.5	434
ζ_ℓ	5.91 X 10^{-3}	4.55 x 10^{-2}
$\zeta_{se} H_{se} x_L$	1.33	18.9
$N_{tu,m}$	11.1	2.2
Sc/Pr	29.7	~16.
$N_{tu,h}$	330.	~35.
$M\lambda/R_u T_e$	14.6	12.3
$T_e - T_L$, (°R)	1.35	3.57

19
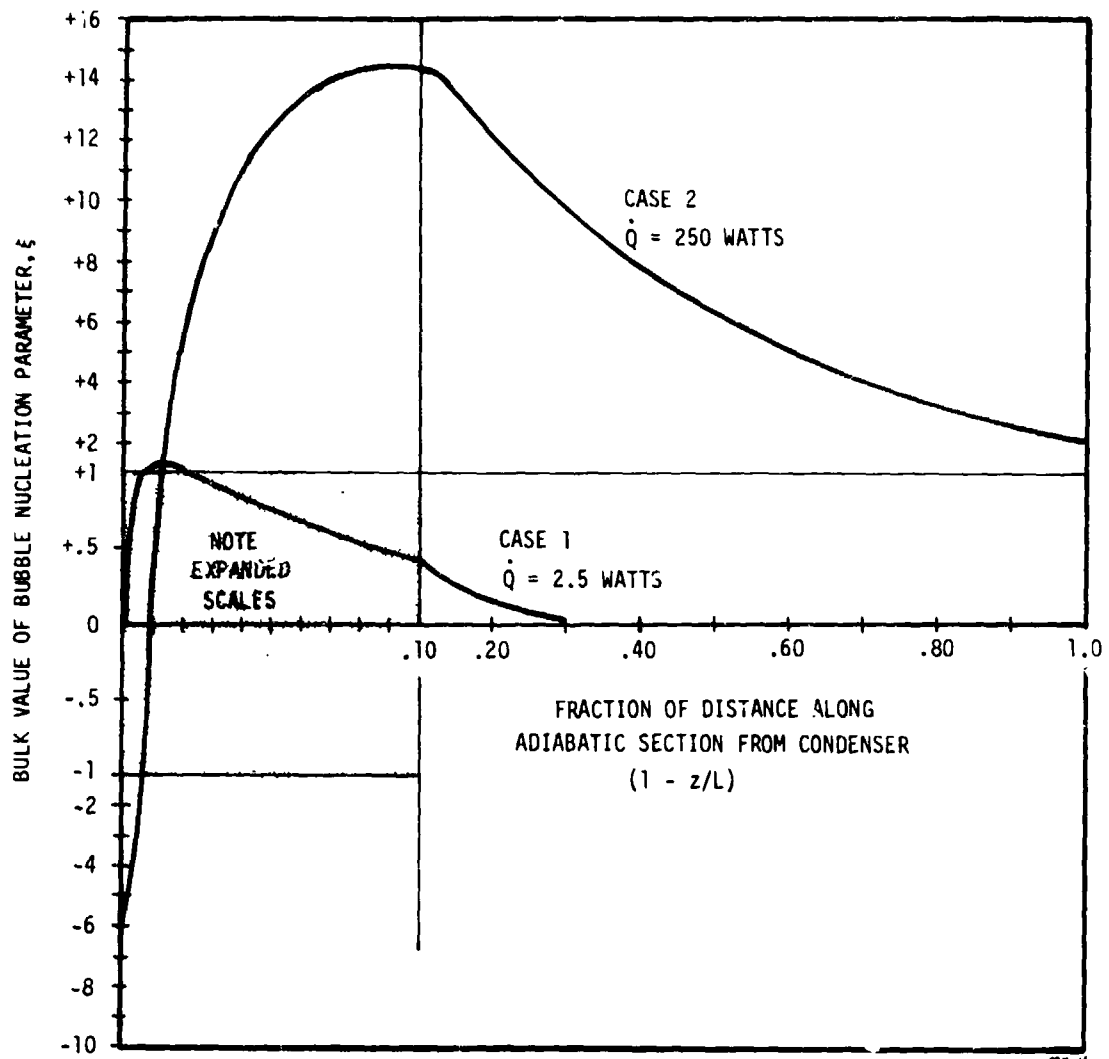
FIGURE 2-1. Danger of Vapor-Lock Versus Distance Along Adiabatic Section.

the fluid rapidly loses its subcooling so that ξ climbs and reaches positive values. However, the gas stripping proceeds rapidly also, and the value of ξ quickly drops to the small value arising from the hydrodynamic load.

In case (2) the subcooling effect is quite strong initially and is only gradually lost, because the N_{tu} for heat transfer (and mass transfer more so) is small at the higher liquid velocities occasioned by the higher heat load. As the subcool is lost, the dissolved gas comes into play, driving ξ positive. Then the gas stripping effect becomes significant and ξ reaches a maximum and decreases. The maximum is seen to be large enough so that a bubble appreciably smaller than the pumping pore size would grow in the artery causing failure.

It is worthy of note that case (2) corresponds to only a 4.4% demand on the pumping capacity of the wick ($\xi_0 = 4.4 \times 10^{-2}$ in Table 2-4). The pore size actually needed in the evaporator is thus over 20 times larger than that chosen in the example. When the size of the potentially troublesome bubble is compared to this large size, the effect of dissolved gas is seen to be large indeed.

The parameter ξ is an inverse measure of the size of pre-existing bubbles which will grow (or collapse) at any position along the heat pipe. As such, it is a measure of the potential for nucleation of vapor bubbles from pre-existing gas stabilized nucleation sites within an artery. If there are nuclei present inside the artery liquid, then vapor bubbles will grow at a nucleation site whenever ξ grows sufficiently large that the critical radius ($r_{cr} = r_e/\xi + 1$) is equal to or less than the size of the pre-existing nucleus.

Typical heat pipe practice involves values of r_e around 5×10^{-3} inches. However, it is difficult to estimate the size of natural nuclei which might exist in a heat pipe artery. If we draw from experience with nucleate boiling from clean surfaces, such nuclei would have radii on the order of 10^{-4} inches. Then ξ would have to rise to a value of order 50 to promote bubble growth. The numerical examples then suggest that such natural nuclei are generally tolerable except perhaps in systems under very high load.

In spite of the quantitative undertainty regarding conditions for bubble growth, the analysis yields useful semi-quantitative results. It demonstrates that, for a given load (given value of r_e), there exists a critical position along the pipe (the maximum in ξ) at which nucleation is most probable. It also allows one to determine the relative probabilities of nucleation for different operating conditions or heat pipe designs by comparing the results for $r_e/\xi_{max} \div 1$.

It is stressed that the theory developed holds for the bulk averages in the fluid. The centerline values of ξ persist at lower values for a longer distance from the condenser and then rise to high values. The wall values are considerably different than the bulk values also. If sizeable nuclei are present only on the walls, the critical position would seem to be just at the transition from the condenser to adiabatic section. But bubbles could not grow to a very large size before encountering subcooled liquid deeper within the artery.

3.0   ANALYSIS OF THE STABILITY OF LARGE BUBBLES IN GAS LOADED
       HEAT PIPE ARTERIES - REPRIMING OF FAILED ARTERIES

A closed artery heat pipe is one having a high permeability
liquid conduit capable of being operated at liquid pressures lower than
can be supported by a vapor-liquid interface of the size of the artery
flow path. In its simplest form an artery is a cylindrical tube running
inside the heat pipe from the condenser to the evaporator. The artery
tube can deliver or receive liquid through a porous web to wicking on
the pipe wall. The wall wicking has a low permeability but a high
capillary pumping ability and serves to distribute the liquid circum-
ferentially over the pipe wall and to provide strong capillary suction
to force flow through the condenser wicking and web, along the artery,
and through the evaporator web and wicking. The web and distribution
wicking will be referred to as secondary or backup wicking in the re-
mainder of this report.

Should a vapor bubble enter the artery at the evaporator end,
for example, through the distribution web or through growth of a gas
bubble nucleated as a consequence of gas in the pipe, such a bubble
will cause the artery to fill with vapor, if the bubble exceeds a
critical size. The vapor plug which then forms eliminates liquid flow
through the high permeability artery path and may cause the evaporator
to dry out and the evaporator temperature to run away. It is of con-
siderable engineering importance to know whether or not the artery will
reprime when the heat load on the pipe is reduced. If repriming occurs,
the pipe can once more be operated at high heat loads with low evaporator
temperature.

Experiments at TRW Systems Group have shown that when arteries
made of scree   prime, a thin sheath of liquid forms and runs along the
screen wall ahead of the main liquid-vapor meniscus. When such an artery
was deprimed by imposing a greater hydrostatic pressure difference than
the screen could support, the artery emptied of liquid and filled with
vapor and air, but a thin sheath of liquid remained intact over the
entire artery wall, as far as visual inspection could determine, although

23

some pores must have admitted the air. The thin sheath of liquid pre-
vented the artery from repriming by trapping air within it. Only when
the sheath was removed by blowing hot air from a heat gun did the artery
reprime.

One can thus envision the following scenario for a gas controlled
heat pipe· A heat pipe artery fails at too high a heat load by entry
of vapor through the evaporator web or a pore on the artery screen wall.
The evaporator dries out, and the evaporator temperature rises rapidly.
A sensor detects the evaporator temperature run away and greatly reduces
the heat load. Since the open artery and secondary wicking continue to
deliver some liquid even after failure of the artery, with the power re-
duced sufficiently the evaporation of the remaining liquid supply cools
the evaporator. As the evaporator cools, the secondary wicking and open
artery are able to supply liquid at a greater distance from the condenser
thus hastening the cooling. When sufficient cooling has occurred, the
secondary wicking reprimes completely, and a sheath of liquid forms over
the artery screen wall. The bubble of vapor and noncondensible gas
trapped by the liquid sheath prevents further repriming except as the
gas diffuses through the sheath of liquid wetting the artery wall.

Counteracting the diffusion of gas through the artery sheath is
the evolution of dissolved gas carried up the liquid-filled portion of
the artery from the gas-blocked portion of the condenser. A gas-
controlled heat pipe, particularly at reduced heat loads, contains an
extensive section of condenser which is subcooled and contains much gas.
A small amount of the gas is unavoidably dissolved in the condensate
and carried up the artery in the dissolved state. Some of the gas is
lost by "stripping" to the counter-flowing vapor stream in the pipe,
but unavoidably the remainder flows with the liquid to the vicinity
of the vapor plug in the artery before the liquid is diverted from the
artery by the plug into the secondary wicking. As the liquid flows
over the cap of the vapor bubble plug, gas is transferred to the
bubble cap interface and evolved into the bubble.

Whether or not the artery reprimes completely then depends upon
whether or not gas diffuses through the artery sheath faster than it is

24

supplied by the bubble cap. In what follows these mass transfer rates
are formulated, and a computer program to determine whether or not a
failed artery will reprime at a given reduced heat load is described.

3.1   Liquid Flow in the Evaporator:

3.1.1   Objectives:

It is desired to develop the demand upon the pumping pores im-
posed by a uniformly distributed heat flux in an evaporator containing
a failed artery. The pressure necessary to sustain the bubble cap is
also desired. The first quantity will be used to establish the maximum
length of evaporator which can be supplied without dry out. Dry out of
a portion of the evaporator would presumably lead to dry out of the
artery sheath as well and would thus liberate the gas blocking the artery.
Then the artery would be free to reprime until formation of a new sheath
again impeded its progress. The maximum length which can be supplied
without dry out is thus taken to be the maximum length of the artery
sheath. The second quantity, the pressure at the bubble cap, will be
compared with the equilibrium pressure established by a balance of the
mass transfer rates into and out of the bubble. If this equilibrium
pressure is lower than the pressure necessary to sustain the bubble, the
bubble will spontaneously reduce in size and vice versa.

3.1.2   Pumping Pore Stress:

The hydrostatic condition of the vapor bubble cap is an equality
of the pressure and surface tension forces. With the assumption of a
hemispherical interface the equality is

$$\frac{2\sigma}{r_a} + P_\ell = P_{gb} + P_{vb} \tag{3-1}$$

Under conditions of negligible vapor side pressure drop and zero gravity,
the pumping pore radius of curvature and pipe pressure are related by

$$P_v = \frac{2\sigma}{r_p} + P_\ell (o) \tag{3-2}$$

25

where $P_{\ell}(o)$ is the liquid pressure at $z = 0$, the end of the evaporator furthest removed from the condenser. The bubble is imagined to exist from $z = 0$ to $z = z_b$. In this portion of the evaporator a parabolic liquid pressure distribution exists

$$P_{\ell}(z) = P_{\ell}(o) + \frac{1}{2} \Delta P_{we} \; (\dot{Q}/\dot{Q}_0) \; (z/z_e)^2 \; , \; z < z_b \qquad (3\text{-}3)$$

where

$$\Delta P_{we} = \frac{\mu_{\ell} \; z_e \; \dot{Q}_0}{K_w A_w \; \lambda} \qquad (3\text{-}4)$$

$$K_w = \frac{D_w^2 \; \dot{\theta}_w}{32 \; \tau_w} \qquad (3\text{-}5)$$

The subscript w refers to the backup or secondary wicking, and z_e is the evaporator length.

In the primed portion of the evaporator, $z_e > z > z_b$, a parabolic liquid pressure distribution also exists, but the pressure gradients are much less steep due to the high permeability of the artery.

$$P_{\ell}(z) = P_{\ell}(o) + \frac{1}{2} \Delta P_{we} \; (\dot{Q}/\dot{Q}_0) \; (z_b/z_e)^2$$

$$+ \frac{1}{2} \Delta P_e \; (\dot{Q}/\dot{Q}_0) \; [(z - z_b)/z_e]^2 \qquad (3\text{-}6)$$

where

$$\Delta P_e = \frac{\mu_{\ell} \; z_e \; \dot{Q}_0}{(K_w A_w + K_a A_a) \; \lambda} \qquad (3\text{-}7)$$

$$K_a = \frac{D_a^2}{32} \qquad (3\text{-}8)$$

At the end of the condenser, assumed to be flooded, the
pressure is

$$P_v = P_\ell (o) + \frac{1}{2} \Delta P_{we} (\dot{Q}/\dot{Q}_0) (z_b/z_e)^2$$

$$+ \frac{1}{2} \Delta P_e (\dot{Q}/\dot{Q}_0) [(z_e - z_b)/z_e]^2$$

$$+ \Delta P_{ad} + \frac{1}{2} \Delta P_c \qquad (3-9)$$

where the last two terms are the adiabatic and condenser section
pressure drops,

$$\Delta P_{ad} = \Delta P_e [(z_{ad} - z_e)/z_e] = \Delta P_e (L_{ad}/L_e) \qquad (3-10)$$

$$\Delta P_c = \Delta P_e [(z_c - z_{ad})/z_e] = \Delta P_c (L_c/L_e) \qquad (3-11)$$

Eq. (3-9) serves to fix P_v in terms of P_ℓ (o), $\dot{Q}$, and z_b.

Equating Eqs. (3-2) and (3-9) yields an expression for pumping
pore demand. Rearranging the expression gives

$$\frac{2\sigma}{r_p} = \left\{ \frac{1}{2} \Delta P_{we} z_b^{*2} + \frac{1}{2} \Delta P_e (1-z_b^{*2}) + \Delta P_{ad} + \frac{1}{2} \Delta P_c \right\} \dot{Q}^* \qquad (3-12)$$

where

$$z_b^* = z_b/z_e \qquad (3-13)$$

$$\dot{Q}^* = \dot{Q}/\dot{Q}_0 \qquad (3-14)$$

27

Since ΔP_{we} is greater than ΔP_e, the demand upon the pumping pore increases with z_b^{*2} as well as $\dot{Q}^*$.

3.1.3 Bubble Pressure:

It remains to determine the bubble pressure difference, $P_{gb} + P_{vb} - P_v$. Eqs. (3-1) to (3-3) combine to give at $z^* = z_b^*$

$$P_b = (P_{gb} + P_{vb}) - P_v = \frac{2\sigma}{r_a} - \frac{2\sigma}{r_p} + \frac{1}{2} \Delta P_{we} \, \dot{Q}^* \, z_b^{*2} \qquad (3-15)$$

This expression may be combined with Eq. (3-12) to give

$$P_b = \frac{2\sigma}{r_a} - \left[\frac{1}{2} \Delta P_e + \Delta P_{ad} + \frac{1}{2} \Delta P_c \right] \dot{Q}^* + \frac{1}{2} \Delta P_e \, \dot{Q}^* \, z_b^{*2} \quad (3-16)$$

This equation states that $\dot{Q}^*$ must be sufficiently small so that the open artery pumping will exceed the primed flow demand,

$$\frac{2\sigma}{r_a} > \left[\frac{1}{2} \Delta P_e + \Delta P_{ad} + \frac{1}{2} \Delta P_c \right] \dot{Q}^* \qquad (3-17)$$

since P_b must be positive in order to drive gas out of the bubble and force z_b^* to zero.

3.2 Transfer through the Artery Sheath:

3.2.1 Mass Transfer:

The mass transfer through the artery sheath is linearly related to P_b, and a quantitative value of the proportionality constant is desired. The physical situation lends itself to an extremely simple model. The mass transfer resistance in the vapor space is small compared to the resistance through the liquid sheath, so the entire liquid

28

side on the interior vapor liquid sheath interface is virtually uniform in mole fraction x_{gb}. Henry's and Raoult's laws then give

$$P_{gb} + P_{vb} = C\, x_{gb} + P_{vi}\, (1 - x_{gb}) \tag{3-18}$$

where C is the Henry constant and P_{vi} is the saturation vapor pressure corresponding to the interior temperature, which is taken to be iso-thermal. In general the temperature T_i will be very slightly less than the prevailing pipe vapor temperature, because of the slight subcooling of the liquid near the bubble cap.

From a simple mass balance it is clear that the mole fraction in the vapor outside the artery at any axial location has bulk mole fraction y_g equal to the bulk mole fraction x_g of the liquid in the wicking at that axial location. Since the mole fraction in the liquid just inside the exterior vapor liquid sheath interface is equal to y_g divided by Henry number H where

$$H = C/P_v \tag{3-19}$$

and since H is enormous for the fluid and noncondensible gas pairs commonly used in heat pipes, the liquid side mole fraction on the exterior of the sheath is negligible. Thus the rate of gas withdrawal from the bubble is, assuming a hemispherical artery end cap,

$$\dot{m}_{sh} = M_g\, \frac{c_\ell \mathcal{D}_\ell}{\delta_a}\, (\pi\, D_a L_e z_b^{\,*} + \pi\, D_a^{\,2}/2) x_{gb}$$

$$\dot{m}_{sh} = \frac{1}{R_{sh,m}}\, x_{gb} \tag{3-20}$$

where δ_a is the artery wall sheath effective thickness and $R_{sh,m}$ is the resistance of the sheath to mass transfer,

$$R_{sh,m} = \frac{\delta_a}{M_g c_\ell \mathcal{D}_\ell \pi\, (D_a L_e z_b^{\,*} + D_a^{\,2}/2)} \tag{3-21}$$

29

Of course, if δ_a is appreciable compared to D_a, the usual logarithmic cylindrical shell relationship would be used in preference to the slab relation above.

Eq. (3-15) of the previous section defined a quantity P_b. We now form the same pressure difference and employ Eq. (3-18) to obtain

$$P_b = P_{gb} + P_{vi} - P_v = (C - P_{vi}) x_{gb} - (P_v - P_{vi})$$

$$P_b = (C - P_{vi}) x_{gb} - \frac{\partial P_v}{\partial T} (T - T_i) \qquad (3-22)$$

The Clausius-Clapeyron relation may be used to obtain the magnitude of $\partial P_v/\partial T$

$$\frac{\partial P_v}{\partial T} = \frac{\lambda M_v}{T} \frac{P_v}{T} \qquad (3-23)$$

3.2.2 Heat Transfer:

At the same time that mass is flowing through the artery sheath out of the bubble, heat is flowing through the artery sheath into the bubble. Again employing a simple slab model for thin sheaths or the cylindrical shell for thick sheaths

$$\dot{Q}_{in} = \frac{k_\ell}{\delta_a} (\pi D_a L_e z_b{}^* + \pi D_a{}^2/2) (T - T_i) \qquad (3-24)$$

$$\dot{Q}_{in} = \frac{1}{R_{sh,h}} (T - T_i) \qquad (3-25)$$

where

$$R_{sh,h} = \frac{\delta_a}{k_\ell \pi(D_a L_e z_b{}^* + D_a{}^2/2)} \qquad (3-26)$$

3.3   Transfer through the Bubble Cap:

3.3.1   Mass Transfer:

A simple model which shows the main physical features of the bubble cap transfer is constructed as follows. Let the mole fraction of the noncondensible which reaches the vicinity of the bubble cap be $x_{g,\infty}$. Suppose a boundary layer exists over the hemispherical cap whose effective thickness is $D_a/Nu_{m,bc}$ and the mole fraction at the edge of this boundary layer is x_{ge}. Finally, the mole fraction at the bubble cap surface is x_{gb}. Gas is brought up the artery and back up wicking at the rate $x_{g,\infty} \dot{Q}/\lambda M_\ell$ moles per unit time. Of this, gas in the amount $x_{ge} \dot{Q}/\lambda M_\ell$ is forced into the back up wicking, because of the vapor bubble plug, and the remainder diffuses through the boundary layer into the bubble. Hence

$$\dot{m}_{bc} = M_g \left[\frac{x_{g,\infty} \dot{Q}}{\lambda M_\ell} - \frac{x_{ge} \dot{Q}}{\lambda M_\ell} \right]$$

$$= M_g \frac{c_\ell \mathscr{D}_\ell Nu_{m,bc}}{D_a} A_{bc} (x_{ge} - x_{gb}) \tag{3-27}$$

Eq. (3-27) above may be represented in engineering circuit terms by a mass current $\dot{m}_{bc}$ flowing in succession through two mass transfer resistances, one $R_{Q,m}$

$$\dot{m}_{bc} = \frac{1}{R_{Q,m}} (x_{g,\infty} - x_{ge}) \tag{3-28}$$

$$R_{Q,m} = \frac{\lambda M_\ell}{\dot{Q} M_g} = \frac{\lambda M_\ell}{\dot{Q}_o M_g} \frac{1}{\dot{Q}^* F(z_b^*)} \tag{3-29}$$

Note that in the evaporator section $F(z_b{}^*)$ is $z_b{}^*$ itself, and in the adiabatic section $F(z_b{}^*)$ is unity. The other resistance is $R_{bc,m}$

$$\dot{m}_{bc} = \frac{1}{R_{bc,m}} (x_{ge} - x_{gb}) \qquad (3-30)$$

$$R_{bc,m} = \frac{2}{M_g c_\ell \mathscr{D}_\ell Nu_{m,bc} \pi D_a} \qquad (3-31)$$

The quantity $x_{g,\infty}$ will have to be found from an analysis to follow in the next section. It is possible now to eliminate x_{ge} and write a more useful expression for $\dot{m}_{bc}$.

$$\dot{m}_{bc} = \frac{1}{R_{Q,m} + R_{bc,m}} (x_{g,\infty} - x_{gb}) \qquad (3-32)$$

3.3.2 Heat Transfer:

In a similar manner, an expression for $\dot{Q}_{bc}$ can be found

$$\dot{Q}_{bc} = \frac{1}{R_{Q,h} + R_{bc,h}} (T_\infty - T_i) \qquad (3-33)$$

where

$$R_{Q,h} = \frac{\lambda}{\dot{Q} c_p} = \frac{\lambda}{\dot{Q}_o c_p} \frac{1}{\dot{Q}^* F(z_b{}^*)} \qquad (3-34)$$

$$R_{bc,h} = \frac{2}{k_\ell Nu_{h,bc} \pi D_a} \qquad (3-35)$$

From the Colburn relationship one would expect that

$$Nu_{m,bc}/Nu_{h,bc} \doteq (Sc_\ell/Pr_\ell)^{1/3} \qquad (3-36)$$

32

where Sc_ℓ and Pr_ℓ are the liquid Schmidt and Prandtl numbers, respectively.

A value of Nusselt number is difficult to fix, because of the variety of geometrical forms which the web can take, and because of the complex three-dimensional nature of the flow occurring near the bubble cap as fluid is withdrawn into the web. It seems improbable that the value would fall below the value for convection at the average liquid velocity over an isolated sphere, in which case the upper limit to R_{bc} would be obtained with $Nu_{bc} = 2.0$. On the contrary, it seems that the value of Nu could be larger than the isolated sphere value. Of course, a lower limit to the sum $R_Q + R_{bc}$ is certainly R_Q itself.

3.4 Bubble-Cap-Sheath Relationships:

3.4.1 Mass Transfer:

Equating mass rate of gas in at the bubble cap, Eq. (3-32), to the mass flow out through the sheath, Eq. (3-20), permits the unknown x_{gb} to be found in terms of $x_{g,\infty}$ and the heat flow $\dot{Q}$ and bubble size z_b.

$$x_{gb} = x_{g,\infty} \ \frac{R_{sh,m}}{R_{sh,m} + R_{bc,m} + R_{Q,m}} \tag{3-37}$$

This value is the static equilibrium value.

At a nonequilibrium state $\dot{m}_{bc}$ may not equal $\dot{m}_{sh}$ in which case the bubble grows or shrinks at a rate governed by

$$\dot{m}_{bc} - \dot{m}_{sh} = \frac{d}{dt}\left(H\, x_{gb}\, \frac{P_i}{R_u T_i}\, M_g\, \frac{\pi}{4}\, D_a^2\, L_e\, z_b^* \right)$$

where P_i is $P_{gb} + P_{vb}$ or $P_b + P_v$. Using the latter,

$$\dot{m}_{bc} - \dot{m}_{sh} = \frac{\pi}{4} D_a^2 L_e \frac{d}{dt}\left\{ z_b^*\, x_{gb}\, H\, \frac{(P_b + P_v)}{R_u T_i} \right\} M_g \tag{3-38}$$

3.4.2 Heat Transfer:

At an equilibrium or quasi-equilibrium thermal state $\dot{Q}_{bc} = \dot{Q}_{sh}$, and Eqs. (3-25) and (3-33) yield

$$T - T_i = (T - T_\infty) \frac{R_{sh,h}}{R_{sh,h} + R_{bc,h} + R_{Q,h}} \qquad (3-39)$$

In a nonequilibrium state, as the bubble shrinks, latent heat is delivered to the sheath wall with the result that

$$\dot{Q}_{bc} - \dot{Q}_{sh} = \frac{d}{dt} \left\{ (1 - x_{gb}) \frac{M_v P_i}{R_u T_i} \cdot \frac{\pi}{4} D_a^2 L_e z_b^* \right\}$$

$$\dot{Q}_{bc} - \dot{Q}_{sh} = \frac{\pi}{4} D_a^2 L_e \frac{d}{dt} \left\{ (1 - x_{gb}) H \cdot \frac{M_v (P_b + P_v)}{R_u T_i} z_b^* \right\} \qquad (3-40)$$

3.4.3 Equilibrium Excess Pressure:

The value of P_b given by Eq. (3-22) which would exist if the bubble were in an equilibrium condition is now denoted as the excess pressure P_x. Eqs. (3-37) and (3-39) then may be substituted to obtain

$$P_x = (C - P_{vi}) \frac{R_{sh,m}}{R_{sh,m} + R_{bc,m} + R_{Q,m}} x_g + \frac{\partial P_v}{\partial T} \frac{R_{sh,h}}{R_{sh,m} + R_{bc,h} + R_{Q,h}} (T - T_\infty)$$

$$(3-41)$$

At equilibrium P_x here will equal P_b in Eq. (3-16).

3.5 Gas Stripping and Heating:

3.5.1 Adiabatic Section Mass Transfer:

Assume that the mole fraction of gas in the condensate leaving the condenser is known to be x_{gc}. In two calculations using the GASPIPE

34

program x_{gc} was found to be on ... order of 10^{-2} divided by Henry number H (Section 2.2). Thus x_{gc} is expected to be quite small, but the product $C x_{gc}$ may be 10^{-2} of P_v and is thus quite important when $2\sigma/r_{\hat{a}}$ is of the same order.

As the liquid flows up the evaporator some gas is stripped from it by the counterflowing vapor. As remarked previously, because of the large value of H and the equality of the bulk values of liquid and vapor mole fractions at any axial station, the vapor may be considered to be pure for purposes of calculating mass transfer from the liquid. Elementary mass exchanger theory then yields for the bulk value of $x_{g,\infty}(z)$

$$x_{g,\infty}(z) = x_{gc} \, e^{-N_{tu,m} \, [(z_c - \lambda)/L_{ad}] \, \frac{1}{\dot{Q}^*}} \tag{3-42}$$

where N_{tu} is the number of transfer units given by

$$N_{tu,m} = \frac{K_{oa}\mathcal{P} L_{ad}}{m_\ell/M_\ell} = \frac{M_\ell \, \lambda \, K_{oa}\mathcal{P} L_a}{\dot{Q}_o} \tag{3-43}$$

The overall mass transfer coefficient effective perimeter product is

$$K_{oa}\mathcal{P} = \cfrac{1}{\cfrac{1}{\pi D_a \cfrac{c_\ell \mathscr{D}_\ell}{\delta_a} Nu_{m,a}} + \cfrac{1}{\pi D_a \cfrac{c_\ell \mathscr{D}_\ell}{\delta_a}} + \cfrac{1}{\pi D_o H \cfrac{c_g \mathscr{D}_g}{D_v} Nu_{m,v}}}$$

Because $Hc_g \mathscr{D}_g$ greatly exceeds $c_\ell \mathscr{D}_\ell$ the last or "gas-side" term is negligible. For this reason $K_{oa}\mathcal{P}$ may be written

$$K_{oa}\mathcal{P} = \frac{\pi D_a \, c_\ell \mathscr{D}_\ell}{\dfrac{D_a}{Nu_{m,a}} + \delta_a} \tag{3-44}$$

35

Again, if δ_a is appreciable compared to D_a, the cylindrical shell relationship is used for the artery wall resistance.

3.5.2 Adiabatic Section Heat Transfer:

The liquid leaves the condenser with an initial subcooling $\Delta T_{\ell,s}$. The GASPIPE program was used to estimate this subcooling, and values of a few degrees Rankine were found. This subcooling is very rapidly lost when the artery wall is thin. The remaining subcooling is

$$T - T_\infty = \Delta T_{\ell,s} \, e^{-N_{tu,h} \, [(z_c - z)/L_{ad}]} \frac{1}{Q^*} \tag{3-45}$$

where

$$N_{tu,h} = \frac{U_{oa} \mathscr{P} L_{ad}}{\dot{m} \, c_{\sim,\ell}} = \left(\frac{\lambda \, U_{oa} \mathscr{P} L_{ad}}{\dot{Q} \, c_{p,\ell}} \right) \tag{3-46}$$

Because of the high heat transfer coefficient for condensation on the outside of the artery, the liquid side governs the heat transfer, and

$$U_{oa} \mathscr{P} = \frac{\pi D_a K_\ell}{\dfrac{D_a}{Nu_{h,a}} + \delta_a} \tag{3-47}$$

The same proviso regarding δ_a/D_a made above is invoked.

3.5.3 Evaporator Section Mass Transfer:

In the evaporator section the simple N_{tu} relationship must be modified, because the mass flow varies with z, as liquid is bled off through the webs to the evaporator. For this reason the mass flow is

$$\dot{m}_\ell(z) = \frac{\dot{Q}_0}{\lambda} \, \frac{\dot{Q}}{\dot{Q}_0} \, \frac{z}{L_e} = \frac{\dot{Q}_0}{\lambda} \, \dot{Q}^* \, z^* \tag{3-48}$$

36

At any location $z_e > z > z_b$ in the liquid filled section of the evaporator artery, the conservation of gas equation takes the form (neglecting the effect of flow into the web on K_{oa}) shown below:

$$(\dot{m}_\ell(z)/M_g) \; \frac{dx_g}{dz} = \; + K_{oa} \mathscr{P} x_g$$

$$z^* \; \frac{dx_g}{dz^*} \; = \; \frac{M_g \, K_{oa} \mathscr{P} \, L_e \, \lambda}{\dot{Q}_o} \; \frac{1}{Q^*} \, x_g$$

$$z^* \; \frac{dx_g}{dz^*} \; = \; \left[N_{tu,m} \; \frac{L_e}{L_{ad}} \frac{1}{Q^*} \right] x_g \tag{3-49}$$

The solution to Eq. (3-49) is

$$x_g = \lambda_{g,e} \; z^{* \, E_m} \tag{3-50}$$

$$E_m = N_{tu,m} \; \frac{L_e}{L_{ad}} \frac{1}{Q^*} \tag{3-51}$$

3.5.4   Evaporator Section Heat Transfer:

By similar reasoning, the subcooling in the evaporator is

$$T - T_\infty = (T - T_\infty)_e \; z^{* \, E_h} \tag{3-52}$$

$$E_h = N_{tu,h} \; \frac{L_e}{L_{ad}} \frac{1}{Q^*} \tag{3-53}$$

3.6   Adiabatic Section Relationships:

3.6.1   Objectives:

It remains to set up relationships for pumping pore stress and bubble pressure, should the bubble project into an adiabatic section. These relationships will replace Eqs. (3-12) and (3-16) in the event that the bubble length does exceed the evaporator length.

3.6.2   Pumping Pore Stress:

Eqs. (3-1) and (3-2) continue in effect, but Eq. (3-3) becomes

$$P_\ell(z) = P_\ell(o) + \Delta P_{we} \dot{Q}^* (z^* - \frac{1}{2}), \quad z_b^* > z^* > 1 \tag{3-54}$$

Eq. (3-6) likewise changes form

$$P_\ell(z) = P_\ell(o) + \Delta P_{we} \dot{Q}^* (z_b^* - \frac{1}{2}) + \Delta P_{ad} \dot{Q}^* \frac{z - z_b}{L_{ad}}$$

$$P_\ell(z) = P_\ell(o) + \Delta P_{we} \dot{Q}^* (z_b - \frac{1}{2}) + \Delta P_e \dot{Q}^* (z^* - z_b^*) \tag{3-55}$$

Eq. (3-9) becomes

$$P_v = P_\ell(o) + \Delta P_{we} \dot{Q}^* (z_b^* - \frac{1}{2}) + \Delta P_e \dot{Q}^* (z_c^* - z_b^*) + \Delta P_c \tag{3-56}$$

This latter expression together with Eq. (3-2) gives the pumping pore stress

$$\frac{2\sigma}{r_p} = \Delta P_e \dot{Q}^* (z_c^* - z_b^* + \frac{1}{2} \frac{L_c}{L_e})$$

$$+ \Delta P_{we} \dot{Q}^* (z_b^* - \frac{1}{2}) \tag{3-57}$$

3.6.3 Bubble Pressure:

The bubble pressure difference P_b is given by Eqs. (3-1), (3-2), and (3-54)

$$P_b = \frac{2\sigma}{r_a} - \frac{2\sigma}{r_p} + \Delta P_{we}\dot{Q}^* \left(z_b^* - \frac{1}{2}\right) \qquad (3\text{-}58)$$

Substituting in Eq. (3-57) results in

$$P_b = \frac{2\sigma}{r_a} - \Delta F_e\dot{Q}^* \left(z_c^* - z_b^* + \frac{1}{2} \frac{L_z}{L_e}\right) \qquad (3\text{-}59)$$

3.7 Critical Deprimed Heat Flow:

3.7.1 Definition:

The critical deprimed heat flow is the heat flow which is sufficiently high so that some value of z_b, between 0 and the value which exists just after formation of the artery sheath, gives rise to a bubble which can exist steadily. A higher value of $\dot{Q}$ would cause the critical bubble to grow by increasing the transfer of gas into the bubble and by increasing the liquid flow pressure losses. The former increases P_x given by Eq. (3-41) by increasing $x_{g,\infty}$, given by Eq. (3-42) or (3-50). The latter causes P_b, given by Eq. (3-16) or (3-59) to fall.

The critical condition is thus defined by the relation

$$P_x = P_b \text{ at } z_b = z_{b,cr} \qquad (3\text{-}60)$$

3.7.2 Method of Calculation:

The ratio P_x/P_b is calculated versus z_b^* for a trial value of $\dot{Q}^*$. The quantity P_b is obtained from Eq. (3-16). Eqs. (3-42) or (3-50) and (3-45) or (3-52) are used to obtain values of $x_{g,\infty}$ and $T - T_\infty$ needed for Eq. (3-41). The computation is stopped at $z = z_c$ or at the point

39

when Eq. (3-12) for the pumping pore stress shows back up wicking dry out. If the maximum value of P_x/P_b is greater than unity a smaller value of $\overset{.*}{Q}$ is tried and vice versa.

3.7.3   Sample Calculations:

Sample calculations were made for selected parameters tabulated in Table 3-1. The results are shown graphed in Figure 3-1. The sample calculations clearly show the beneficial effects of thin artery wall and long adiabatic length for achieving a high value of critical deprimed heat flow.

3.8   Conclusions:

Analysis and calculations show conclusively that a thin artery wall and an adiabatic section for gas stripping are highly desirable. Even with such features, however, the maximum heat load which can be sustained during repriming was found to be only about a tenth of the load which could be delivered by an open artery. Since this open artery capacity is presumably only a small fraction of the design capacity, the load which can be sustained during repriming is very small indeed.

A load in excess of the repriming load but smaller than the open artery capacity will not cause failure of the pipe (burnout), but will also not allow the artery to reprime. A periodic destruction and re-forming of the artery sheath will occur. On the other hand, the absence of any load will also impede priming because, at equilibrium, the vapor core in the evaporator will not be swept of gas, and there will exist very little diffusion potential for the gas to escape the artery.

Thus, the results indicate that, to prime an artery in a gas-loaded heat pipe which contains a gas stabilized bubble, it is necessary to operate the heat pipe at a load sufficient to sweep the gas from the evaporator but below the critical repriming value. Unfortunately, the analysis does not yield rate data, and it is therefore not yet possible

TABLE 3-1

SELECTED PARAMETERS FOR SAMPLE CALCULATION

FLUID PROPERTIES (WATER):

    LATENT HEAT   HFG = 9.90000E+02 BTU/LB

    SURFACE TENSION   ST = 4.27000E-03 LB/FT

    LIQUID:

        DENSITY   RHOL = 6.10000E+01 LB/FT3

        CONDUCTIVITY   CONL = 3.90000E-01 BTU/HRFTF

        KINEMATIC VISCOSITY   VISL = 1.40000E-02 FT2/HR

        SCHMIDT NUMBER   SCL = 6.41000E+01

        PRANDTL NUMBER   PRL = 2.16000E+00

        SPECIFIC HEAT   CPL = 1.00000E+00 BTU/LBF

    HENRY CONSTANT   CATM = 1.30000E+05 ATMOS

    VAPOR MOLECULAR WT   VWM = 1.80000E+01

    GAS MOLECULAR WT (NITROGEN)   GWM = 2.80000E+01

ARTERY CHARACTERISTICS:

    INSIDE DIAMETER   DAI = 6.00000E-02 INCHES

    AREA   AAI = 2.83000E-03 SQ INCHES

    PERIMETER   PAI = 1.89000E-01 INCHES

    WALL THICKNESS   DELAI = 8.00000E-03 INCHES

BACK-UP WICK:

    FLOW PORE   DBI = 1.20000E-02 INCHES

    VOLUME VOID FRACTION   VOID = 8.00000E-01

    TORTUOSITY   TORT = 3.00000E+00

TABLE 3-1

SELECTED PARAMETERS FOR SAMPLE CALCULATION

(CONTINUED)

AREA   ABI = 1.00000E-02 SQ INCHES

MIN PUMPING PORE DIAMETER   DMINI = 1.20000E-02 INCHES

OPERATING CONDITIONS:

EVAPORATOR TEMPERATURE   TE = 6.37600E+02 DEG R

VAPOR PRESSURE   PV = 1.03700E+03 LB/FT2

SUBCOOLING   TSUB = 1.35000E+00 DEG R

MOLE FRACT OF GAS IN EQUIL WITH COND   YCON = 2.42000E-02

ARTERY NUSSELT NUMBER   ANU = 3.65000E+00

BUBBLE CAP NUSSELT NUMBER   BCNU = 1.00000E+04

NOMINAL LOW LEVEL HEAT FLOW   QMIN = 2.46000E+01 BTU/HR

PIPE CHARACTERISTICS:

EVAPORATOR LENGTH   XLEI = 6.00000E+00 INCHES

ADIABATIC LENGTH   XLAI = 3.00000E+00 INCHES

CONDENSER LENGTH   XLCI = 2.40000E+01 INCHES
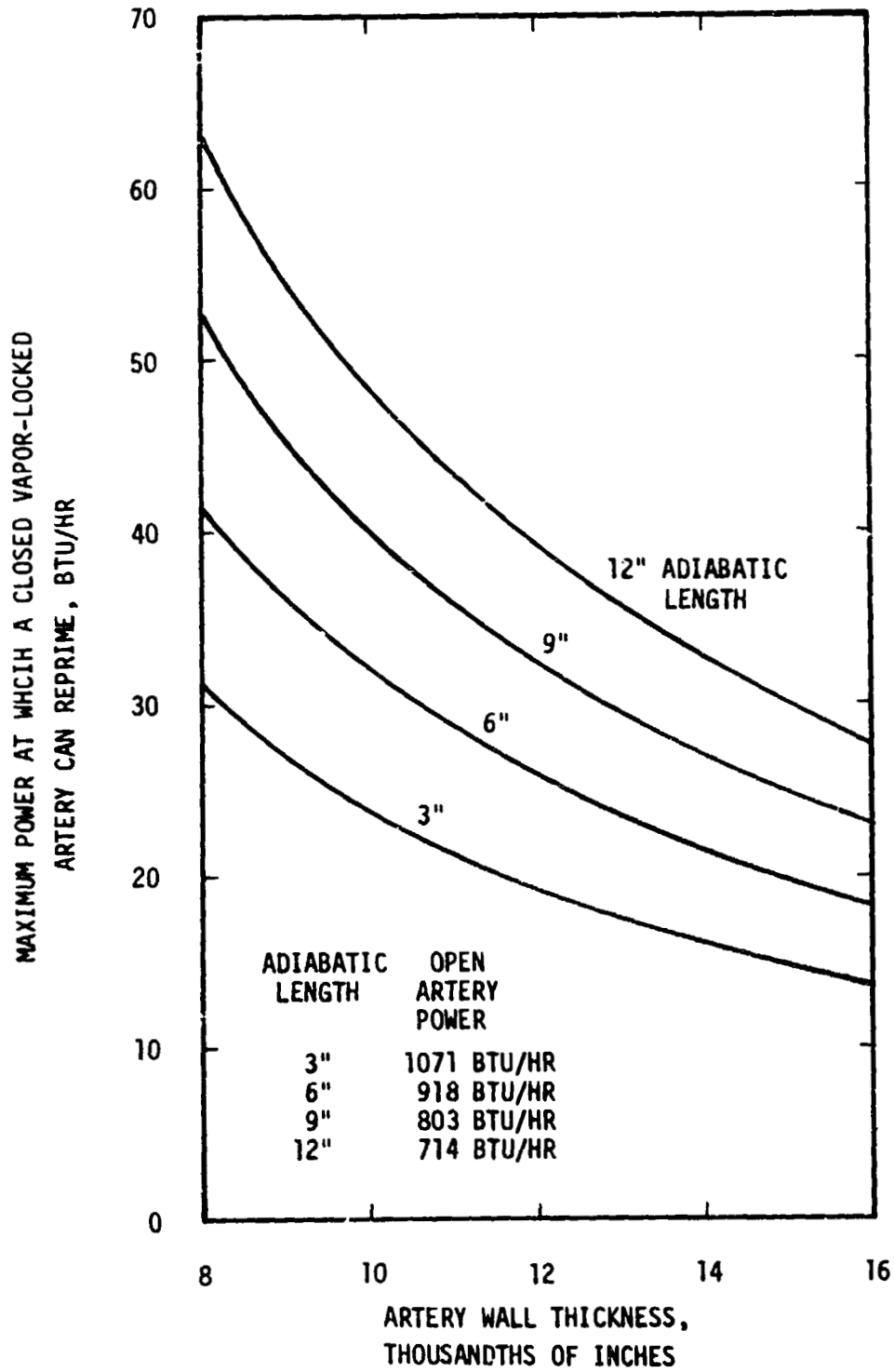
FIGURE 3-1. Calculated Values of Maximum Re-priming Load for an Artery Containing a Gas - Stabilized Vapor Bubble vs. Artery Wall Thickness and Length of the Adiabatic Section.

to analytically evaluate the practicality of this approach. Some experimental results obtained at TRW Systems Group on ammonia-helium heat pipes have shown that very low loads (2-4 watts) for extended periods (16 hours) were necessary to successfully achieve priming.

4.0   SCALING LAWS FOR ACCELERATED LIFE TESTING

With the heat pipe rapidly becoming a serious design element in
the solution of many spacecraft thermal control problems, there exists
a major impetus for understanding the mechanisms and developing scaling
laws for life limiting processes. A need for achieving very long lived
high reliability heat pipe systems in a rapidly changing technology
necessitates the employment of accelerated testing techniques.

Within the realm of spacecraft temperature control devices,
potential failure processes and criteria can be defined. Efforts on
this task have directly addressed the demonstration that quantitative
relations can be established between a life limiting process and specific
materials compatibility, test temperature, and heat transport rate.

In considering the general problem of developing scaling laws
for accelerated life testing, TRW Systems defined a broad program and
approach which involved multiple materials systems, extensive material
tests, and a several year time phased effort. Because of funding
limitations, the present task was of reduced scope, but did not obviate
any of the concepts included in the broader program. Rather, this task
represented a feasibility study to determine the extent to which a
scaling law might be developed for accelerated life testing in a specific
heat pipe system. If a successful scaling law could be established
for a specific system, it might provide justification for undertaking
the broader program which would include all materials combinations of
interest in spacecraft thermal control and all life limiting processes.

Nickel-water heat pipes were selected for study for a number of
reasons: (1) it was of interest to accurately study hydrogen gas evolution
which occurs during corrosion within the heat pipe, and which occurs in other
materials systems with possible important heat pipe applications as well;
(2) past experience showed this couple exhibited a high enough corrosion
rate to permit experimental study of gas generation in a reasonable time
period; (3) the simplicity of studying a system consisting of pure (un-
alloyed) materials; and (4) the commercial availability of the materials.
Actually, Ni 200 was selected because fine screen was available up to

45

250 mesh, which was desirable for the study of wick degradation. However, it was found that in order to comprehensively examine the more important effect of hydrogen evolution in detail, wick degradation could not be included in the program. Thus, a higher purity grade of nickel could have been employed, but this was not an important consideration.

The primary objective was to formulate an accurate scaling law for the specific example of the water-nickel heat pipe which predicts the useable lifetime at reference (low) operating conditions from data taken at accelerated (high) operating conditions. It is emphasized that this task was not concerned with achieving a water-nickel compatibility solution. However, it was necessary to maintain sufficient control over the starting materials and fabrication techniques to allow the separation of temperature and fluid circulation effects.

4.1   Accelerated Testing:

4.1.1   Heat Pipe Materials and Construction

A total of 16 heat pipes were constructed from nickel 200 materials for the experimental phase of this program. Containers were 17.5" in length with 1/2" OD and 0.035" walls. Two layers of 250 mesh screen were installed and the end caps and closure tubes were machined from 1/2" and 1/4" diameter rods, respectively. Care was taken to ensure that all the heat pipes were as nearly the same as possible in terms of materials and construction procedures. All containers were constructed from nickel 200 tube of the same heat number and the same was true of the screen and rods from which the end caps and pinch-off tubes were constructed. Efforts were made during welding to use the same temperature and complete the weld in the same length of time for each heat pipe. A schematic diagram of the heat pipes subjected to accelerated testing is shown in Figure 4-1.

In order to remove the oxide film produced during TIG welding on the internal surfaces of the heat pipes, all 16 heat pipes were baked out in vacuum for 2 hours and 26 minutes at 700°C and then reduced in hydrogen for 30 minutes at 732°C. A test specimen subjected
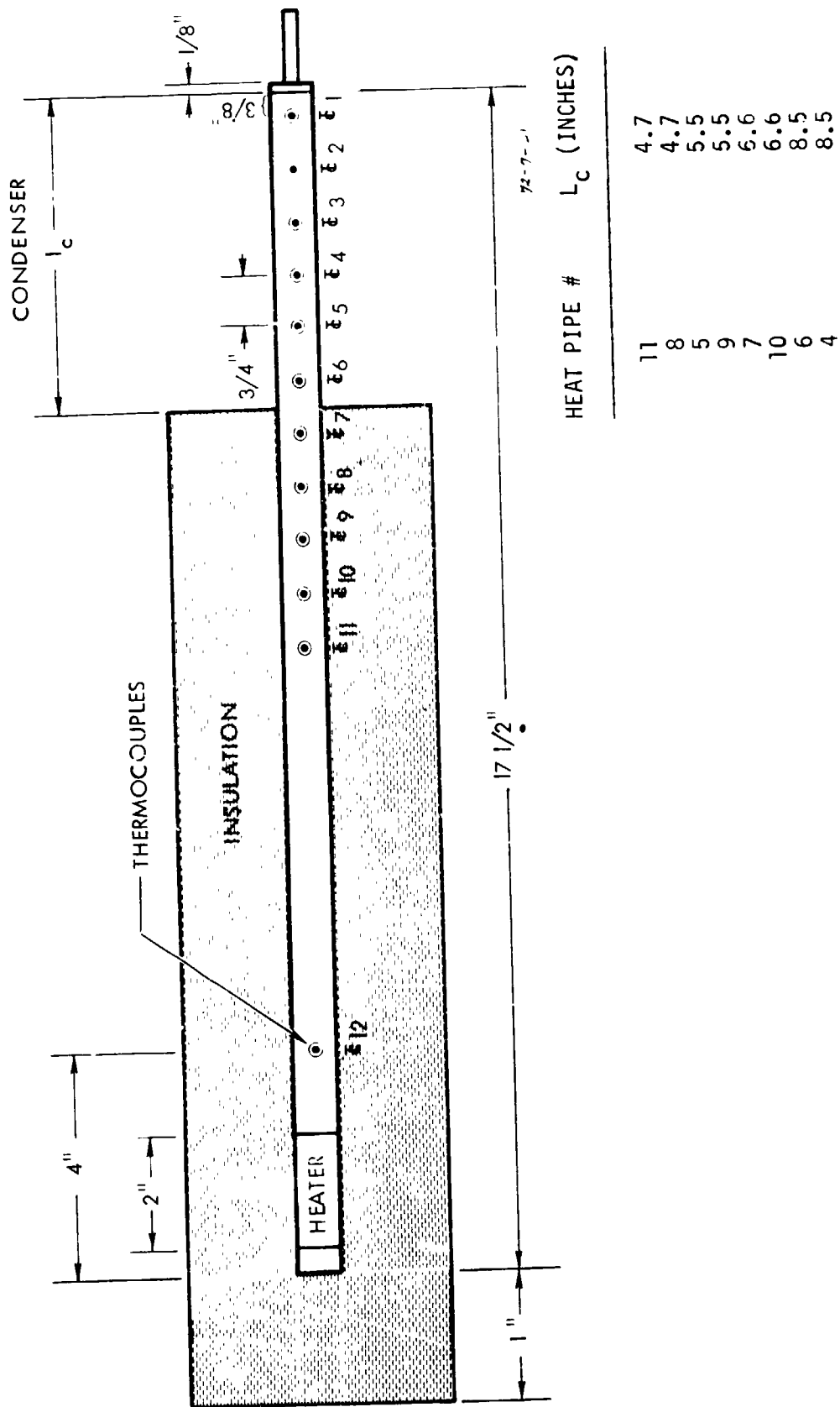
46

FIGURE 4-1. Accelerated Life Testing Nickel-Water Heat Pipe.

HEAT PIPE #	L_c (INCHES)
11	4.7
8	4.7
5	5.5
9	5.5
7	6.6
10	6.6
6	8.5
4	8.5

to this reduction procedure showed no oxide film remaining on internal surfaces after processing. After vacuum bake-out and reduction in hydrogen, the heat pipes were stored with plastic caps over the fill cubes. The heat pipes were filled with 2.0 ml of triply distilled and degassed water just prior to the initiation of testing. Chromel/alumel thermocouples were spot-welded to the outside of the heat pipes and 2" long wire wound resistance heaters were installed on the evaporator sections prior to filling. Aerotube pipe insulating material was installed to allow four different condenser lengths L_c, which permitted operating with different flow rate, at the same temperature and vice versa.

4.1.2 Measurement of Noncondensible Gas Evolution

As gas is evolved during operation of a heat pipe, it is carried to the condenser end causing a blockage and consequent temperature profile along the outer wall. Assuming ideal gas behavior, the amount of gas present may be calculated from the temperature profile. If the condenser end is divided into equal intervals and the temperature at the center of each interval is T_i, then under steady-state conditions the number of lb.-moles of gas n is given by the ideal gas law as:

$$n = \frac{\Delta V}{R_u} \sum_{i=1}^{N} \frac{P_{gi}}{T_i} \tag{4-1}$$

In (4-1), ΔV is the volume of each interval, R_u is the gas constant, and

$$P_{gi} = P_{va} - P_{vi} \tag{4-2}$$

is the partial pressure of gas at the center of the ith interval. In (4-2), P_{va} is the total pressure (the vapor pressure corresponding to the temperature in the adiabatic section) and P_{vi} is the vapor pressure in the ith interval.

A data reduction computer program was used to determine the quantity of gas in a heat pipe at any given time from the measured steady-state wall temperature profile. This method is based on the

48

assumption that the wick surface temperature, and hence the vapor-gas mixture, is very close to the wall temperature in the gas blocked region of the condenser. This assumption has been found to be valid through calculations with the TRW Gaspipe Program [11].

In practice, each pipe was divided into 3/4" elements with a chromel-alumel thermocouple placed in the center of each interval. The thermocouple temperature readings were punched directly into the computer program, which automatically carried out the operations indicated by equations (4-2) and (4-1), and printed out the total number of lb.-moles of gas in the pipe. Trial calculations indicated that the discrepancy between using a 0.5" element and a 1.0" element was less than one percent.

4.1.3 Accelerated Testing Conditions

It was assumed, based on previous studies of water heat pipes [12, 13], that the gas generation rate would be a strong function of the operating (vapor) temperature. For this reason a constant temperature, controlled flow chamber, in which all life testing and accelerated testing of heat pipes in this program were carried out, was designed and built. The chamber is shown schematically in Figure 4-2. A boxer fan blows air into a heating chamber and then through mixing baffles into a plenum region. The air then flows through a 200 mesh layer of screen and a 1" thickness of 1/8" cell honeycomb to uniformly distribute and straighten the flow into the test region. The test region is covered with a spun glass cover to eliminate drafts from the environment. In addition, the entire chamber is insulated with 1" of urethane foam to further minimize environmental effects. The temperature of the air entering the test region is maintained constant at 80°F by modulating the heater (light bulbs) power through a proportional controller using a reference thermocouple. In the course of the program, the chamber demonstrated set point control of approximately ± 0.5°F, and was unaffected by convective air currents in the room. However, laboratory temperature changes of ± 3°F, which occurred occasionally, were found to result in changes in the chamber temperature of ± 1°F. Thus, the
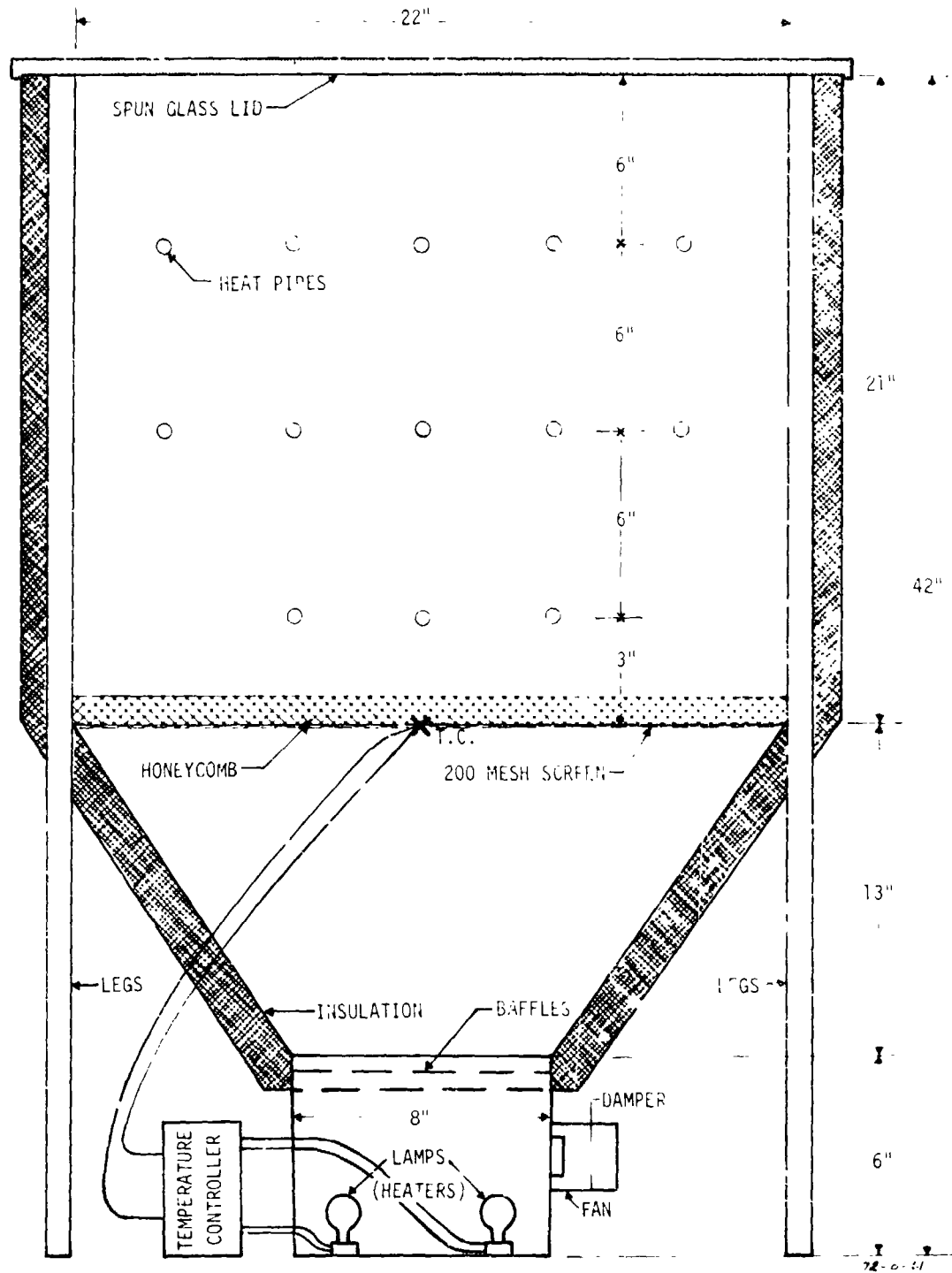
FIGURE 4-2. Schematic of Accelerated Life Test Chamber.

chamber was effective in reducing ambient temperature variations, but did not entirely eliminate them. The test region contains three racks at different levels to hold the heat pipes.

The accelerated testing phase of the program was begun by operating three heat pipes at temperatures of approximately 150°F, 250°F, and 350°F   This initial testing stage was carried out in order to determine approximately the time and temperature dependence of the gas generation function in order to draw up a detailed test plan. Gas generation curves for two of these heat pipes operating at accelerated temperatures of approximately 150°F and 250°F are shown in Figures 4-3 and 4-4. These data were taken during the initial testing period of the program and the temperature was not well controlled, as the scatter in the data indicates. The curves are shown only to indicate the strong temperature dependence. The apparent parabolic behavior was not found with more accurate data taken later in the program.

Based on these initial results, a test plan was drawn up to begin life testing of three reference condition heat pipes and five accelerated condition heat pipes held at higher temperatures. The three reference condition heat pipes were set operating in the 80.0 ± 0.5°F constant temperature chamber in a slight reflux mode at 85.0 ± 0.5°F and 0.42 watts.

The five accelerated condition heat pipes were held at constant temperatures of 135°F, 150°F, 165°F, 180°F, and 195°F (isothermally) with zero flow rate. These isothermal heat pipes were held to within ± 0.5°F of the indicated temperatures by completely wrapping the pipes with heat tape and convering with two layers of insulation. The temperature difference betweer any two points on a heat pipe was less than 0.5°F. Thus, the fluid flow rate in the isothermal heat pipes were essentially zero. The only time fluid flow occurred was during the approximately one hour periods when the heat pipes were operated at 100°F, as heat pipes, for the purpose of measuring the temperature profiles. In order to measure the amount of gas generated by high temperature exposure, the heat pipes maintained under isothermal conditions were taken out of the constant temperature chamber temporarily for

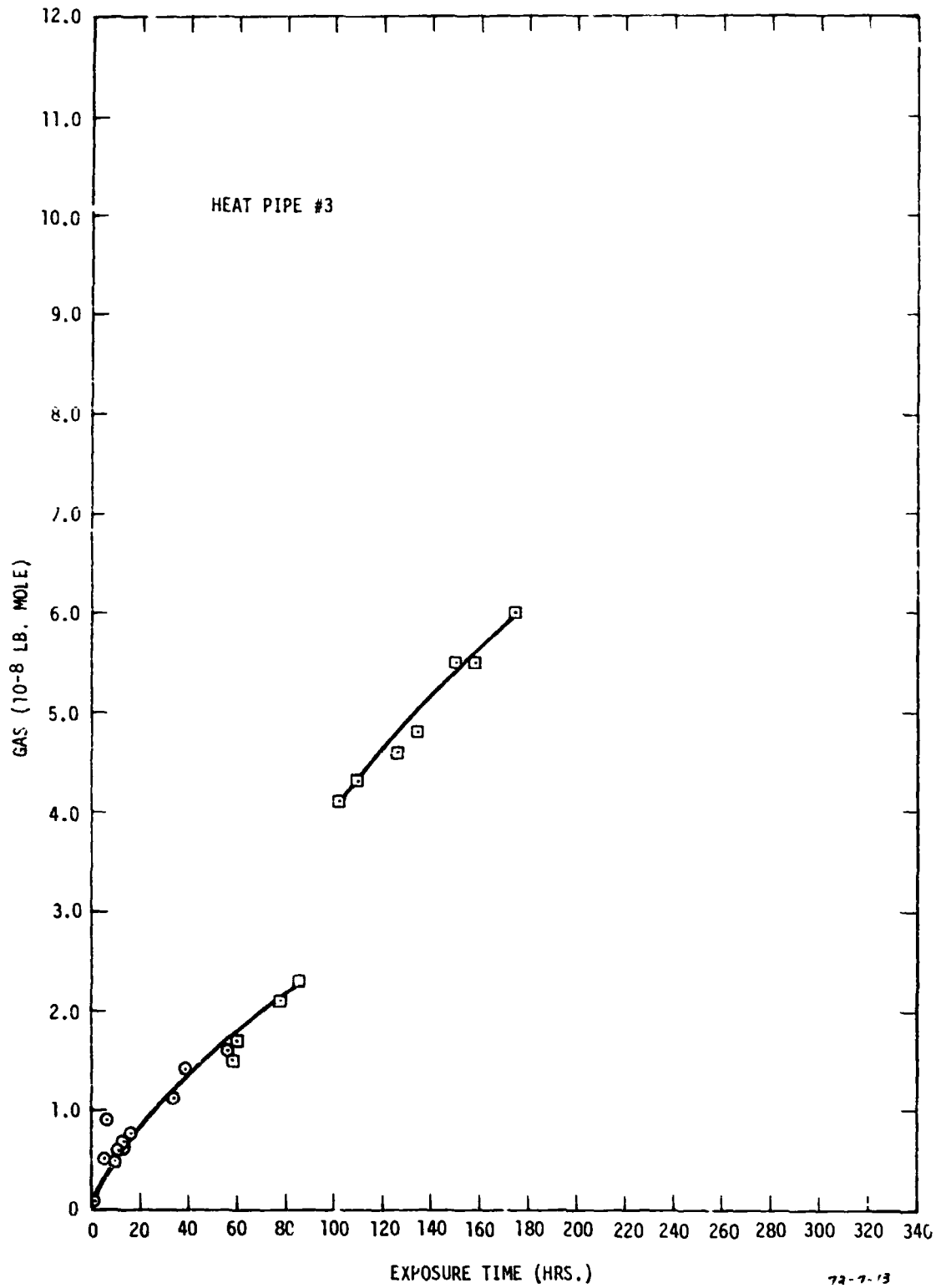FIGURE 4-3. Gas evolution in nickel-water heat pipe #3
             operated at accelerated condition at 150 ±
             3°F. The step in the curve may have resulted
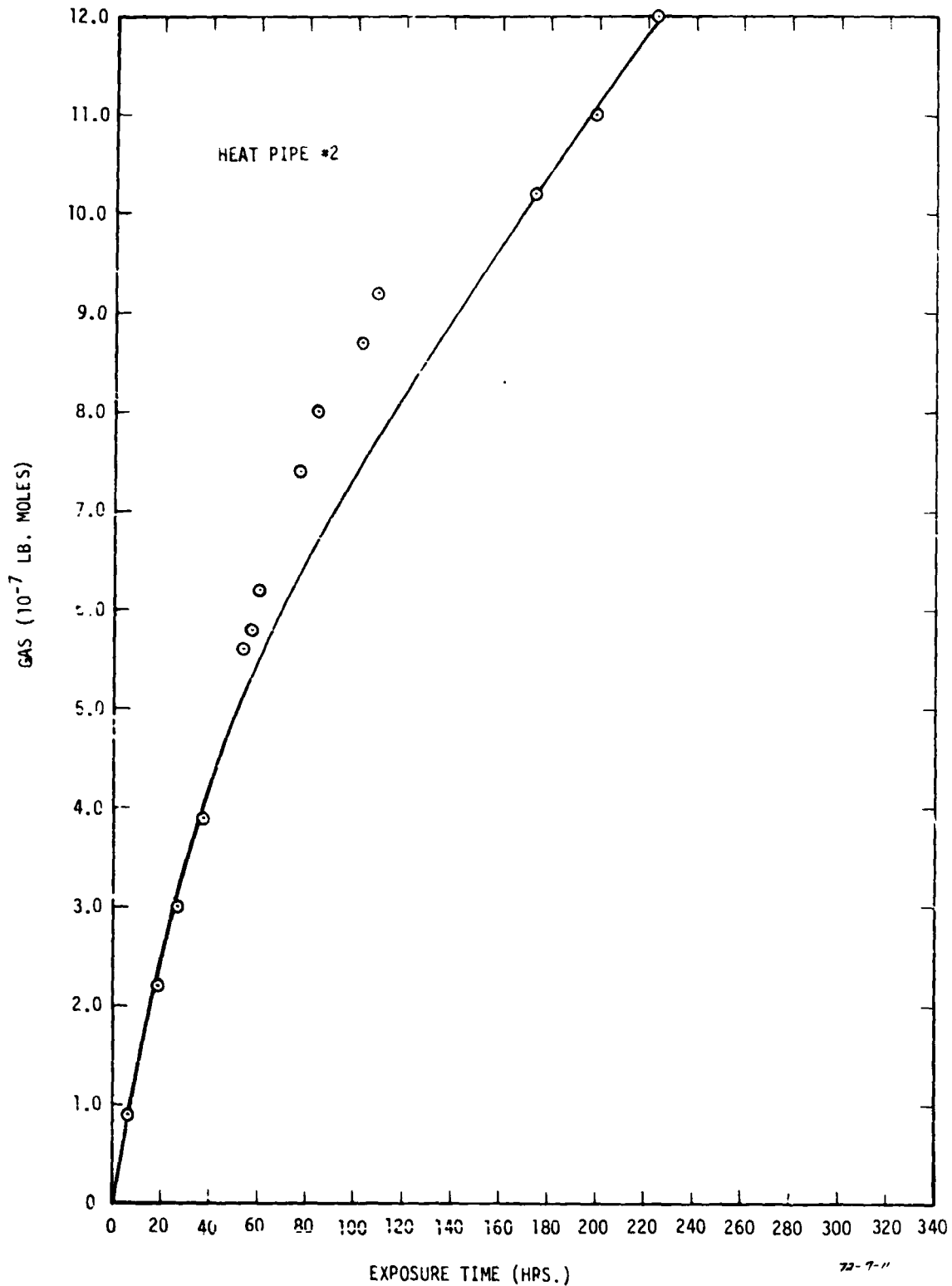   from an unrecorded temperature increase.

FIGURE 4-4. Gas evolution in nickel-water heat pipe #2 operated at accelerated condition between 250°F and 280°F. Data scatter is probably due primarily to variation in temperature.

removal of the heat tape and placed back in the chamber and operated as heat pipes for the purpose of recording the temperature profiles. After recording the temperature profiles, these heat pipes were removed from the chamber, wrapped with heat tape again, and placed in the chamber for further high temperature exposure.

Accelerated testing under isothermal conditions was carried out for a number of reasons. When operated as a heat pipe (with fluid flow) the gas generated in a pipe builds up as a function of time and the consequent change in the temperature profile at the condenser means that the vapor temperature in the adiabatic section can be held constant only if the power is continuously decreased or more condenser length is continuously uncovered. The first method requires a temperature controller for each heat pipe for good accuracy and allows the flow rate to decrease, while the second would require a great amount of time in maintenance if the insulation were moved by hand. It was desired to study the temperature dependence with these heat pipes, independent of the flow rate. Thus, it was decided to test under isothermal conditions (with zero flow rate) and it was found possible to hold the temperatures almost precisely constant over an extended (1290 hours) period using only the temperature controller on the chamber.

Contrary to expectations, a strong temperature dependence did not appear with the five heat pipes held at accelerated temperatures of 135°F, 150°F, 165°F, 180°F, and 195°F under isothermal (zero flow rate) conditions, as shown in Figure 4-5. With these heat pipes the general behavior appears to be initial (possibly parabolic) passivation, but at much reduced rates compared to heat pipes operated with non-zero flow. The 150°F data of Figure 4-3 (heat pipe mode) is reproduced in Figure 4-5 for comparison. It thus appears that the flow rate is an important variable in gas generation in nickel-water heat pipes.

The gas generation in the three reference conditions heat pipes is shown as a function of time in Figure 4-6. As discussed above, the amount of gas was calculated from the temperature profile with a computer program based on ideal gas behavior. The scatter in the data may result from the fact that the results of the computer program are quite
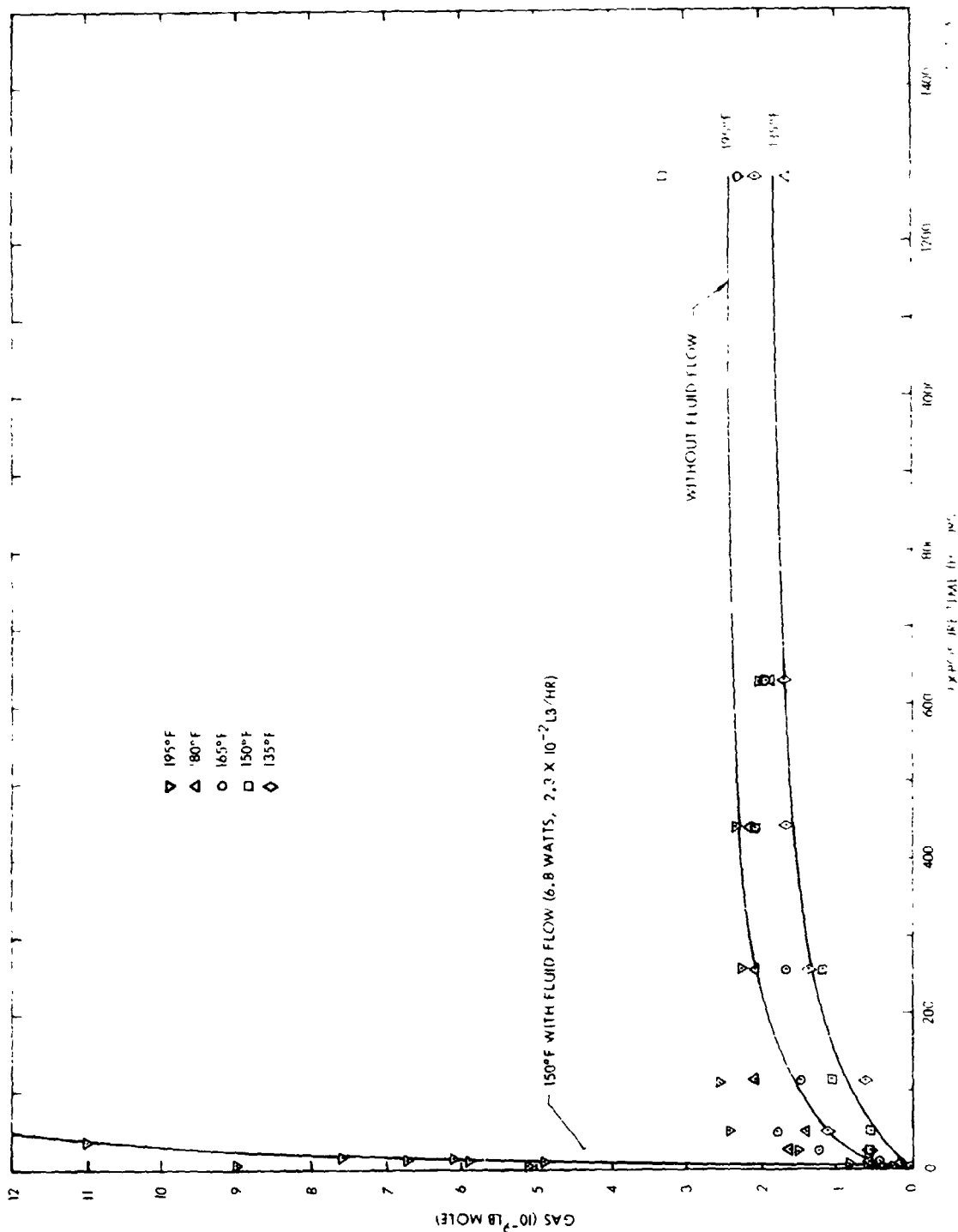
FIGURE 4-5. Gas evolution in nickel-water heat pipes operated at accelerated, isothermal conditions between 135°F and 195°F compared with that of heat pipe #3 operated in heat pipe mode at 150°F.
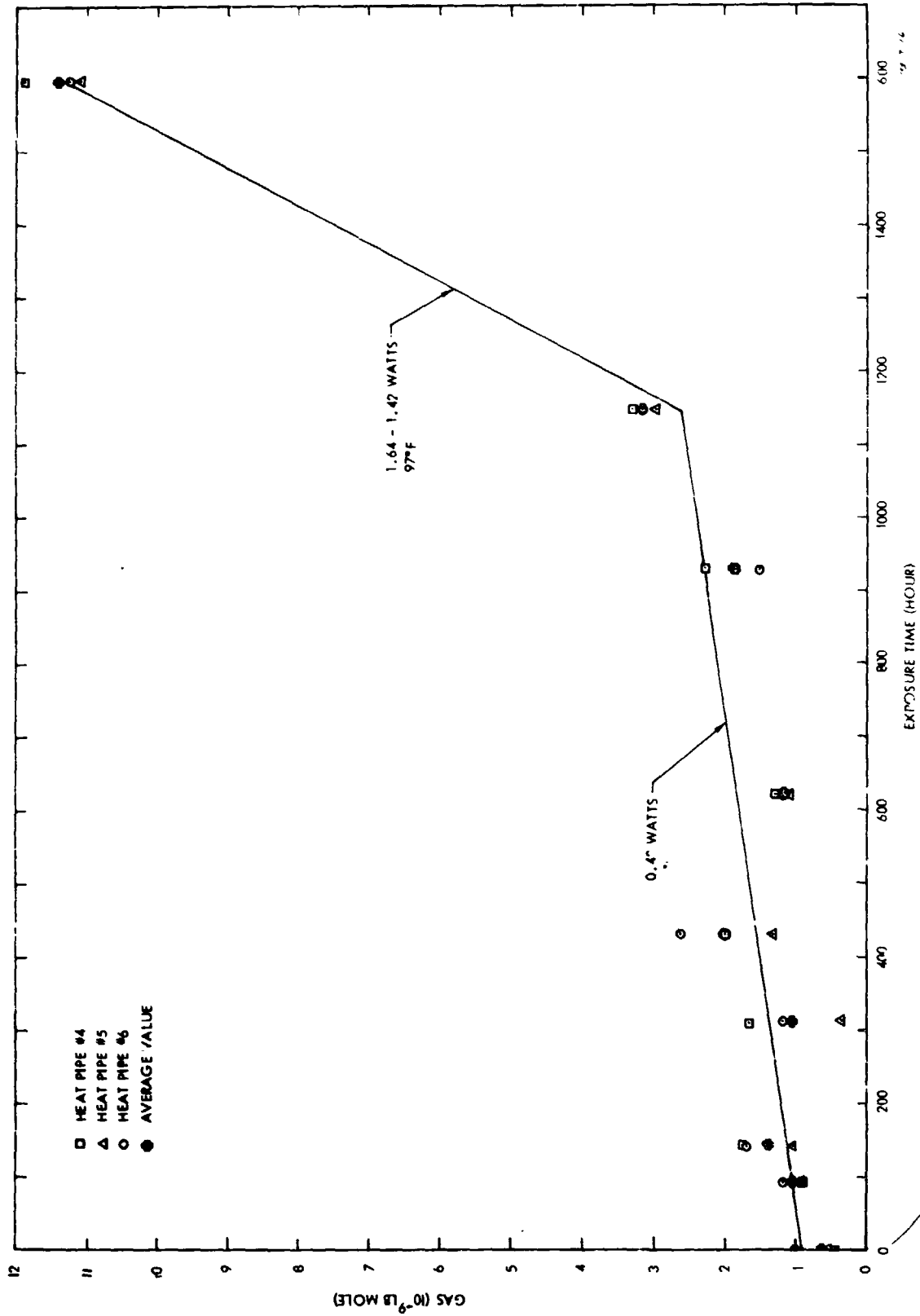
FIGURE 4-6. Gas evolution in reference condition nickel-water heat pipes operated at 85°F for 1150 hours and 97°F beyond 1150 hours.

sensitive to small variations in the thermocouple readings, particularly for small amounts of gas (10×10^{-10} lb.-mole range). These heat pipes were operated at $85.0 \pm 0.5°F$ for 1150 hours, except for two brief periods (of approximately 2 hours) at 97°F. Within the scatter of the data, only a linear time dependence can be assumed. Sufficient accuracy was not obtained to determine an initial period of parabolic passivation. After 1150 hours at 85°F, the temperature was increased to 97°F in order to improve the accuracy of the gas measurements. A rapid increase in gas was noted beyond this point up to the total 1600 hours exposure indicating a change in the corrosion behavior.

Having determined that the flow rate is an important variable in gas generation in nickel-water heat pipes, in that the gas evolution rate is very low with zero flow rate, but high at the same temperature when the heat pipes are operated normally with fluid flow, it was decided to carry out acce⌐rated testing with controlled, non-zero fluid flow. In order to examine the flow rate dependence together with the temperature dependence, eight heat pipes were operated at accelerated conditions up to 188 hours. The heat pipes employed in this phase of the program were the five tested previously with zero flow and the three reference conditions heat pipes (from which sufficient reference conditions data had been collected). All these heat pipes contained only a small amount of gas as a result of previous testing. New heat pipes were not employed in this phase of the program, primarily because the available funding was not sufficient to cover the instrumentation and processing costs. It was initially intended to operate one set of four heat pipes at the same flow rate and different temperatures and a second set of four at the same temperature and different flow rates. These conditions could not be met exactly in practice. After establishing the accelerated testing conditions for each heat pipe, the power was reduced as gas was generated as a function of time in order to hold the temperature constant throughout the testing period. This was done because it was felt that the temperature dependence would be stronger than the flow rate dependence, as was found to be the case. The heat pipes were operated under the following accelerated conditions, where the power levels in paren-

57

thesis are the initial and final values, respectively: 177°F (9.0 - 8.1 watts), 163°F (6.3 - 5.2 watts), 153°F (6.0 - 4.9 watts), 152°F (6.7 - 6.1 watts), 152°F (5.7 - 5.0 watts), 152°F (6.4 - 5.8 watts), 152°F (5.4 - 4.4 watts), and 151°F (6.0 - 5.6 watts). The results of these measurements are shown in Figures 4-7, 4-8, and 4-9. In all cases the time dependence appears to be linear within the accuracy of the data obtained. Beyond 100 hours of exposure the data may begin to be of reduced accuracy because the area exposed to the indicated temperature becomes reduced as gas builds up in the condenser. The resulting re-duction in gas generation as the temperature falls along the condenser could be taken into account by an iterative method but the accuracy of the data does not appear to warrant such a treatment. For this reason, the curves were drawn with emphasis on the interval below 100 hours of exposure. Displacements in a number of the curves apparently resulted from unrecorded increases or decreases in the temperature.

4.2   Phenomenological Corrosion Model and Analysis:

4.2.1   Phenomenological Model

A phenomenological model of heat pipe degradation in the nickel-water system was developed which incorporates corrosion and oxidation theory and contains parameters which may be determined by experiment. This model is based on the concept of extrapolation from accelerated conditions to predict behavior at reference (normal) conditions. It is thus explicitly assumed that the chemical and physical mechanisms responsible for heat pipe degradation at accelerated conditions are the same in nature at the reference conditions. In this preliminary formulation only non-condensible gas generation has been considered. Effects of wick degradation, which were expected to be of less importance in this system, were not treated because the accelerated testing phase did not leave sufficient funding for this additional activity.

It is known that a clean nickel surface corrodes uniformly at a linear rate (0.001 mpy) after long duration exposure to distilled water at room temperature [14]. The initial behavior of nickel in water
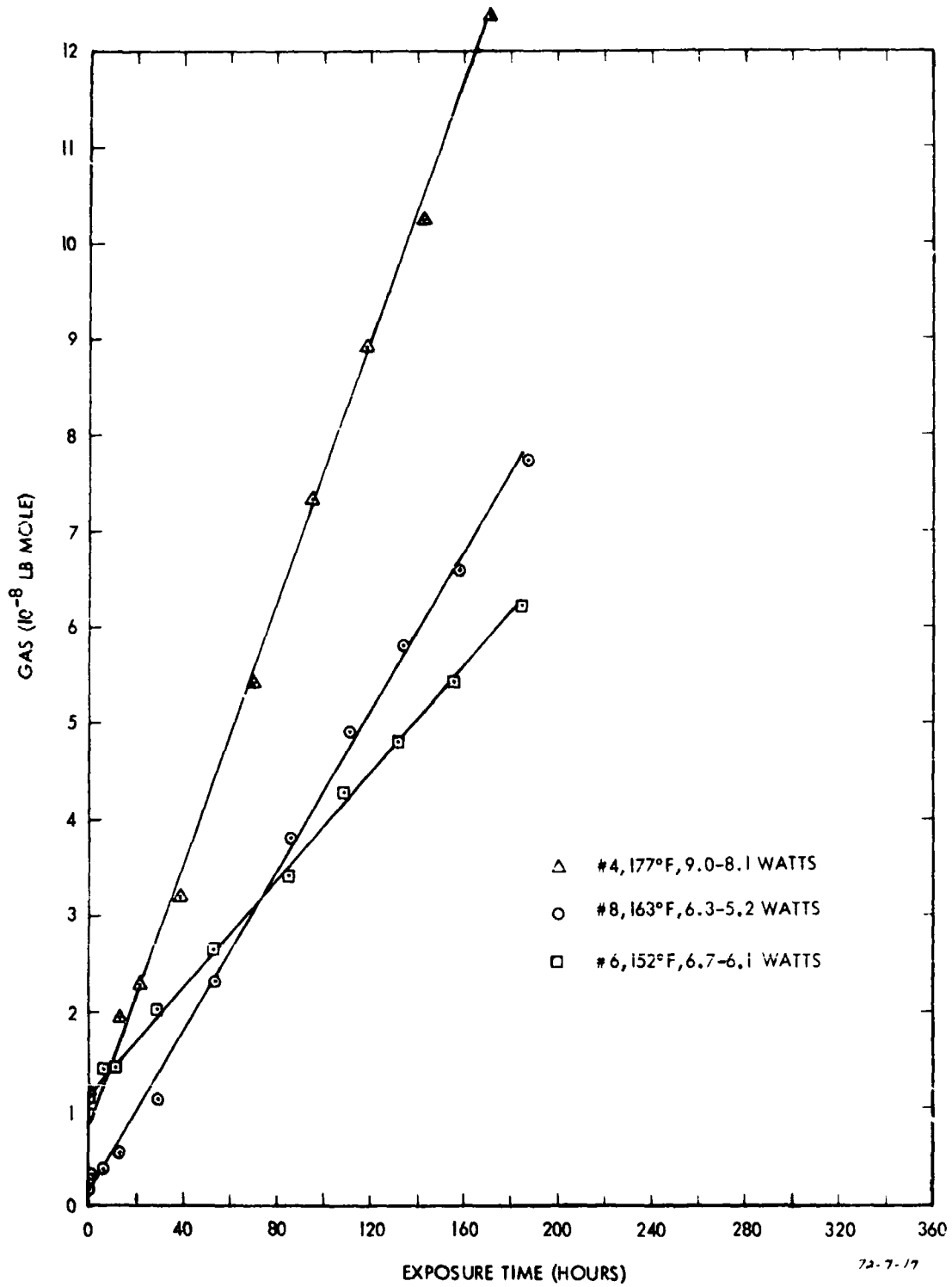
FIGURE 4-7. Gas evolution in accelerated condition: nickel-water heat pipes.
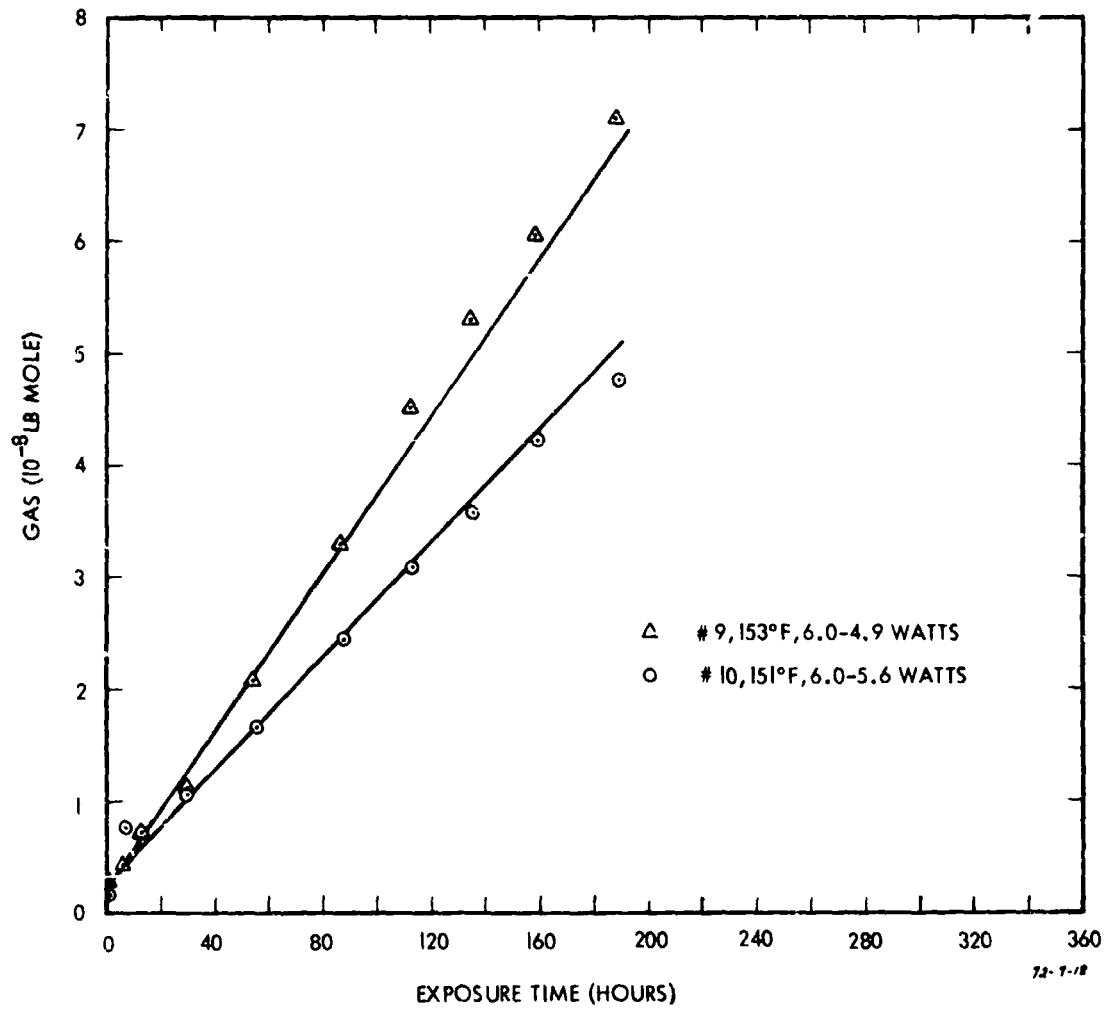
FIGURE 4-8. Gas evolution in accelerated condition:
nickel-water heat pipes.
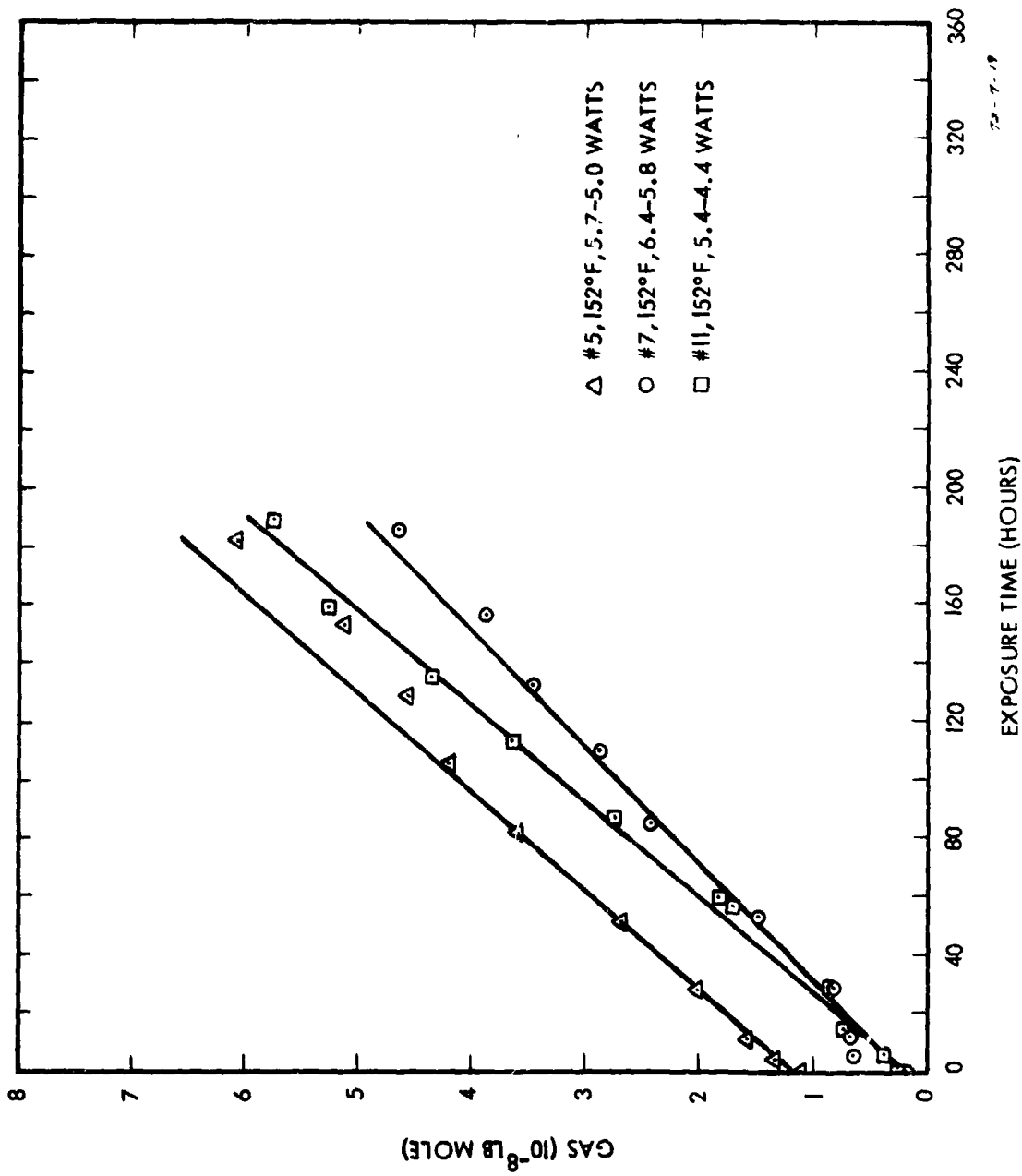
FIGURE 4-9. Gas evolution in accelerated condition: nickel-water heat pipes.

has to our knowledge not been studied in detail. Assuming clean, un-passivated nickel surfaces in the heat pipes, corrosion will occur at all nickel surfaces under the influence of mobile, local corrosion cells. At each cell nickel oxide and/or nickel hydroxide will be generated at the anode [15], and hydrogen gas at the cathode [16], according to the reactions:

$$Ni + H_2O \longrightarrow NiO + H_2 \tag{4-3}$$

$$Ni + 2 H_2O \longrightarrow Ni(OH)_2 + H_2 \tag{4-4}$$
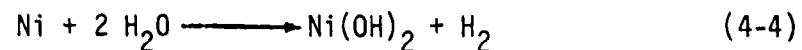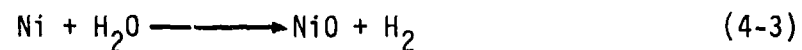
For each molecule of nickel oxidation product one molecule of hydrogen gas is evolved. Since the long duration corrosion rate of nickel is very small at room temperature, a protective film of the oxidation corrosion products must be formed during the initial exposure. It appears likely that the film will grow by migration of Ni^{++} ions toward the film-water interface and by O^{--} ions toward the nickel-film inter-face under the influence of the electrical potential established across the film in the electrochemical cell. Assuming a constant potential, oxidation theory predicts passivating film growth will occur at a parabolic rate [17]. Hydrogen evolution will thus have the same time dependence, giving:

$$n(t,T) = F(T)\, t^{1/2} \tag{4-5}$$

where n is the number of lb.-moles of hydrogen, t is the time, and F(T) is some function of the temperature T. This relationship has been found to describe hydrogen evolution from steel in boiling water [18], but is not common to the (long duration) corrosion of metals generally. Over long periods of time, uniform corrosion with a linear time dependence occurs more commonly. Thus, after the initial passivation the hydrogen evolution may be expected to obey:

$$n(t,T) = F(T)\, t \tag{4-6}$$

The function F (T) may be determined empirically if necessary by measuring the hydrogen evolution at a series of temperatures and plotting n vs. t^a for each temperature, where a = 1/2 for initial passivation and a = 1 for long-term uniform corrosion. The slope $\frac{\delta n}{\delta y}$ = F (T), y = t^a of each temperature curve generates the function F (T). However, from the mechanisms of film growth assumed in the model, migrating ions will experience an activation energy Q in moving from one interstitial site to the next [17]. In this case the temperature dependence will be-have as $e^{-Q/kT}$, where k is Boltzmann's constant, giving:

$$F (T) = Be^{-Q/kT} \qquad (4-7)$$

where B is a proportionality constant. This is the relationship found with the oxidation of many metals, which is essentially the model assumed here. From a plot of lnF vs. 1/T, B and Q may be determined. Having determined these parameters by measuring the gas evolution at accelerated conditions the gas evolution at any time may be calculated for heat pipes operated at reference conditions from:

$$n (t,T) = Bt^a e^{-Q/kT} \qquad (4-8)$$

$$a = 1/2 \text{ (initial passivation)}$$

$$a = 1 \text{ (long-term, uniform corrosion)}$$

This model is incomplete in certain respects and might be developed further in a more extensive study. It ignores a number of mechanisms and effects which might be included in a more complete model. Four of the more important effects may be:

1. The corrosion rate of many metals is increased when fluid flows over the surface as opposed to a stagnant situation, in which case the heat transport rate must be taken into account. It is shown below that the flow rate dependence is in the form of a threshold.

2. As gas is generated and collects at the condenser
   end of a heat pipe, the temperature of the affected
   'ength will drop, reducing the area of high tem-
   perature gas generation. This effect was partly
   accounted for by more heavily weighing the early
   data as discussed in Section 4.1.3.

3. Hydrogen gas in solution has been reported to
   reduce the corrosion rate of nickel in water [19].
   In this case, the initial gas evolution rate would
   be less than parabolic.

4. No efforts were made to establish the parameters
   controlling the proportionality constant - B.
   Petrick [13] suggests that the surface area of
   the heat pipe components (wall and wick) wetted
   by the liquid represents one such parameter.

4.2.2 Analysis and Prediction of Reference Condition Gas Evolution Rate

Except for the case of the initial exposure of the isothermal
(zero flow) heat pipes, the data obeys a linear time dependence
corresponding to uniform corrosion, as shown in Figures 4-6 ∽ 4-9.
The data during initial exposure in the 10×10^{-10} lb.-mole range was
not of sufficient accuracy to allow identification of initial passi-
vation. Plotting $\log \frac{\partial n}{\partial t}$ vs. 1/T results in the curve shown in Figure
4-10, indicating that corrosion in these nickel-water heat pipes is
described by Eq. (4-8) with a = 1, within the accuracy of the data.
Calculating the parameters Q and B from the slope and intercept, re-
spectively, results in:

$$Q = 10.29 \times 10^{-20} \text{ joules,}$$

$$B = 0.9699 \text{ lb.-mole/hr.}$$
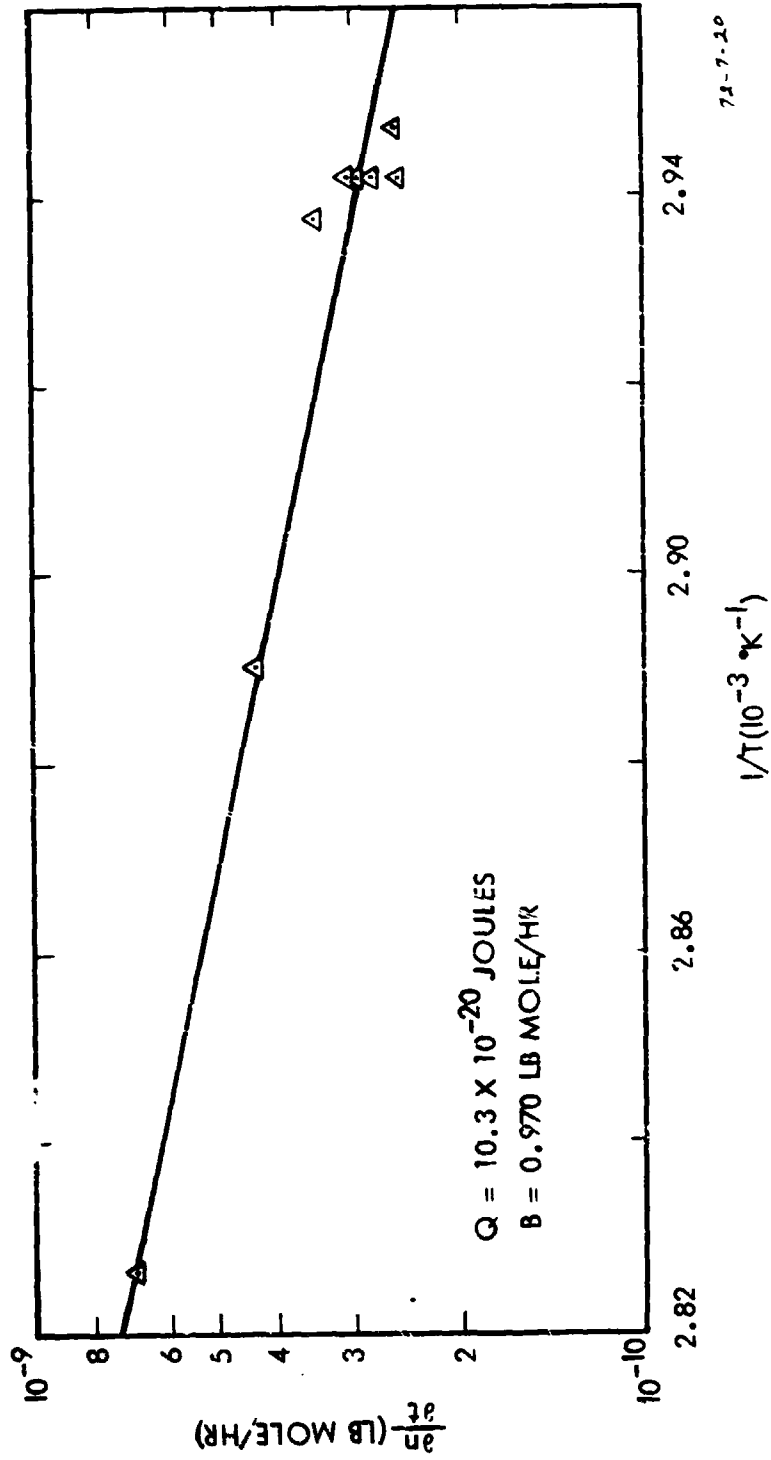
FIGURE 4-10. Temperature dependence of gas evolution in nickel-water heat pipes.

Table 4-1 compares the actual and predicted gas evolution in the reference condition heat pipes. As discussed above, the flow rate appears to be an important variable in gas generation in these nickel-water heat pipes. However, flow rate is usually most important in cases of crevice corrosion, which is not important with the nickel-water system. In other cases, only a moderate flow is required for general uniform corrosion to remove insulating gas bubbles or depleted solution from the surface. That is, there may be a threshold in the flow rate, above which normal, general corrosion with hydrogen evolution occurs. This appears to be the case in the corrosion of the nickel-water heat pipes tested in this program. As seen in Figure 4-6, a change in the gas generation rate appears to occur on changing the reference operating conditions from 85°F at 1.37×10^{-3} lb/hr flow rate to 97°F at 4.67×10^{-3} lb/hr flow rate. This change in behavior appears to result from the increase in flow rate and not from an increase in temperature. Comparison with the curves in Figure 4-5 shows that gas generation in the high temperature, zero flow rate, heat pipes was low and similar to the behavior found at 85°F with 1.37×10^{-3} lb/hr flow rate. Furthermore, at flow rates above 4.7×10^{-3} lb/hr the dependence on flow rate does not appear in the data, as may be seen by a comparison of the gas generation curves in Figure (4-9) taken at the same temperature but at different circulation rates. It thus appears that the flow rate dependence f is in the form of a threshold f_t, below which gas evolution is very low and above which normal, uniform corrosion takes place. Eq. (4-8) for uniform gas generation may thus be written:

$$n(t,T) = Bte^{-Q/kT}, \qquad (4-9)$$

$$f > f_t$$

$$1.4 \times 10^{-3} < f_t < 4.7 \times 10^{-3} \text{ lb/hr}$$

$$B = 0.9699 \text{ lb.-mole/hr}$$

$$Q = 10.29 \times 10^{-20} \text{ joules,}$$

with T in °K.

TABLE 4-1

ACTUAL AND PREDICTED GAS EVOLUTION
IN REFERENCE CONDITION NICKEL-WATER HEAT PIPES

VAPOR TEMPERATURE (°F)	POWER INPUT (WATTS)	FLUID FLOW RATE (10^{-3} LB/HR)	TOTAL EXPOSURE TIME (HR)	QUANTITY OF NONCON-DENSIBLE GAS EVOLVED (LB.-MOLE)	
				ACTUAL	PREDICTED
85	0.42	1.37	1149	17.5×10^{-10}	226.3×10^{-10}
97	1.64-1.42*	5.39-4.67*	447	88.0×10^{-10}	96.3×10^{-10}

* Initial and final values, power was continuously decreased
during exposure to maintain the vapor temperature at 97.0°F.

Further experimentation would be required to determine the precise value of f_t, the sharpness of the threshold, and behavior of the gas evolution below threshold.

As shown in Table 4-1, the proposed phenomenological model severely over-predicts the gas evolution for the reference condition below threshold but predicts the reference condition gas evolution above threshold reasonably well, over-predicting by 9.4%.

As an example of accelerated life testing and the scaling law represented by Eq. (4-9), let it be assumed that heat pipes are required for a particular application to be operated at 85°F, but at a power input resulting in a flow rate greater than threshold. If the useful lifetime is considered to be limited by gas evolution amount to 200×10^{-10} lb.-moles, solving Eq. (4-9) for t results in a predicted lifetime of $t_{life} = 1015$ hours $\pm$ 9%.

4.3   Comparison With Literature:

Although there exists an abundance of literature on the general question of corrosion, there has been very little published on gas

generation in heat pipes. In fact, the only quantitative study of this phenomenon which we have found is the work of Petrick [13] on the stainless steel - water system. Aside from this work there has been a "rule-of-thumb" discussed among heat pipe researchers that the gas generation rate doubles for every 10°C increase in temperature, although we have not been able to locate any publication to this effect. It is of interest, however, to compare the results of this program to those of Petrick and to the "rule-of-thumb."

If we assume that we are considering heat pipes operating above the threshold flow rate, an expression for the temperature difference necessary to double the gas generation rate is easily derived from Eq. (4-9). Let the gas generation rate at temperature T_2 be twice that at T_1. Then,

$$\left. \frac{\partial n}{\partial t} \right|_{T_2} = B e^{-Q/kT_2} = 2 \cdot \left. \frac{\partial n}{\partial t} \right|_{T_1} = 2 \, B e^{-Q/kT_1} \qquad (4\text{-}10)$$

If we set $T_2 = T_1 + \Delta T_d$, where ΔT_d is the temperature difference required to double the generation rate, Eq. (4-10) can readily be written

$$\frac{\left. \dfrac{\partial n}{\partial t} \right|_{T_1 + \Delta T_d}}{\left. \dfrac{\partial n}{\partial t} \right|_{T_1}} = 2 = \exp\left[\frac{Q}{k}\left(\frac{\Delta T_d}{T_1(T_1 + \Delta T_d)} \right) \right]. \qquad (4\text{-}11)$$

Taking logarithms and solving for ΔT_d yields

$$\Delta T_d = \frac{T_1^2 \ln 2}{\dfrac{Q}{k} - T_1 \ln 2}. \qquad (4\text{-}12)$$

The important thing to note in this result is that the rate doubling temperature differential is not a constant, as suggested by the "rule-of-thumb," but depends on the operating absolute temperature level. The higher the operating temperature level, the greater the temperature

difference required to double the gas generation rate.

What is constant is the activation energy - Q, and a better "rule-of-thumb" would be to establish an average value of Q to be used with Eq. (4-9). However, if a rate doubling temperature differential is preferred, it must at least be referenced to a standard temperature - say 20°C (293.16°K). If we let ΔT_d^* be the value of ΔT_d at standard conditions, Eq. (4-12) reduces to

$$\Delta T_d^* = \frac{5.957 \times 10^4}{\frac{Q}{k} - 203.2} \tag{4-13}$$

where k = 1.38 x 10^{-23} joules/°K (Boltzmann Constant), and Q is expressed in joules.

If we now substitute the activation energy for nickel-water systems found in this study (Q = 10.29 x 10^{-20} joules) into Eq. (4-13), we find that $\Delta T_d^* = 8.2$°K. This is not far removed from the 10°C "rule-of-thumb."

To compare TRW's results with those of Petrick [13], it must first be emphasized that two different material systems and different processing techniques were used. Petrick worked with water/304 stainless steel heat pipes, while this study used water/Nickel 200 pipes. Further, he used a completely different method of calculating gas inventories in which he froze the heat pipe and extracted the gas, using a mass spectrometer to determine the composition and quantity of gas present.

In analyzing his test data for fifteen heat pipes run at three temperature levels (100, 200 and 300°F), Petrick observed that gas accumulated linearly with time up to 92 days. This is similar to the time dependence found in this study, as given by Eq (4-9).

In attempting to formulate a temperature dependence, however, Petrick simply used an empirical best fit of his data yielding

$$\frac{\partial n}{\partial t} = CT^{3.62} \tag{4-14}$$

69

where C is an empirical constant and T is in degrees Centigrade.

Eq. (4-14) would appear to be of limited use in that it is simply a curve fit and does not represent any physical or chemical mechanisms. However, Petrick's data are themselves valid and can serve as an independent test of the analysis presented herein, leading to Eq. (4-7). His published data for the hydrogen generation rate as a function of temperature are shown in Table 4-2.

TABLE 4-2

PETRICK'S GAS GENERATION DATA [13]

H_2 GENERATION RATE ($\mu g/cm^2$ - day)	T (°K)	1/T (1/°K)
9.63×10^{-5}	310.94	.003216
1.69×10^{-3}	366.49	.002729
1.54×10^{-2}	422.05	.002369

To test the model inherent in Eq. (4-7), we can plot the gas generation rate vs. the inverse absolute temperature (1/T) on semi-log paper, as was done for TRW's data on Figure 4-10. This is done for Petrick's data on Figure 4-11. As is apparent, the data falls on a straight line indicating that Eq. (4-7) properly describes the functional dependence on temperature for Petrick's results as well as TRW's.

Furthermore, extracting a value for the activation energy - Q from the slope of the line, one obtains: $Q = 8.25 \times 10^{-20}$ joules. This compares with TRW's value of 10.29×10^{-20} joules for the nickel-water system.

It is also of interest to calculate the rate doubling temperature differential for Petrick's system. From Eq. (4-13) with $Q = 8.25 \times 10^{-20}$
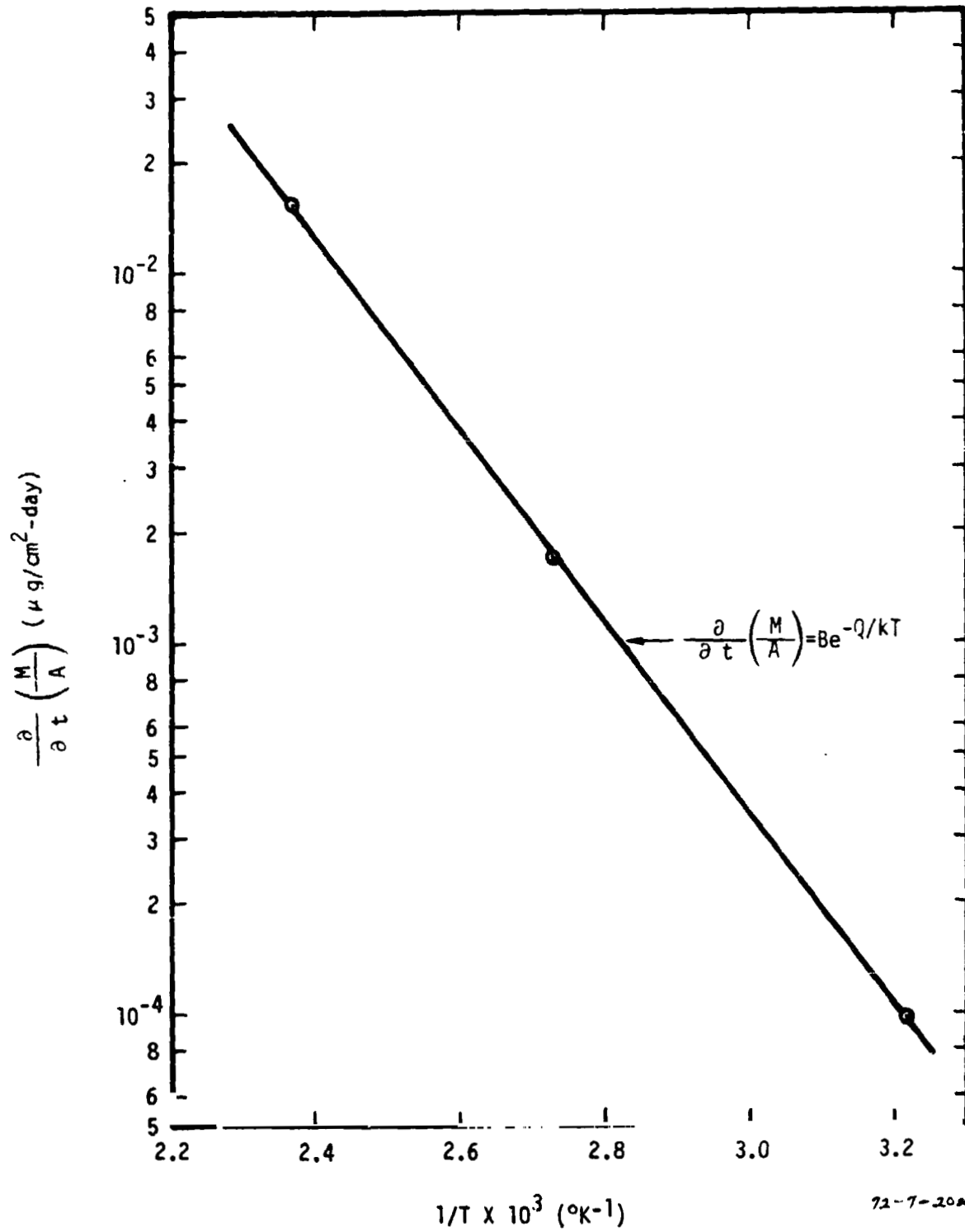
FIGURE 4-11. Temperature dependence of gas generation rate for stainless steel/water heat pipes (data from [13]).

joules, we calculate: $\Delta T_d^* = 10.3°K$. In this case the 10°C "rule-of-thumb" is remarkably close to correct.

4.4 Conclusions and Recommendations:

From a study of hydrogen evolution in nickel-water heat pipes under accelerated and reference conditions it has been found possible to accurately predict, calculating with Eq. (4-9), the lifetime of a heat pipe operating at reference conditions from data taken at accelerated conditions, provided the fluid flow rate is greater than a threshold value. For flow rates less than threshold the hydrogen evolution rate is much reduced, but a precise lifetime cannot be calculated within the scaling law. However, this is not of great importance as the advantage of heat pipes lie in the area of large heat transport, which is the case covered by the accelerated testing model. Further investigations of accelerated testing of nickel-water heat pipes should include an accurate determination of the threshold flow rate, the sharpness of the threshold, and the behavior of hydrogen evolution below threshold. Evidently, effects of wick degradation are completely dominated by the large hydrogen evolution in this particular heat pipe system.

Of considerable significance is that fact that the data published by Petrick for stainless steel-water systems shows a similar functional dependence on time and temperature as that taken at TRW for nickel-water systems. Furthermore, the activation energies for the two cases are nearly the same (8.25×10^{-20} vs. 10.29×10^{-20} joules). This suggests that the results may be fairly general for similar systems and are not too sensitive to small variations in the purity of the water or surface condition of the wicks and walls, since substantially different processing techniques were used.

Also of interest is the fact that the 10°C "rule-of-thumb" for the temperature differential necessary to double the gas generation rate was quite close to correct for both studies if referenced to standard conditions (20°C).

72

The results of this study have been most encouraging and suggest that the generation of scaling laws for accelerated testing of life limiting processes is indeed feasible. It is believed that the success of this feasibility study now provides the motivation for an expanded effort in this area.

5.0   DEVELOPMENT OF A VAPOR FLOW MODULATION VARIABLE
       CONDUCTANCE HEAT PIPE

In an earlier publication [3] it was shown that the control
capability of passive, gas-controlled, variable-conductance heat pipes
is sensitive to variations in the environmental conditions. This is
because the sink temperature influences both the gas temperature
and the partial pressure of vapor within the gas blocked region of
the pipes. Thus, variations in sink temperature cause variations in
the gas blocked condenser length and, hence, in the evaporator temperature.
This is particularly troublesome in cases where the sink temperature
varies significantly and approaches the operating temperature. Conditions
such as these characterized as the AHPE flight experiment on tne OAO-C
spacecraft, requiring the use of a sophisticated hot non-wicked reservoir
design in order to achieve the required 10°F control range [8, 10].

Because of this limitation, TRW has been studying alternate
control techniques which are relatively insensitive to sink temperature
variations. Two such systems have been examined; excess fluid control
and vapor flow modulation. Of the two, vapor flow modulation appeared
to be the preferred scheme for spacecraft thermal control applications.
Thus, this scheme was selected for the design, fabrication and test of
a laboratory prototype.

5.1   Excess Fluid Control:

This control technique is closely related to non-condensible
gas control. It utilizes the same fundamental control approach - that
of passively varying the condenser area to accommodate changing heat
rejection requirements. However, it differs from ordinary gas-control
concepts in two princip-l ways. Rather than rely on the compressibility
of a noncondensible gas mixed with working fluid vap i tc accommodate
changes in inactive condenser volume, this scheme uses an isolated
extensible container (bellows, bladder, etc.) containing a control
fluid. Also, excess working flu'1 is used to block the condenser
rather than a gas diffusion barrier. Such a system is shown
schematically in Figure 5-1.

74
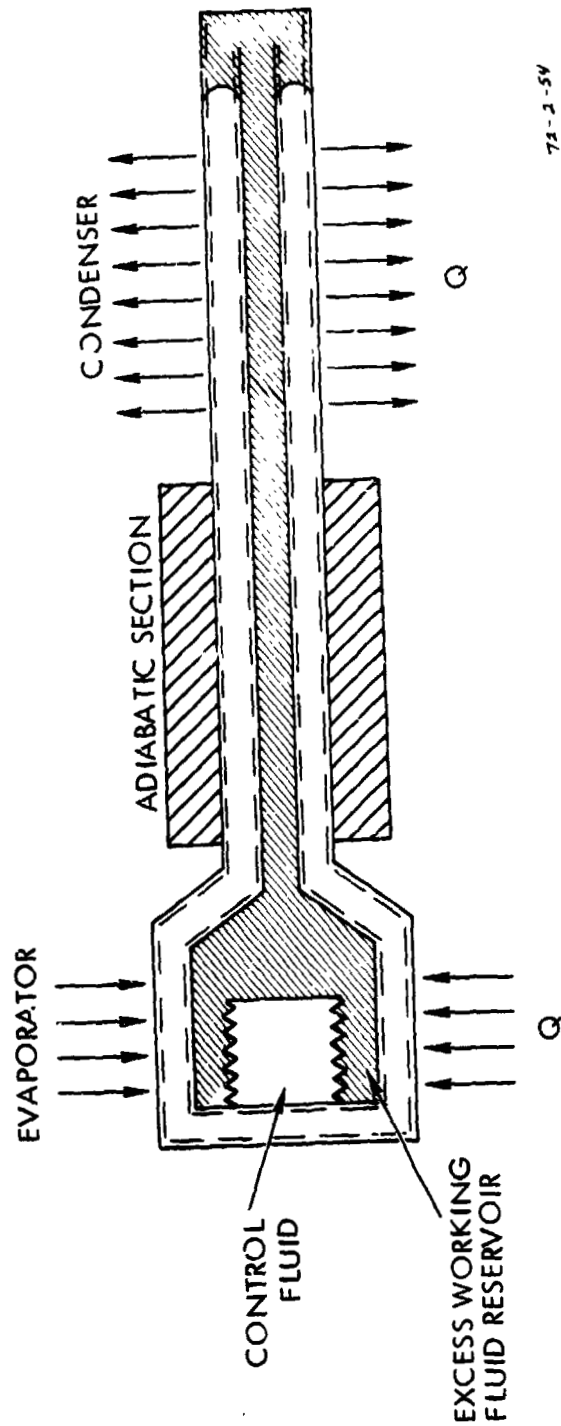
FIGURE 5-1. Schematic diagram of excess liquid controlled Variable Conductance Heat Pipe.

Clearly this scheme is comparitively insensitive to variations in sink tempearture. In the gas controlled heat pipe, the partial pressure of vapor mixed with the gas increases the "effective" gas volume in a temperature dependent way. Furthermore, the volume of the gas itself is a relatively strong function of temperature. In comparison, the volume of the excess liquid used to block the condenser in the excess fluid control scheme is a relatively weak function of temperature.

Another related advantage of this technique is that its transient behavior is not influenced by diffusion effects between gas and vapor, as is the case with hot reservoir gas controlled heat pipes, since there is no gas in the system.

On the other hand, this technique also suffers some obvious disadvantages. It introduces difficulties in 1-G testing in that gravity tends to cause the excess fluid to puddle in the condenser rather than reside as shown in Figure 5-1. To permit 1-G testing, it is therefore necessary to design the heat pipe with an internal capillary structure to retain the fluid against gravitational forces. This is a practical approach, as was demonstrated by the successful applications of liquid condenser blockage to effect a heat pipe diode [20].

The 1-G requirement also constrains the geometry and location of the excess fluid reservoir. However, placing the reservoir outside and **below** the evaporator, coupled to it through the saddle, provides a sat isfactory solution for both 0-G and 1-G operation, as shown in Figure 5-2.

Another disadvantage to this approach is that it is limited to applications where the effective sink temperature is above the freezing point of the working fluid. If the working fluid freezes in the "shut-off" end of the condenser, the reservoir is decoupled from the operating portion of the pipe by the solid plug, causing a loss of control.

5.2   Vapor Flow Modulation:

This approach to heat pipe control involves a different primary control principle than the gas or liquid condenser flooding

76
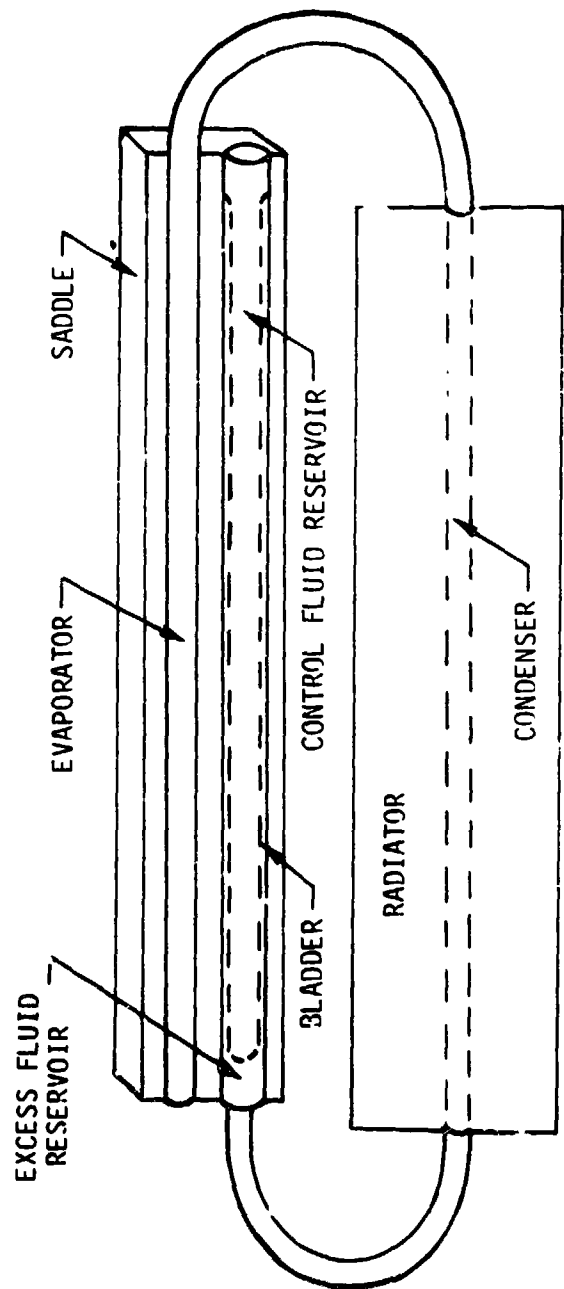
FIGURE 5-2. Schematic of Excess Fluid Control System Amenable to 1-g Testing.

techniques. That is tu throttle the vapor flow between the evaporator and condenser sections of the heat pipe, giving rise to a pressure difference between the two regions and, with it, a corresponding temperature difference. In this way, the overall temperature drop can be varied for any given heat flux; i.e., the heat pipe has a variable thermal conductance.

The principal limitation of this technique is that the pressure drop across the throttling valve comes "off the top" of the available capillary head. This pressure drop must not exceed the capillary head or vapor will "blow through" the wick. This establishes a maximum value (blow-through limit) for the evaporator-to-condenser temperature difference, dependent on the wick, working fluid and operating temperature. Furthermore, whatever the magnitude of the throttling pressure drop, it reduces the hydrodynamic capacity of the heat pipe. An analytical model for vapor flow modulation heat pipes including blow through limits and operating characteristics was previously reported in Ref [3].

To implement this control mechanism effectively, a promising approach is to passively actuate the throttling valve with a control fluid within an extensible container, as with the excess fluid control technique. This is shown schematically in Figure 5-3.

As with excess fluid control, this technique is relatively insensitive to the magnitude and variability of the sink conditions. In fact, as opposed to gas control concepts, performance improves as the effective sink temperature approaches the evaporator temperature in that smaller evaporator-to-condenser pressure differentials are involved and more of the capillary head is available to circulate the fluid.

EVAPORATOR   CONDENSER

THROTTLING VALVE

CONTROL
FLUID   Q

FIGURE 5-3. VAPOR MODULATED HEAT PIPE
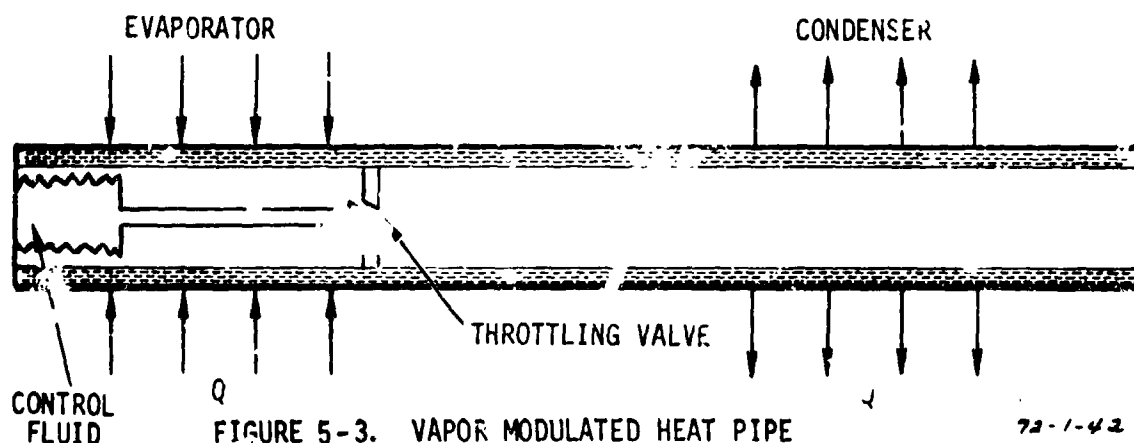
In comparison with excess fluid control, the vapor flow modulation technique does not suffer similar geometric design constraints to permit 1-G testing. Also, since the entire condenser is active at all times, it is not subject to failure if the sink temperature falls below the freezing point of the working fluid, as long as the condenser itself does not fall below this temperature. On the other hand, this scheme requires a valve which inherently reduces reliability. Also, the limited capillary pressures available constrain the system to operate at rather low absolute pressures if significant evaporator-to-condenser temperature differentials are required.

5.3   Control Fluids and Extensible Containers:

As was seen in the previous two sections, control of the evaporator temperature of a heat pipe can be achieved through the use of a bellows, bladder or other extensible container located within or thermally coupled to it. Within the control fluid container may be a vacuum, a single phase liquid or gas, a two-phase single component or a two-phase mixture. As the temperature of the evaporator changes, the difference between the vapor pressure of the working fluid in the pipe and the pressure of the control fluid, if any, within the bellows causes the bellows to deflect. The movement of the bellows may be used for compensating control. This section presents some considerations leading to selection of a control fluid and container.

5.3.1   The Displacement of the Bellows:

Consider an impermeable bellows which contains fluid 1 and is surrounded by a heat pipe working fluid 2. Both are assumed to be in thermodynamic equilibrium at temperature T. One end of the bellows is attached to a stationary wall as shown in Figure 5-4.

The linear displacement x from the equilibrium position of the bellows is given by

$$F = Kx = A(P_1 - P_2) \tag{5-1}$$

where K is the spring constant, assuming elastic deformation of the bellows. The change in x with a change in temperature is
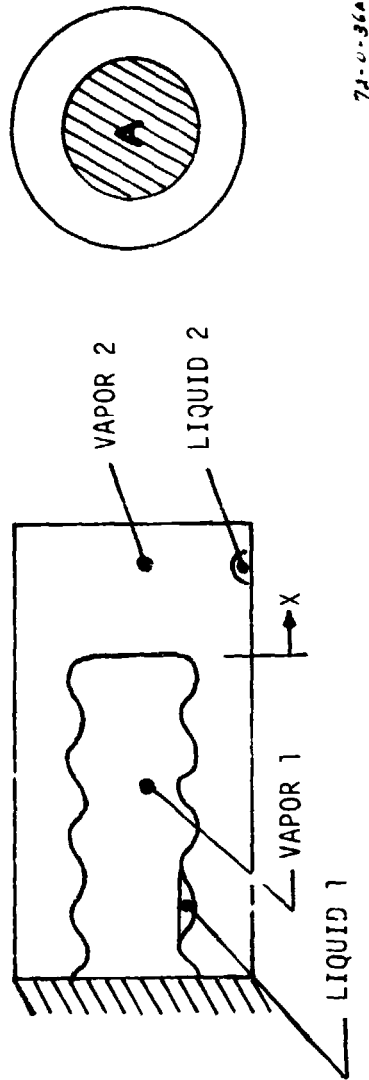
FIGURE 5-4. Model for Deflection of Bellows.

$$\frac{dx}{dT} = \frac{A}{K}\left(\frac{dP_1}{dT} - \frac{dP_2}{dT}\right) \tag{5-2}$$

The following descriptive terms are used to distinguish the algebraic sign of dx/dT:

PUSHER $dx/dT > 0$ $dP_1/dT > dP_2/dT$

PULLER $dx/dT < 0$ $dP_1/dT < dP_2/dT$

For maximum control sensitivity, it is clear that the bellows (or bladder) deflection should be a strong function of temperature; i.e., $dx/dT \gg\limits_{<<} 0$. From Eq. (5-2), we see that this suggests a small spring constant - K. However, it is also obvious that a soft, weak bellows or bladder cannot sustain an appreciable load or pressure difference, as might exist when the heat pipe experiences temperatures far removed from the design point. Thus, a trade-off exists between control sensitivity and off-design system integrity in establishing the bellows stiffness.

5.3.2 Control Fluid Selection:

Eq. (5-2) indicates that a good control fluid is one with a value of dP/dT far removed from that of the working fluid. However, it is also clear that, in order to gain the benefits of using an extensible container with a small spring constant, the pressure inside and outside of the container should be nearly equal; i.e., $P_1 \doteq P_2$.

5.3.2.1 Two-Phase Control Fluids:

The use of a two-phase control fluid is attractive in that its pressure is a function of temperature alone, independent of the container volume. The working fluid 2 is in two-phase equilibrium. Therefore, its pressure is given approximately by the Clausius Clapeyron relation

$$P_2 \doteq P_0 \, e^{-(T_{z2}/T_{b2})(T_{b2}/T-1)} \tag{5-3}$$

where T_b is the boiling point at pressure $P_0 = 1$ atmos and T_z is $\lambda M/R_u$, where R_u is the universal gas constant and M the molecular weight.

The dP_2/dT term is then

$$\frac{dP_2}{dT} = \frac{P_2}{T}\left(\frac{T_{z2}}{T}\right) \tag{5-4}$$

The P, T relationship for the control fluid depends, of course, on its nature; i.e., whether the bellows is evacuated, filled with a gas, a liquid, or a two-phase fluid or mixture of fluids. In the case of a two-phase control fluid, P_1 obeys a relationship similar to Eq. (5-3).

$$P_1 \doteq P_0\, e^{-(T_{z1}/T_{b1})(T_{b1}/T-1)} \tag{5-5}$$

In this case (if $P_1 \doteq P_2$)

$$\frac{dP_1}{dT} - \frac{dP_2}{dT} \doteq \frac{P}{T^2}\,(T_{z1} - T_{z2}) \tag{5-6}$$

We see that T_{z1} should be much greater than T_{z2} for a good "pusher" fluid and much lower for a good "puller". In addition, we desire P_1 and P_2 to be nearly equal so:

$$\frac{T_{z1}}{T_{b1}}\left(\frac{T_{b1}}{T} - 1\right) = \frac{T_{z2}}{T_{b2}}\left(\frac{T_{b2}}{T} - 1\right) \tag{5-7}$$

If the working fluid and the operating temperature are fixed, T_{b1} is related to T_{z1} through Eq. (5-7).

$$T_{b1} = \frac{T_{b2}}{\dfrac{T_{b2}}{T} - \dfrac{T_{z2}}{T_{z1}}\left[\dfrac{T_{b2}}{T} - 1\right]} \tag{5-8}$$

For example, consider methanol operating at 292°K. For methanol $T_{b2} = 338.12$ and $T_{z2} = 4250°K$. Eq. (5-8) gives T_{b1} versus T_{z1} as shown in the third column of Table 5-1.

TABLE 5-1

Boiling Point of Control Fluid versus Vapor
Pressure Parameter T_z of Control Fluid

Operating Temperature 293°K

T_b, Boiling Point Desired for Working Fluid

T_z	Water	Ammonia	Methanol
°K	°K	°K	°K
2700	475.6	239.7	370.6
2900	457.9	241.4	363.8
3100	441.7	244.1	358.4
3300	428.5	246.6	353.6
3500	417.5	248.9	349.5
3700	408.3	251.0	346.0
3900	400.0	252.9	342.8
4100	393.3	254.5	340.0
4300	387.1	256.1	337.3
4500	381.6	257.5	335.0
4700	376.6	258.9	333.0
4900	372.5	260.3	331.4
5100	368.4	261.4	329.8
5300	364.8	262.5	328.2
5500	361.6	263.4	326.3

To see whether there are suitable candidates for pusher control fluids we search for one with T_{z1} much greater than T_{z2} and with a boiling point close to the value indicated. Similarly, for a good puller, we seek T_{z1} much less than T_{z2} with the same boiling point criterion. The values of T_b and T_z for a number of fluids are shown in Table 5-2.

Comparison of Table 5-1 with Table 5-2 shows that there appear to be no two-phase "pusher" fluids which are satisfactory for two of the three commonly used ambient temperature heat pipe working fluids, water, ammonia, and methanol. In the case of water only one fluid in the table, n-propyl alcohol, has a greater T_z, but it is only slightly greater. The desired boiling point for a value of $T_z = 4960°K$ is $372°K$, and the actual boiling point of n-propyl alcohol is $370.4°K$. In the case of ammonia, there is no trouble finding a fluid with a greater T_z. However, the boiling points of the fluids in Table 5-2 are all too high. In the case of methanol, only the other alcohols and water have greater values of T_z. But the values of T_b for these fluids are all too high. Thus, there is not a single candidate in the Table for use as a "pusher" fluid with ammonia or methanol.

A similar search for two-phase "puller" control fluids shows that there are no candidates in the table for use with ammonia (values of T_z are too high), a possible (although not very good) candidate for water (di-ethyl ketone) and several candidates (carbon tetrachloride and ethyl iodide) which appear satisfactory for use with methanol.

Another way of looking at the stated requirements and conclusions is to consider the pressure-temperature curves for the system. This is shown in Figure 5-5. Since both the control and working fluids are presumed to be two-phase fluids, the P, T curves are unique for each of them. In terms of Figure 5-5, the requirements for a good control fluid are 1) that the two-curves cross at a temperature T_a which is very close to the design point $(P_1 \doteq P_2)$, and 2) that the slopes of the curves be very different at this point $(\frac{dP_1}{dT} \gg \frac{dP_2}{dT})$. An inability to find a control fluid with T_{z1} much greater than (pusher) or much less than (puller) T_{z2} is equivalent to saying the slopes of the P, T curves are not sufficiently different at the desired control point.

TABLE 5-2

Vapor Pressure Parameters for Some Fluids

Fluid	Boiling Point T_b		Latent Heat λ	Molecular Weight M	Control Parameter T_z
	°C	°K	cal/g	g/g-mole	°K
Acetone	56.5	329.7	124.5	58.1	3640
Ammonia	-33.5	239.7	327.4	17.03	2790
Benzene	80.1	353.3	94.3	78.1	3710
Tert-butyl alcohol	82.5	355.7	130.5	74.1	4860
Carbon tetrachloride	76.8	350.0	46.4	153.8	3600
Chloroform	61.3	334.5	59.0	119.4	3550
Diethylamine	55.5	328.7	91.0	73.1	3350
Diethyl ketone	102.7	375.9	90.8	36.1	3940
Ethyl alcohol	78.4	351.6	204.0	46.1	4740
Ethyl iodide	72.2	345.4	45.6	156.0	3580
Ethylene chloride	83.6	356.8	77.3	99.0	3850
Ethylidene chloride	57.3	330.5	67.1	99.0	3350
Methyl acetate	57.1	330.3	98.1	74.1	3660
Methyl alcohol	65.0	338.2	262.8	32.04	4250
Methyl propionate	79.9	353.1	79.0	88.1	3510
Isopropyl alcohol	82.3	355.6	159.0	60.1	4810
N-propyl alcohol	97.2	370.4	164.0	60.1	4960
Sulfur dioxide	-10.0	263.2	92.7	64.1	2990
Trichloroethylene	87.0	360.2	57.3	131.4	3790
Water	100.0	373.2	539.6	18.01	4860
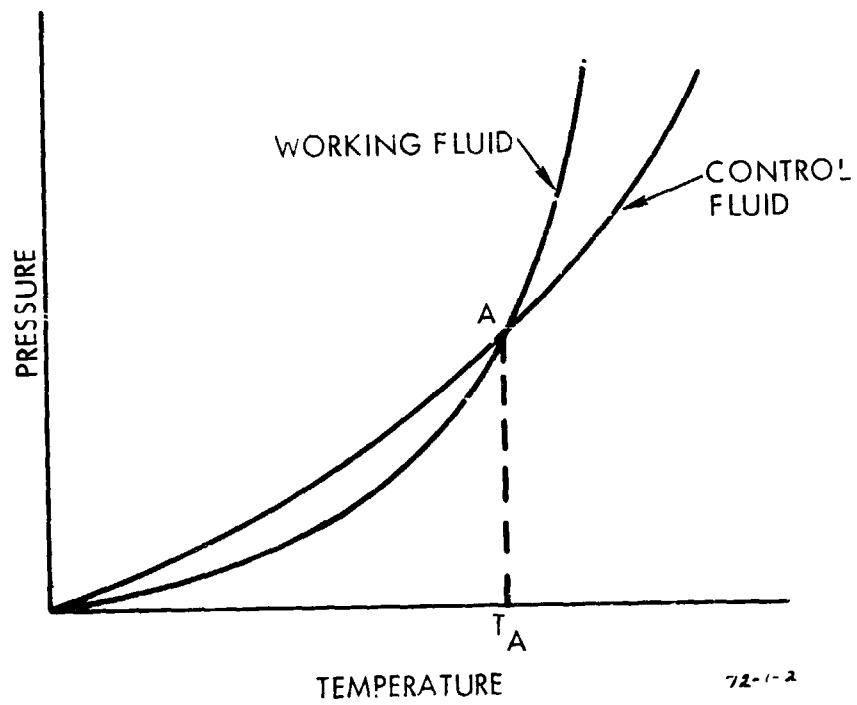
FIGURE 5-5. Pressure - Temperature Relationship for Extensible Container Control System Using a Two-Phase Control Fluid.

Similarly, an inability to obtain a control fluid with the appropriate boiling point T_{b1} (as given by Eq. 5-8) is tantamount to saying the two P, T curves don't cross near the design point.

5.3.2.2 Two-Component Control Fluids:

Since there appear to be few single-component two-phase control fluids for use with the desired working fluid, it is of interest to consider the possibility of using mixtures. For example, in seeking a "pusher", if there is found a fluid with a desirable $T_{z1} > T_{z2}$ but which has too low a value of T_{b1} (i.e., the fluid is too volatile), it is possible to mix it with another less volatile fluid, preferably with the same value of T_{z1}, to obtain a match for P_1 and P_2.

Consider an ideal solution of two components, one more volatile (subscript m), the other less volatile (subscript ℓ). The vapor pressure of the mixture is

$$P_{mix} = X_m \, P_m + X_\ell \, P_\ell \qquad (5-9)$$

where X_m and X_ℓ are the mole fractions of the liquid. Substituting from Eq. (5-5) yields

$$P_1 = P_0 \left[X_m e^{T_{z1}/T_{bm}} + X_\ell e^{T_{z1}/T_{b\ell}} \right] e^{-T_{z1}/T} \qquad (5-10)$$

$$X_m + X_\ell = 1 \qquad (5-11)$$

Comparing Eqs. (5-5) and (5-10) shows that an equivalent T_{b1} can be defined by

$$e^{T_{z1}/T_{b1}} = X_m e^{T_{z1}/T_{bm}} + (1-X_m)e^{T_{z1}/T_{b\ell}}$$

$$T_{b1} = T_{z1}/\ell n \left\{ X_m e^{T_{z1}/T_{bm}} + (1-X_m)e^{T_{z1}/T_{b\ell}} \right\} \qquad (5-12)$$

It is then possible to obtain the desired value of T_{b1} by varying X_m. Solving for X_m we find

$$X_m = \frac{e^{T_{z1}/T_{b1}} - e^{T_{z1}/T_{b\ell}}}{e^{T_{z1}/T_{bm}} - e^{T_{z1}/T_{b\ell}}} \qquad (5\text{-}13)$$

Eqs. (5-10), (5-12) and (5-13) hold only for $T_{z\ell} = T_{zm} = T_{z1}$ and are therefore useful only for conceptual design. For actual design one would use real mixture vapor pressures obtained from experiment.

Eqs. (5-9) - (5-13) apply to a mixture of two phase fluids. An alternative approach is to use a combination of a single two-phase fluid and a noncondensible gas. In this way it is possible to arbitrarily raise P_1 so that it matches P_2 at any desired set point. This relaxes the requirement on the two-phase component of the control fluid in that T_{b1} can be equal to or less than the value given by Eq. (5-8).

By introducing a noncondensible gas, however, the control fluid pressure is no longer a unique function of temperature, but also depends on the container volume. If large displacements are involved this results in a reduced control sensicivity.

5.3.2.3 Single Phase Control Fluids:

If we eliminate the two-phase fluid altogether, and simply utilize a ncncondensible gas as the control fluid, the pressure can again be readily adjustable to match that of the working fluid so that $P_1 = P_2$ at the control point. Furthermore, the temperature dependence of the gas pressure is weak compared with the two-phase working fluid, yielding a very large difference in dP/dT. Thus, a single phase gas represents an attractive puller type control fluid. This system would yield performance similar to gas controlled heat pipes except that the gas is isolated (free of vapor) and at nearly constant temperature. Thus, it would be relatively insensitive to variations in sink temperature.

As opposed to a single phase gas, one can also utilize a single phase liquid as the control fluid. Liquids are relatively incompressible and, at constant volume, exhibit very high values of dP/dT [Reference 21]. Thus, liquids make excellent pusher type control fluids, provided very small volume changes are required for control.

88

5.4 Excess Fluid Control Vs. Vapor Flow Modulation:

Both the excess fluid and vapor flow modulation control schemes
show promise for development cf variable conductance heat pipes which
are relatively insensitive to variations in sink temperature. Part of
TRW's task was to examine both schemes in terms of their practicality
and, in conjunction with NASA-ARC personnel, select the most promising
for hardware development. The following paragraphs present a comparison
of the two schemes from numerous points of view relative to design and
implementation. These comparisons are summarized in Table 5-3.

5.4.1 Required Displacement of Extensible Container:

Since the excess fluid control scheme operates by virtue of
condenser blockage, similar to gas control, it is necessary that the
vapor-liquid interface be variable over the entire condenser length.
Thus, the volumetric displacement of the control fluid container must
be at least equal to the vapor void volume of the condenser (see
Figure 5-1) plus any variation in excess fluid volume due to changes
in liquid and vapor density with temperature. This represents a
relatively large displacement.

The function of the extensible container in the vapor flow
modulation technique is to provide linear motion to the valve stem.
By using a small area bellows, one can achieve substantial linear
motion with very little volumetric displacement. Furthermore, by
designing the valve with a very short stroke, the result is a system
requiring minimal volumetric displacement of the extensible container.

5.4.2 Type of Extensible Container:

One might consider pistons, bellows or bladders as potential
candidates for an extensible control fluid container. In general,
pistons appear to be unsuitable because of leakage past the seals.
Similarly, bladders are frequently avoided because of mass diffusion
problems, although this does not appear insurmountable. The preferred
structure seems to be the bellows which is inherently free of both
leakage and diffusion. Furthermore, from a heat pipe fabrication point
of view, a metallic bellows can be heated to high temperatures for
proper vacuum bakeout during processing. Nonmetallic bladders or piston

TABLE 5-3.

COMPARISON BETWEEN EXCESS FLUID CONTROL AND VAPOR FLOW MODULATION TECHNIQUES

CONSIDERATION	EXCESS FLUID CONTROL	VAPOR FLOW MODULATION
Required Displacement of Extensible Container	Large Displacements: Must Exceed Condenser Void Volume.	Small Displacements: Must Provide Motion of Valve Stem.
Type of Extensible Container	Large Soft Bellows or Bladder.	Small Bellows. Stiffness Dependent On Control Fluid.
Control Fluid	Need Puller Type. Two Phase Fluid and/or Noncondensible Gas.	Can Use Pusher or Puller. Gas, Liquid or Two Phase Fluid.
Mechanical Motion	Substantial Motion of Bellows or Bladder.	Small Motion of Bellows Plus Motion of Valve Stem and Seat.
Working Fluid	No Fundamental Limitation. Prefer Low Pressure Fluids.	Limited to Low Pressure Fluids by "Blow-Through" Failure.
Wick Constraints	No Fundamental Limitation.	Need High Capillary Pressure. Requires Arteries.
1-G Testing Constraints	Requires Capillary Structure In Condenser. Constraints On Reservoir Geometry and Location.	No Unusual Constraints.
Thermal Characteristics		
Sink Temperature	Sink Must Be Above Freezing Point.	Condenser (Not Sink) Must Be Above Freezing Point.
Set Point Control and Sensitivity	Fixed Set Point and High Sensitivity With Two Phase Control Fluid. Variable Set Point and Moderate Sensitivity With Noncondensible Gas.	Variable Set Point and High Sensitivity With Liquid Control Fluid.

seals represent a constraint in this regard.

In the case of excess fluid control, the large displacement requirements combined with a desire for high contro¹ sensitivity dictate the use of a large extensible container with little resistance to displacement; e.g., a "soft" (low spring constant) bellows or bladder.

In contrast, the small displacement requirements of the vapor flow modulation scheme permit use of a small bellows of greater stiffness. The actual stiffness requirements depend on the control fluid selected, as will be seen later.

The stiffness requirement of the extensible container is an important factor, for it strongly influei .es the integrity of the system under off design conditions. The pressure differential across the bellows is a function of the system temperature and, depending on the fluids chosen, can be quite large if the temperature deviates from th design point appreciably. Unless the bellows is stiff enough to support such differentials other means must be provided to protect it.

5.4.3   Control Fluid:

The excess fluid control system, as depicted in Figure 5-1 and 5-2, requires a puller type control fluid so that the container contracts and available condenser area increases as the temperature increases. Thus, the field is limited to a noncondensible gas, a two-phase fluid, or a combination of the two. As shown in 5.3.2.1, however, it is difficult to find satisfactory two-phase control fluids for all working fluids of interest. A pure gas or a mixture of gas and a two-phase fluid appears most suitable.

The vapor flow modulation concept can utilize either a pusher or puller type control fluid, depending on which direction one establishes for the valve to seat (Figure 5-3 calls for a "puller"). Thus, this provides no restriction on the control fluid. A particularly attractive approach to this system, made possible by the very small displacements required, is to use a single phase liquid as a pusher fluid. Because a liquid is relatively incompressible, the displacement of the bellows

is essentially independent of both the working fluid vapor pressure
and the bellows stiffness. Thus, very strong bellows may be used
which provides a rugged structure and alleviates protection problems
at off-design temperatures.

5.4.4 Mechanical Motion:

Both systems require mechanical motion to operate. The
excess fluid scheme requires substantial motion of a very soft bellows
or bladder, with associated fatigue possibilities. The vapor modulation
scheme also requires motion of a bellows, but the motion is small and
the bellows can be very strong. However the latter scheme also
requires motion of a valve stem through a guide and repetitive sealing
of a valve. This gives rise to potential sticking problems although,
once again, the use of a very stiff bellows minimizes this concern.

5.4.5 Working Fluid:

The excess fluid control scheme imposes no fundamental constraints
on the working fluid over and above those common to all heat pipes. However,
the pressure differential across the bellows or bladder at off-design
conditions will be greater for high pressure fluids. Consequently, the
use of lower pressure fluids will simplify the problem of assuring
system integrity.

In the case of vapor flow modulation, the control function is
provided by establishing a pressure differential between evaporator
and condenser which yields a corresponding saturation temperature
differential. This and all other pressure drops in the circulation
loop must be overcome by the capillary head. Typical values for
capillary pressure are on the order of tens of psf. Thus, it is clear
that the working fluids are limited to those with low absolute vapor
pressures in the operating temperature range if significant evaporator-
to-condenser temperature differentials are to be achieved. Water and
the alcohols (methanol, ethanol, propanol. etc.) are typical candidate
fluids which exhibit low vapor pressures in the temperature range of
interest in spacecraft thermal control.

5.4.6 Wick Constraints:

The excess fluid control scheme imposes no unusual constraints on the pr mary wick design. Either hcmogeneous or arterial wicks may be used. In fact, the use of arteries is simpler than with the gas control technique for the system is presumably gas free and problems of gas bubble ent apment are minimized.

The vapor flow modulation technique, however, almost certainly requires the use of arteries. It is necessary to generate as high a capillary head as possible to overcome the throttling pressure drop. This requires very small pumping pores which, to avoid excessive liquid flow resistance, calls for an arterial wick structure.

5.4.7 1-G Testing Constraints:

The need for ground testing of the heat pipe places considerable constraint on the design of excess fluid controlled heat pipes. In order to achieve condenser blockage it is necessary to include sufficient capillary structure in the condenser to assure that the fluid will bridge the voids and not puddle on the bottom. In addition, there are limitations on the geometry and location of the excess fluid reservoir. Since this cannot readily contain a capillary structure to avoid puddling (it must permit motion of the control fluid bellows or bladder), the equivalent effect must be obtained geometrically. Figure 5-2 shows a satisfactory approach to the problem. By placing the reservoir external to and below the evaporator and condenser, gravitational forces act to keep liquid in the reservoir rather than in the condenser.

In contrast, the vapor flow modulation concept suffers no unusual constraints for 1-G testing.

5.4.8 Thermal Characteristics:

5.4.8.1 Sink Temperature:

With the excess fluid control scheme, the portion of the condenser which is liquid blocked will tend to fall in temperature and equilibrate with the sink. If the fluid freezes near the end of the condenser, the liquid reservoir will be ecoupled from the

93

active portion of the pipe by the solid plug and the control function
will be lost. Thus, this scheme is limited to applications where the
effective sink temperature does not fall below the freezing point
of the working fluid.

In the case of vapor flow modulation, the control function
is independent of the condenser. Freezing is still a problem, however,
since a frozen condenser cannot return fluid to the evaporator. But
the limitation is on the condenser, not the sink temperature. The
condenser is nearly isothermal in this case, and it is quite acceptable
to have the condenser above and the sink below the freezing point of
the working fluid. There will of course be heat rejection under such
circumstances, but this can be quite small for a condenser near the
freezing point of a fluid such as methanol (F.P. = -144°F).

5.4.8.2 Set Point Control and Sensitivity:

If a two-phase control fluid is used for an excess fluid
controlled heat pipe, the nominal set point is fixed at the inter-
section of the vapor pressure curves of the control and working
fluids. However, the pressure of a two-phase fluid is not a function
of volume and thus the entire condenser can be turned on or off with
a pressure (and hence temperature) change only equal to that necessary
to expand or compress the control fluid container. If a "soft"
container (e.g., bladder) is used, this can be accomplished with
hardly any change in temperature at all. In other words, this system
offers extremely good control sensitivity.

Unfortunately, as discussed in Section 5.4.3, two-phase control
fluids are not readily available for most cases of interest. Rather,
a mixture of a noncondensible gas and a two-phase fluid, or a pure
noncondensible gas seem more promising. In such cases, the nominal
set point can be varied according to the gas inventory (partial
pressure); but the control sensitivity is reduced due to the
volume-dependent pressure characteristics of the gas.

The vapor flow modulation concept seems best implemented
with a liquid control fluid. In this case the nominal set point
corresponds to the evaporator temperature at which the valve

just closes. This can be easily varied over a wide range by simply adjusting the liquid inventory in the extensible container.

As well as a variable set point, this scheme also has the potential for very high control sensitivity. The motion of the valve per unit change in temperature of the liquid in the extensible container is an independent design variable controlled by the volume and geometry of the container. It is a simple matter to design the system so that the valve stem travels its full span with only a few degrees change in control fluid temperature.

5.4.9   Summary and Conclusions:

Based upon the previous considerations, the vapor flow modulation scheme was selected as the preferred approach for hardware development. The principle reasons for this choice were:

a. Vapor modulation requires much less motion of the control fluid extensible container, allowing the use of a bellows which facilitates fabrication and increases reliability.

b. The vapor flow modulated pipe can operate with the sink temperature substantially below the freezing point of the working fluid since no portion of the condenser length is shut off and the fluid need not freeze. This feature gives the scheme a much broader range of application.

c. The vapor throttling valve can be actuated with a single phase liquid control fluid since only small motions of the valve are required. Thus, large forces and stiff bellows can be used, making the system more rugged and less sensitive to temperatures outside of its design operating range.

5.5   Design of a Prototype Vapor Flow Modulation Heat Pipe:

In designing the prototype heat pipe several ground rules were established to provide experimental flexibility and facilitate modification if necessary. These were as follows:

95

o All components must be made of a single material
   which is compatible with both water and methanol
   to permit testing with either as the working fluid.

o At least one end cap must be flanged to permit
   disassembly of the system.

o The entire valve assembly must be removable so that
   modification or replacement is possible if necessary.

o The design must provide outside access to the control
   fluid container to allow modification of the set
   point without disassembling the heat pipe.

o Size and weight would not be considered constraining
   factors in that the heat pipe is a developmental
   version.

A schematic diagram of the prototype heat pipe, indicating
the key components and layout, is shown on Fig. 5-6. The following
paragraphs describe the design of the specific heat pipe components,
consistent with the aforementioned ground rules.

5.5.1   Materials:

5.5.1.1 Metal Components:

Monel 400 was selected for all metal components of the heat
pipe. TRW has accumulated over 20,000 hours of life test data showing
Monel 400 to be compatible with water. Further, although life test
data of monel and methanol were not available, it is known that
methanol is compatible with both copper and nickel, monel's principal
components.

5.5.1.2 Working Fluid:

The working fluid was chosen to be water, with methanol as
an alternative. Water is a particularly attractive fluid for
vapor modulation heat pipes because of its high surface tension
(high capillary pressure) and low vapor pressure at temperatures of
interest. This allows a large range in operating conditions without
exceeding the "Blow through Limit," as discussed in reference [3].
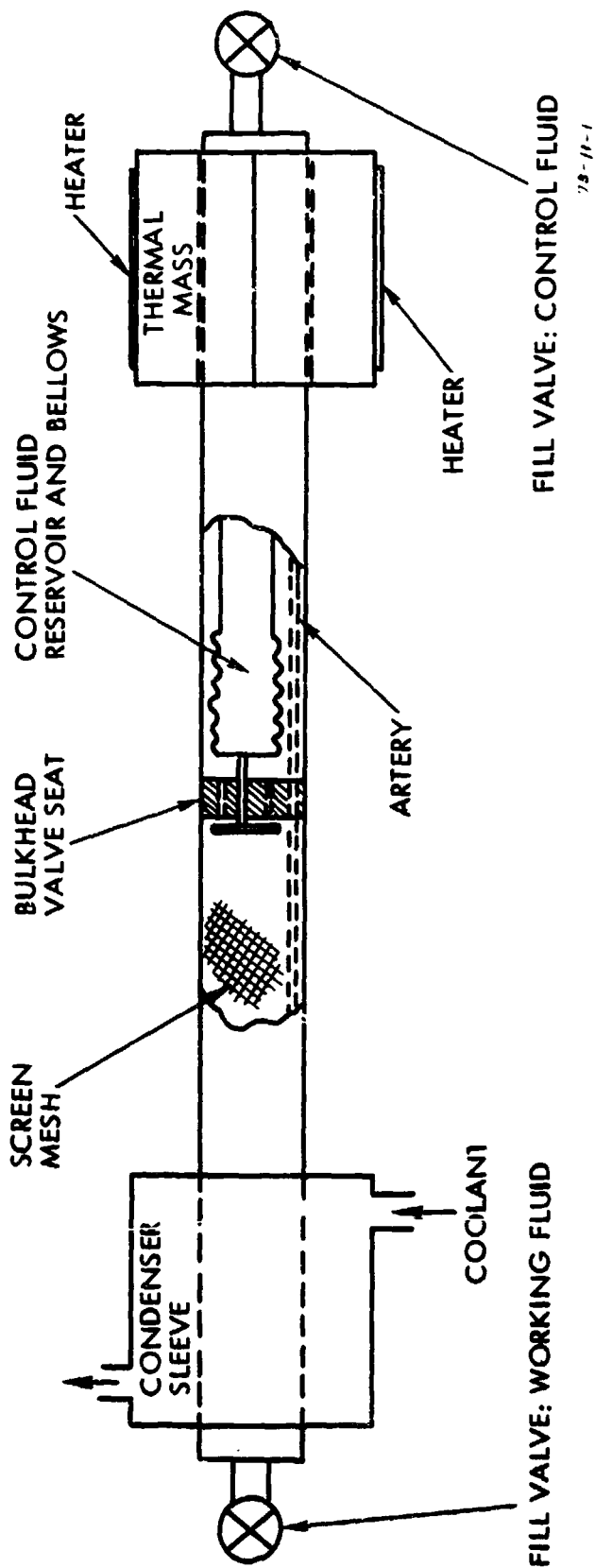
FIGURE 5-6. Vapor Modulation Heat Pipe: Schematic of Prototype.

However, water does have a high freezing point which limits the sink temperature to relatively high values. Substituting methanol allows testing at very low sink temperatures although its operating range is somewhat limited by vapor blow-through.

5.5.1.3 Control Fluid:

In selecting a control fluid, the principal criteria were compatibility and the coefficient of volumetric expansion. A good control fluid has a high coefficient which maximizes the displacement of the valve stem with changes in fluid temperature. Table 5-4 lists the coefficients of volumetric expansion for numerous potential control fluids. As can be seen, methanol exhibits one of the highest values.* Since methanol is presumably compatible with monel, it was selected.

Table 5-4

VOLUMETRIC EXPANSION FOR POTENTIAL CONTROL FLUIDS AT AMBIENT TEMPERATURES

ETHANOL	$\beta = 0.61 \times 10^{-3}$ $(°F^{-1})$
METHANOL	0.80×10^{-3}
MERCURY	0.10×10^{-3}
PETROLEUM	$0.40 - 0.50 \times 10^{-3}$
TURPENTINE	0.54×10^{-3}
WATER	0.115×10^{-3}
PHENOL	0.50×10^{-3}
BENZENE	0.77×10^{-3}
ACETIC ACID	0.80×10^{-3}

*Several fluids with higher values of β have recently been reported in reference [22]

5.5.2   Valve Design:

The heart of the vapor flow modulation concept is the throttling valve between the evaporator and condenser sections. This valve opens and closes so as to automatically adjust the pressure drop through it to maintain the evaporator pressure within the design control range. Desired valve characteristics are as follows:

- o Since the control fluid (Methano" liquid) is a pusher type, the valve must open when the stem moves toward the condenser.

- o The valve must be of sturdy construction and operate under large enough forces to prevent sticking.

- o In the fully open position the valve should offer very little resistance to vapor flow.

- o For maximum control sensitivity the valve should be designed so that the flow area is a very strong function of stem displacement. This suggests a poppet type valve as opposed to a needle valve.

- o .he valve must be removable from the assembly to permit modifications if necessary.

A valve design which satisfactorily meets all of these criteria is shown on Figure 5-7. A disc-type valve head seats against a ring-type seal of semi-circular cross-section. Vapor flows axially through six holes in the valve body and then radially outward through the space between head and seat. The valve stem passes through a seventh hole in the center of the body. The valve body has an external screw thread which interfaces with the bulkhead, allowing easy removal.

5.5.3   Bulkhead Design:

The purpose of the bulkhead is to separate the evaporator and condenser sections such that vapor can flow only through the valve, and liquid only through the wick system (artery). Also, in this first prototype system, the bulkhead had to include a screw thread

SECTION AA PLUS VALVE STEM AND HEAD

VALVE STEM

VAPOR FLOW
PASSAGES

VALVE BODY

BULKHEAD
INTERFACE

VALVE HEAD

VALVE SEAT

APPROX. SCALE: |———— 0.25 IN.

FACE VIEW OF VALVE BODY

.068 DIA.

A

A

100
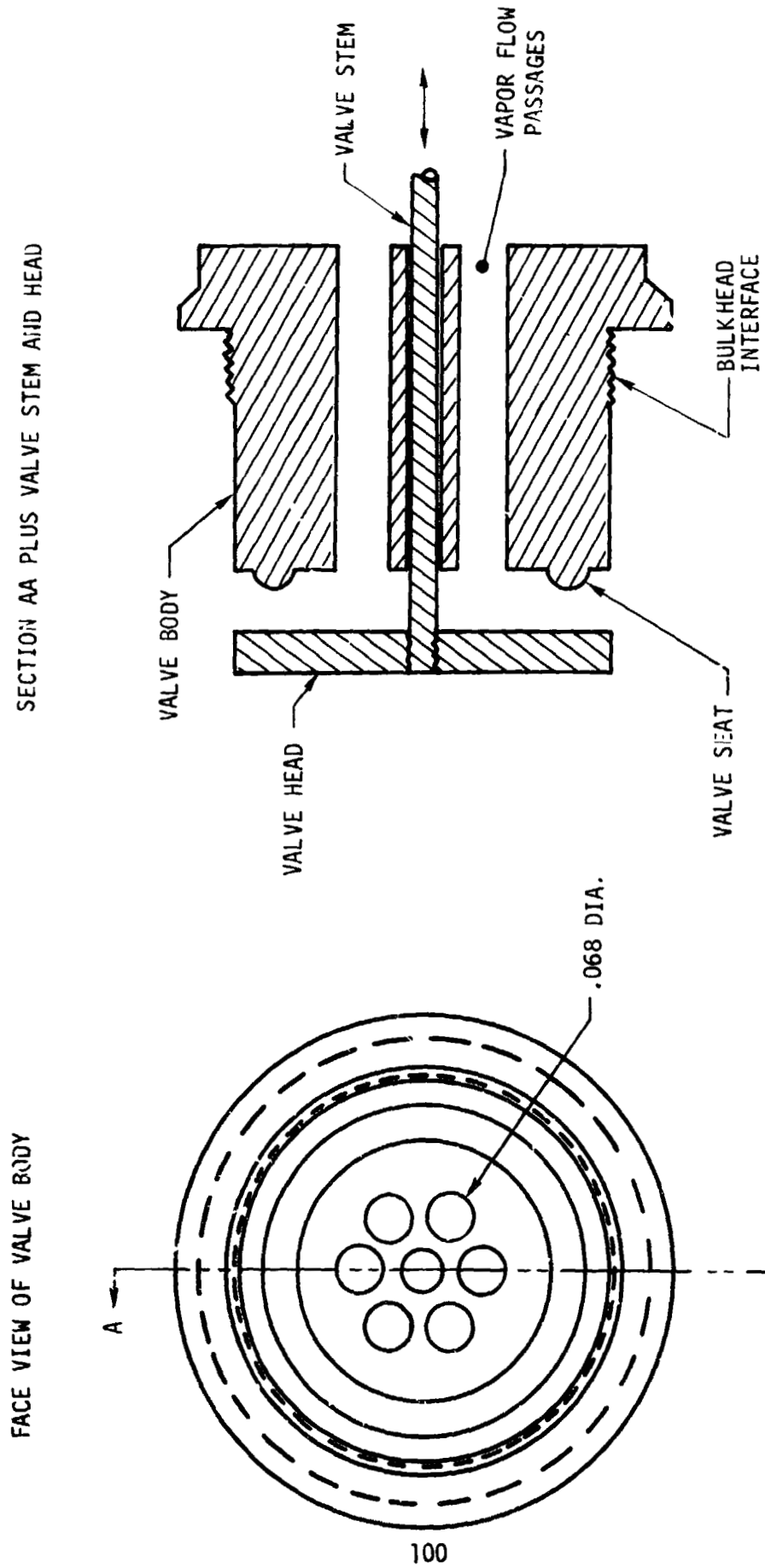
FIGURE 5-7. Throttling Valve Prototype Heat Pipe

interface with the valve body to allow easy removal of the latter. In addition, since there may exist a substantial temperature difference across the bulkhead between the evaporator and condenser sections, it should provide sufficient thermal resistance to heat conduction so that heat leakage is acceptably low when the valve is closed. The low thermal conductivity of monel (12.5 Btu/hr-ft-°F) facilitates this last requirement.

The bulkhead was designed as a monel disc, 0.35 in. thick, with a female threaded hole for the valve body and a small through hole for the artery. It is shown in a photograph on Figure 5-10.

5.5.4 Control Fluid Reservoir and Valve Actuator:

In designing the control fluid reservoir and valve actuator, the following requirements were established:

o The design had to be rugged, suggesting a small bellows with a stiff spring constant plus overload protection in case of temperatures far outside of the control range.

o The design would utilize a standard bellows.

o To maximize control sensitivity, the reservoir volume should be large.

o The design had to include external access to the reservoir to permit adjustment of the control fluid inventory and, hence, the nominal heat pipe set point.

o The design had to include a capability for small mechanical adjustments in the position of the end of the bellows which actuates the valve.

The ultimate design, satisfying all these criteria, is shown schematically in Figure 5-8. A small standard bellows was connected to an 8 in. long, 3/8 in. O.D. tube with an externally threaded connector. A 1/4 in. O.D. tube was connected to the other end of the 3/8 in. tube, representing the reservoir fill tube. The volume of these elements represent the volume of the control fluid.

VAPOR FLOW

VAPOR FLOW HOLES

VALVE STEM

VALVE BODY

SUPPORT SLEEVE

ADJUSTMENT SCREW

BELLOWS
1 IN. LONG
.545 O.D.
.360 I.D.

SPRING LOADED
BASE OF VALVE
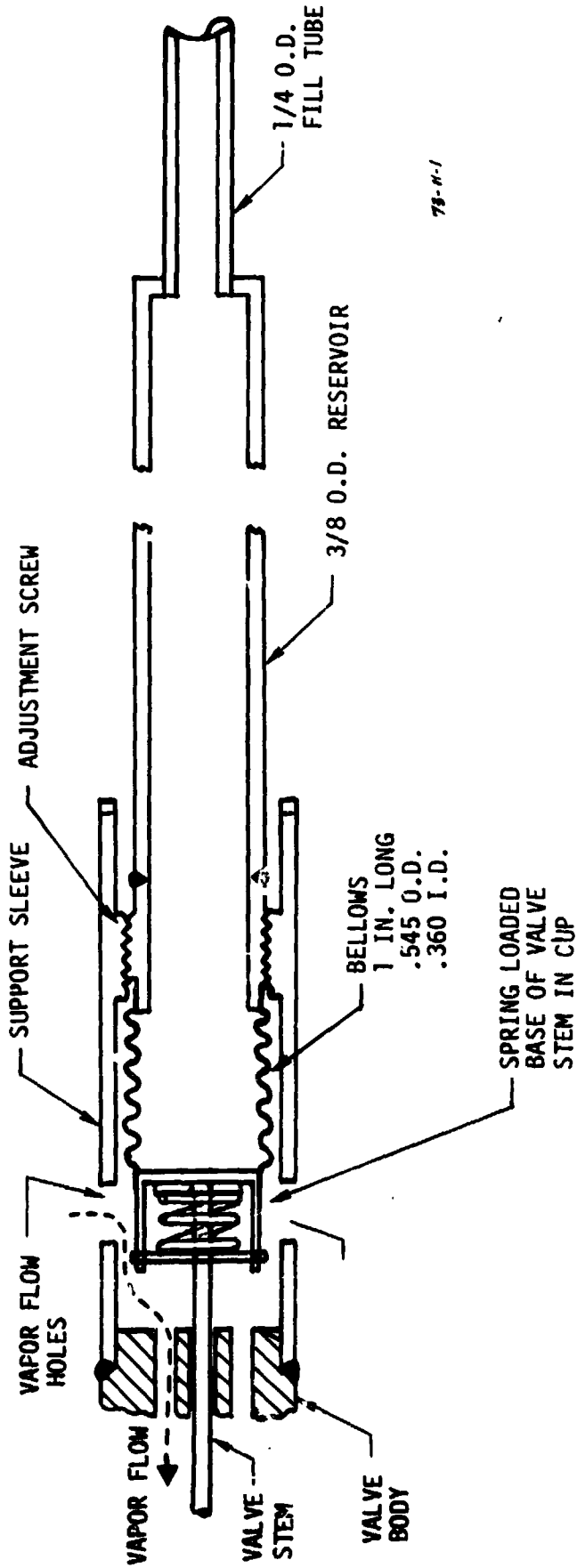STEM IN CUP

3/8 O.D. RESERVOIR

1/4 O.D.
FILL TUBE

FIGURE 5-8.   Control Fluid Reservoir and Valve Actuator - Prototype Heat Pipe

An inverted cup was welded to the other end of the bellows which served as the valve actuator. Rather than hard mounting the valve stem to the bellows, the connection was made with a pinned spring and disc to provide overload protection to the valve stem. The bellows and valve actuator assembly was screwed into a sleeve which was welded to the valve body. This screw thread connection allowed adjustment of the valve actuator position with respect to the valve body. The sleeve provided overpressure protection for the bellows and also served as the point of contact with which the entire valve and control fluid reservoir assembly could be inserted or removed from the bulkhead. Four holes drilled into the sleeve provided the vapor flow path to the valve body. Details of the assembly are shown in the photographs of Section 5.6.

5.5.4.1 Anticipated Control Range:

The volume of the control fluid container (excluding the fill tube) was approximately 0.91 in^3. Using 0.80×10^{-3} $°F^{-1}$ for the methanol coefficient of expansion (Table 5-3), and an effective bellows area of 0.161 in^2 (manufacturer's data), one can calculate the displacement of the valve stem with temperature as follows:

$$\frac{dx}{dT} = \frac{V\beta}{A_{eff}} \qquad (5-14)$$

$$\frac{dx}{dT} = \frac{0.91 \ (0.8 \times 10^{-3})}{0.161} = 4.5 \times 10^{-3} \ in/°F$$

Once the valve opens to the point where the throat area equals that of the holes in the valve body, it can be considered fully open. The area of the holes equals 2.18×10^{-2} in^2, and the area of the throat equals 1.18 in^2 per inch of stem displacement. Thus, a stem displacement of only 0.0185 in. is sufficient to fully open the valve. Based on the previous calculation for $\frac{dx}{dT}$, this corresponds to a temperature change of 4.1°F. Thus, the anticipated control range of the heat pipe; i.e., the range in control fluid temperature to fully open and close the valve, is approximately 4°F.

5.5.5 Wick Syst n:

The requirements on the wick system are that it provides a large capillary head and a low flow resistance. The large capillary head is necessary to accommodate the press.ire drop across the valve, and the low flow resistance to assure that most of the capillary head is available for this vapor pressure drop.

These requirements are best satisfied with an arterial wick structure. Thus, the pipe was designed with a single 0.0625 in. diameter artery along the bottom made with two layers of 300 mesh monel screen. In both the evaporator and conjenser sections the artery was spot welded to circumferential wicks (four layers of 300 mesh monel screen), themselves spot welded to the tube walls.

The circumferential wicks ended at the bulkhead and the arteries in the evaporator and conden. r were connected through the bulkhead by a 1/16 in. O.D. x .006 wal. monel tube. Thus, liou flowed through the bulkhead only through the artery.

Additional wicking in the pipe included a double layer of 300 mesh monel on the external surface of the control fluid reservoir (excluding the bellows), and transfer wicks providing communication between the control fluid reservoir and the evaporator wall. The wicking structure is shown in Figure 5-9.

5.5.6 Tubing and End Caps:

The heat pipe tube was designed in two 12 inch sections welded to opposite sides of the bulkhead. The tube was sized at 1.0 in. O.D. x 0.035 in. wall thickness to facilitate installation of the wicking and valve assembly. Smaller and lighter tubing might ultimately be used for a flight system, but the large diameter was more consistent with the requirements of an experimental prototype.

The condenser end of the heat pipe was capped with a welded disc containing a 1/4 in. fill tube for charging the pipe with working fluid.

The evaporator end of the pipe was designed with a flanged end cap using an 0-ring seal. This was necessary to permit installation

RESERVOIR - 2 LAYERS

TRANSFER WICKS -
2 LAYERS, 5 TURNS
TO FORM TUBES

EVAPORATOR

CIRCUMFERENTIAL WICKS

EVAPORATOR ARTERY

BULKHEAD ARTERY (EVAPORATOR AND
CONDENSER ARTERIES
SPOT WELDED TO TUBE)

CIRCUMFERENTIAL
WICKS - 4 LAYERS

ARTERY - 2
LAYERS, 1/16 I.D.

SPOT WELDS

CONDENSER

BULKHEAD

CONDENSER ARTERY
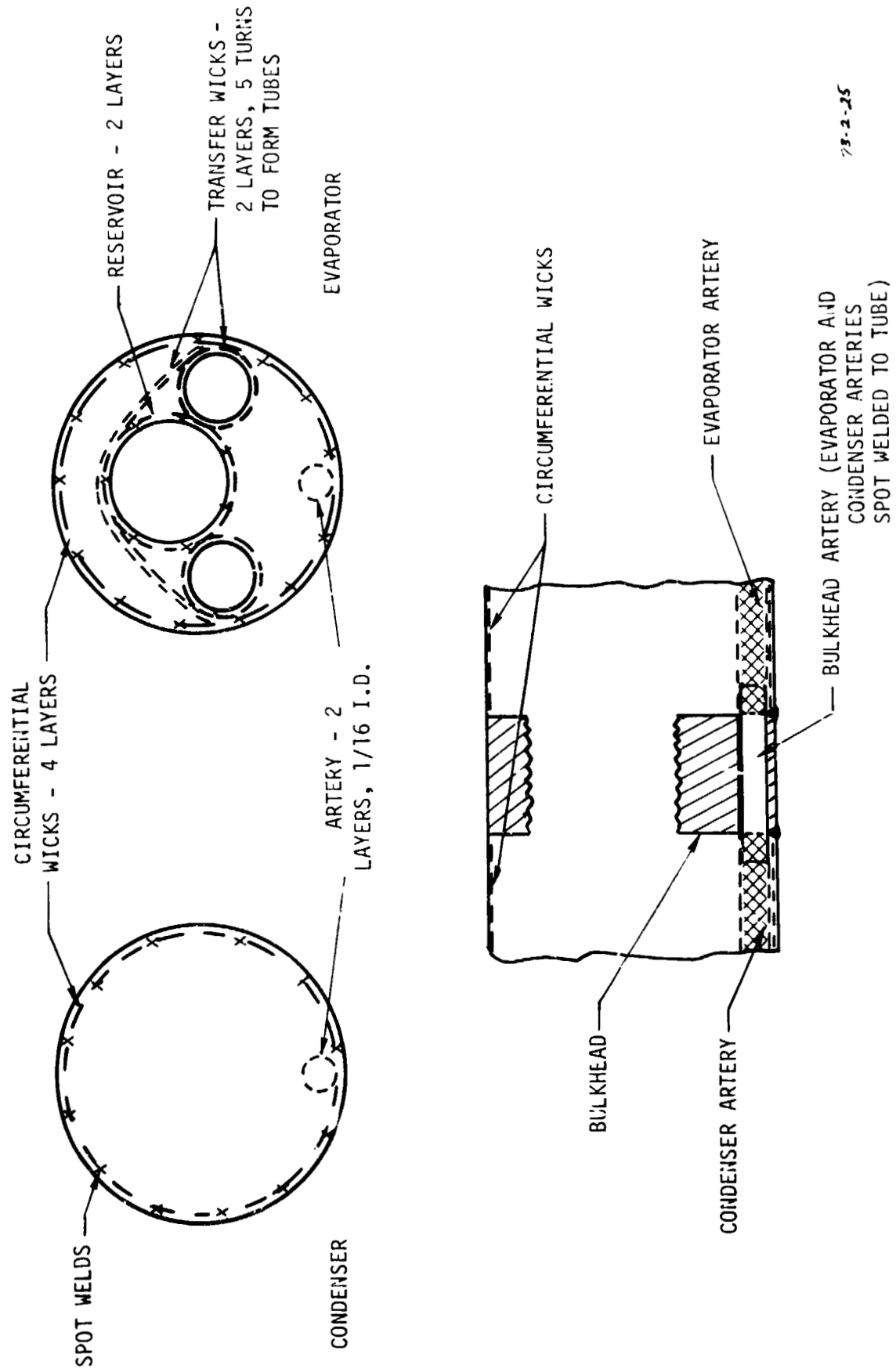
ALL WICKING: 300 MESH MONEL SCREEN

FIGURE 5-9.   Wick System - Prototype Heat Pipe

105

and removal of the valve-reservoir subassembly. The 1/4 in. fill tube
for the control fluid reservoir passed through a hole in the flange -
sealed by a second O-ring and bolted washer. With this design it
was possible to externally adjust the control fluid inventory without
disassembling and reprocessing the heat pipe.

The tubing, end caps, flanges, etc. are shown in the
photographs of Section 5-6.

5.6   Fabrication of the Prototype Heat Pipe.

5.6.1   Piece Part Manufacture:

All of the components of the heat pipe except the O-rings
were fabricated from the same material - monel 400. The wicks were
cut from 300 mesh screen. The bellows was a standard purchased
part with an 0.005 in. wall, 0.161 in. effective area, 1.0 in. free
length and 82.5 lbs./in. spring rate. All other parts were machined
from monel tubing or rod stock.

The principal components of the heat pipe (excluding wicks)
are shown on Fig. 5-10.

5.6.2   Assembly:

The heat pipe assembly utilized an all-welded construction
except for the valve-bulkhead screw connection and the flanged seals
at the evaporator end. In building up the system, the two sections
of tube were individually wicked and then welded to both sides of the
bulkhead. The condenser end cap, fill tube and evaporator flange
were then welded on. The control fluid reservoir-bellows-valve
subassembly was welded and fitted together as a separate unit which
screwed into the bulkhead. Figures 5-11 and 5-12 show the heat pipe
in partial states of assembly.

In building up the heat pipe all components were repeatedly
cleaned at the piece-part, subassembly and assembly levels by
ultrasonically agitating them in acetone and Freon 113 following a
TCE vapor degrease.
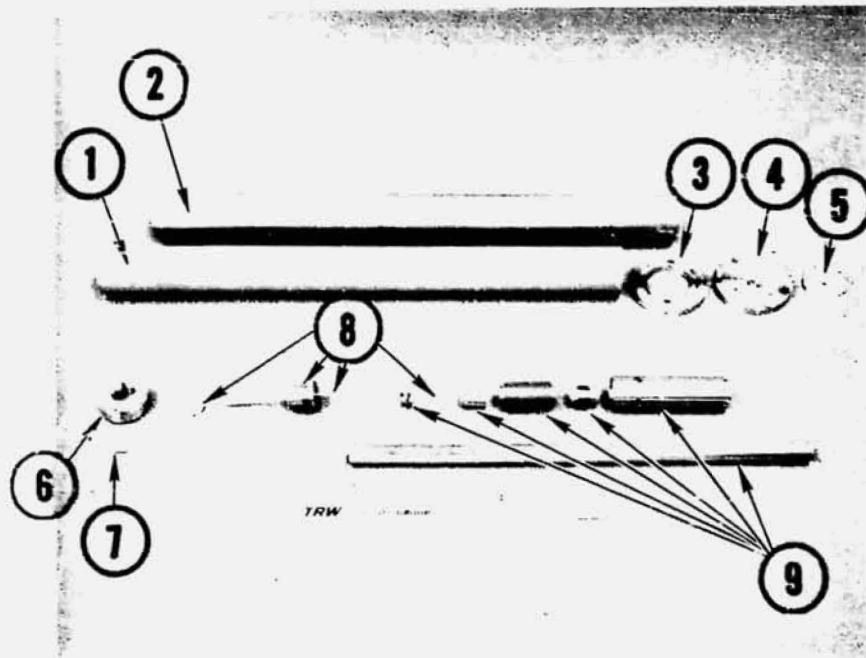
FIGURE 5-10. Vapor Modulation Heat Pipe Components (incomplete).

1. Evaporator tube
2. Condenser tube
3. Evaporator flange
4. Evaporator end cap
5. Bolted washer to seal control reservoir fill tube
6. Bulkhead
7. Bulkhead artery
8. Valve components (poppet, body and seat, stem, actuating disc)
9. Control fluid reservoir assembly components (relief spring, inverted cup, bellows, threaded connector, support sleeve, reservoir tube)
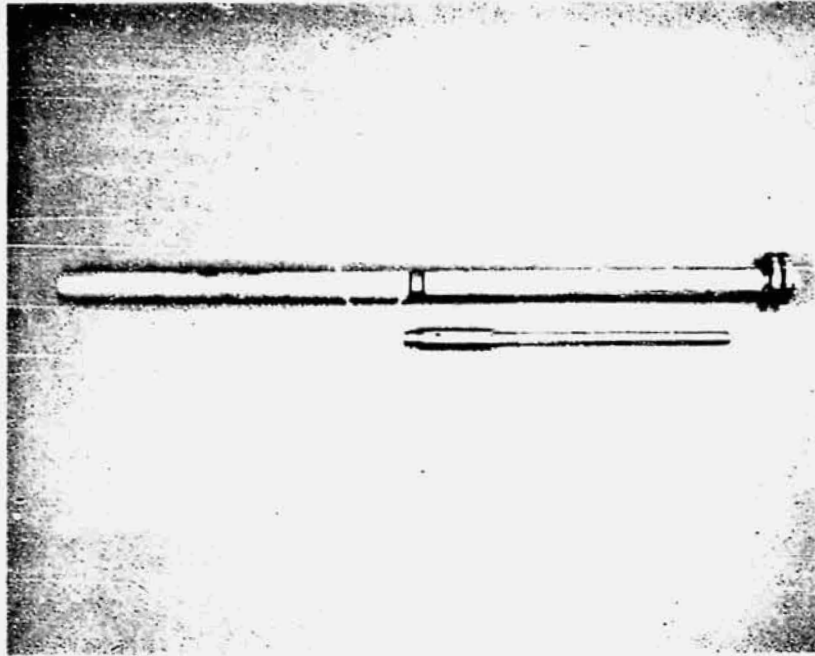
FIGURE 5-11. Partially Assembled Heat Pipe
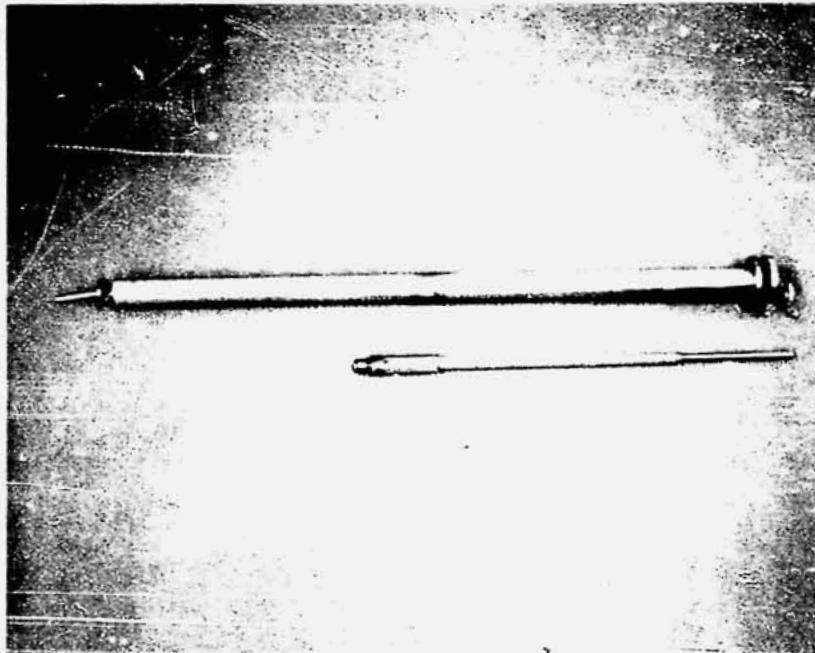
FIGURE 5-12. Partially Assembled Heat Pipe

5.7   Testing of the Prototype Heat Pipe.

The test program for the prototype heat pipe was exploratory in nature; i.e., to determine the characteristics of vapor flow modulation devices in order to lay the groundwork for design of flight systems. Two major areas of investigation were identified as follows:

> o What were the control characteristics of the
> pipe? Would it perform with the anticipated
> control range? Was it truly insensitive to
> sink temperature variations as theorized? Would
> the system exhibit transient overshoots, under-
> shoots and/or hysteresis? Would the system exhibit
> stable operation, etc.?

> o What were the limits of operation? What was the
> capacity of the system as a function of its set
> point temperature and condenser temperature?
> Was the operating regime bounded by the theory
> as discussed in Reference [3]?

5.7.1   Test Apparatus:

To perform the investigation an experimental apparatus was con-structed as shown in Figs. 5-13 and 5-14.

An 8 in. condenser was established on the downstream side of the valve by circulating ethanol through a plastic jacket sealed to the pipe with O-rings. The sink temperature was controlled using a constant tem-perature circulating bath for the coolant with liquid nitrogen as a re-frigerant for the bath.

Similarly, an 8 in. evaporator was established by mounting heated aluminum blocks on the upstream portion of the pipe. Two clam-shell blocks were bolted to the pipe, each with 60 watt (at 110 volts) heaters bonded to them.

There was some concern that the control system might prove unstable unless the thermal time constant of the control fluid reservoir was small compared with the heat source. Thus, a 1/32 in. Teflon sleeve was placed between the aluminum blocks and the pipe to serve as a thermal resistance.
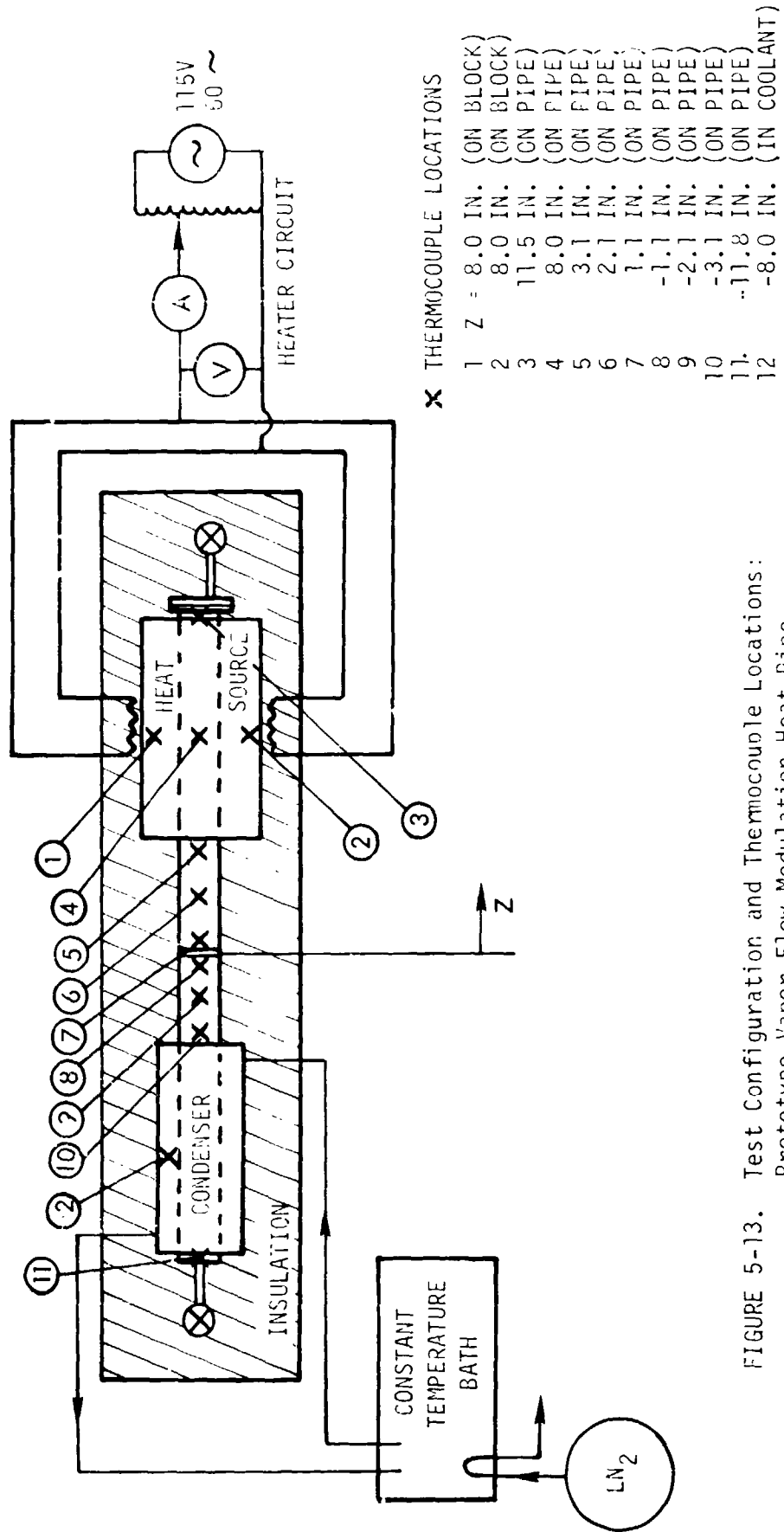
FIGURE 5-13. Test Configuration and Thermocouple Locations: Prototype Vapor Flow Modulation Heat Pipe.

✕ THERMOCOUPLE LOCATIONS

1	Z = 8.0 IN.	(ON BLOCK)
2	8.0 IN.	(ON BLOCK)
3	11.5 IN.	(ON PIPE)
4	8.0 IN.	(ON PIPE)
5	3.1 IN.	(ON PIPE)
6	2.1 IN.	(ON PIPE)
7	1.1 IN.	(ON PIPE)
8	-1.1 IN.	(ON PIPE)
9	-2.1 IN.	(ON PIPE)
10	-3.1 IN.	(ON PIPE)
11.	-11.8 IN.	(ON PIPE)
12	-8.0 IN.	(IN COOLANT)

FIGURE 5-14.   Prototype Vapor Flow Modulation Heat Pipe
On Test Stand.

The thermal capacity of the blocks was 1.175 Btu/°F and the resistance of the Teflon was 0.11 hr.- °F/Btu, yielding a thermal time constant of 0.13 hr. for the heat source. This compares with a value on the order of 0.005 hr. for the control fluid reservoir. It was anticipated that the heat pipe would be tested with and without the heater blocks to study the effect of this parameter.

The system was instrumented with twelve copper-constantan thermocouples located as shown on Fig. 5-13. Nine thermocouples were placed on the heat pipe, most in the region near the valve. The other three were located on the heater blocks and in the circulating ethanol coolant. The thermocouples were read with a 12 point recording potentiometer.
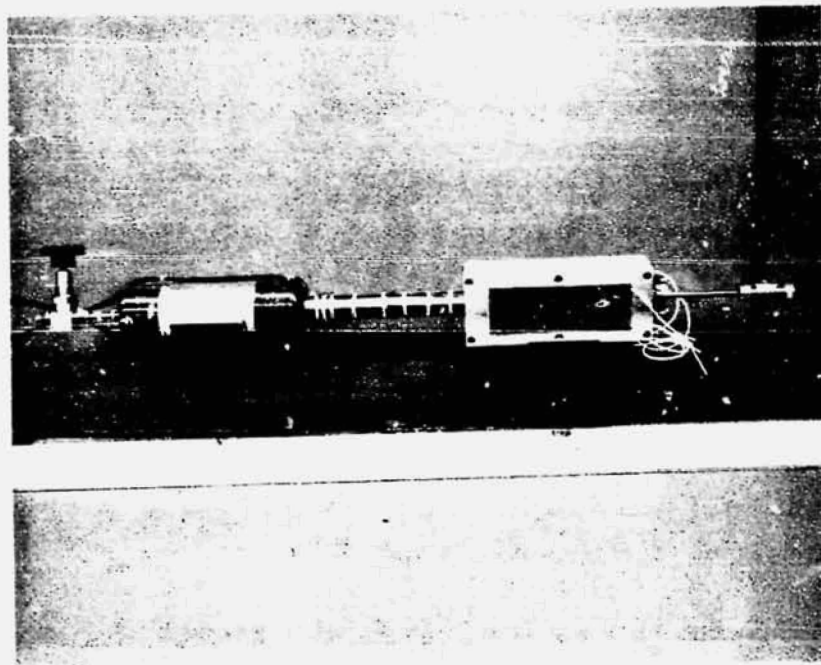
Additional instrumentation included an ammeter, voltmeter, and auto-transformer for controlling and measuring the input power.

The test assembly, as shown in Fig. 5-14, was subsequently insulated with urethane foam to a minimum thickness of 2 inches.

5.7.2   Test Results - Control Characteristics:

Once the experimental system was de-bugged and fully operational, an initial test (Test 1) was run to explore the control characteristics of the pipe and uncover any unanticipated behavior. This test was run with the pipe level and covered a range in input power from 5 to 75 watts, and a range in sink conditions from 26 to 84°F. The heat pipe performed extremely well, as shown on Fig. 5-15. Measured data at key points during the test are presented in Table 5-5.

The pipe was first heated to 90°F with the coolant (sink) set at 84°F to establish an equilibrium condition above the anticipated control range. With the input power maintained at 20 watts, the sink set point was lowered to 60°F. This brought the heat pipe into its control range and a small temperature difference began to appear across the valve. The sink set point was now lowered to 40°F and the evaporator temperature fell only 20°F while a 25°F temperature differential developed across the valve. This indicated that the valve had properly closed in response to the small drop in evaporator temperature.

The input power was then increased to 50 watts and the system
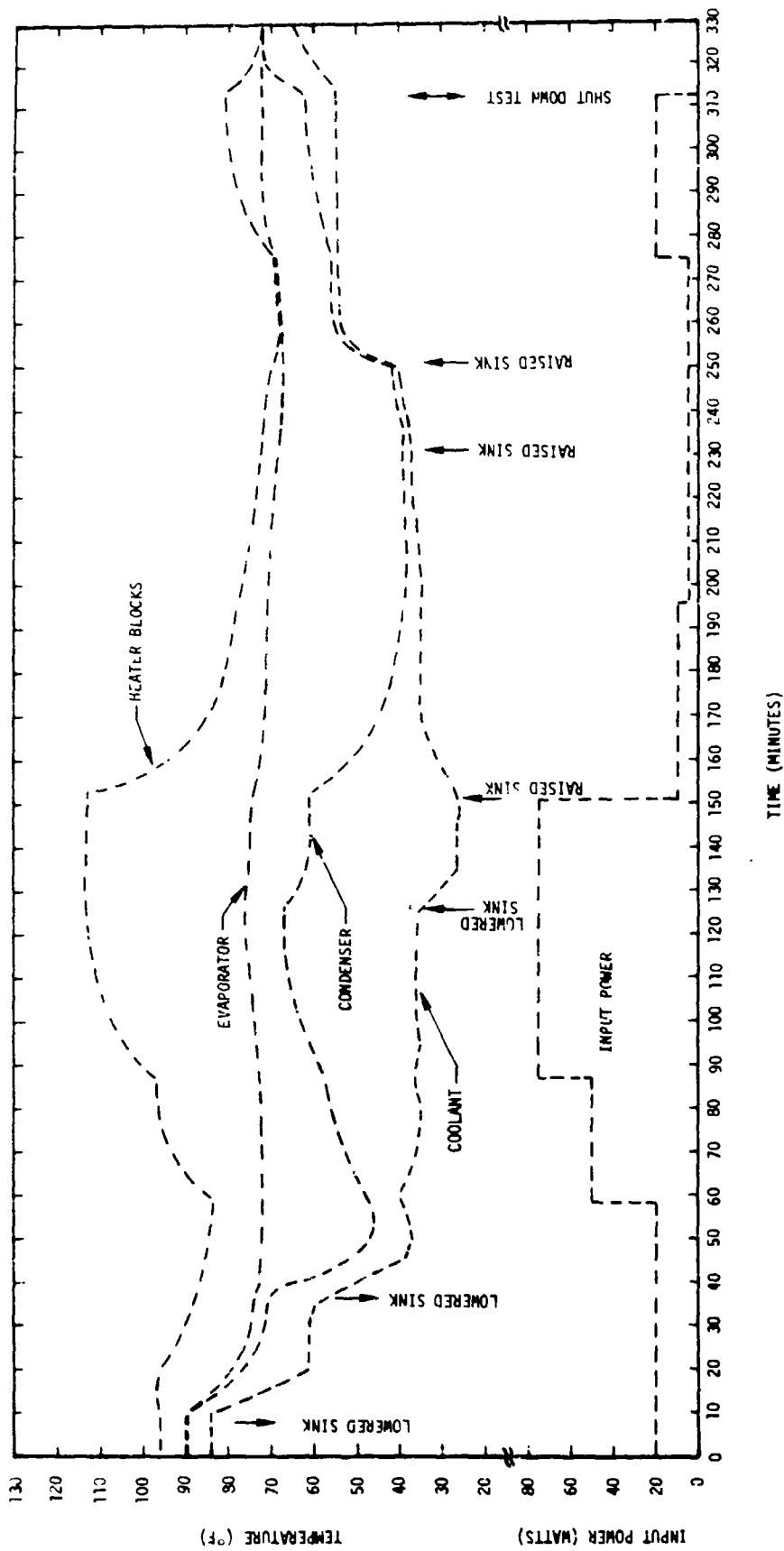
FIGURE 5-15. Test 1 Results.

TABLE 5-5. MEASURED DATA - TEST 1

TEMPERATURES (°F)

TIME (MINUTES)	POWER (WATTS)	HEATER BLOCKS		EVAPORATOR		ADIABATIC SEC. UPSTREAM			ADIABATIC SEC. DOWNSTREAM			CONDENSER	SINK
		1	2	3	4	5	6	7	8	9	10	11	12
5	20	95.5	96.5	91.5	91.0	90.5	90.0	90.0	89.5	89.5	89.0	89.0	84.0
35	20	86.0	88.0	75.5	75.0	74.5	74.0	73.5	71.0	70.5	70.0	70.0	59.0
55	20	84.0	83.0	73.0	72.5	72.0	72.0	72.0	46.0	46.0	46.0	46.0	38.0
85	50	97.5	95.5	73.0	73.5	73.0	72.5	72.5	57.5	57.5	57.0	57.0	36.0
125	75	114.0	117.5	74.5	78.5	76.5	76.0	76.0	67.5	67.0	56.5	66.5	35.5
150	75	114.5	112.0	73.5	76.5	75.5	74.5	74.5	61.0	60.5	60.5	60.0	26.0
195	10	78.5	77.5	72.0	71.0	70.5	70.5	70.5	38.0	39.0	39.0	39.5	34.5
230	5	72.5	72.0	68.5	68.0	68.0	68.0	68.0	38.0	39.0	39.0	39.0	36.5
250	5	72.5	72.0	67.5	67.0	67.0	67.0	67.0	41.5	42.0	42.0	42.0	40.5
275	5	69.0	68.5	68.5	68.5	68.5	68.5	68.5	56.0	55.5	55.5	55.5	54.5
310	20	81.0	80.5	73.0	72.5	72.0	72.0	71.5	62.5	62.5	62.5	61.5	54.5

115

responded with a small increase in evaporator temperature and a large increase in condenser temperature; again, a proper response indicating an opening of the valve.

A further increase in input power pointed up the first design deficiency in the system. Although the condenser rose in temperature with respect to the evaporator, the temperature drop across the valve only fell to 9°F while the evaporator temperature rose to 76°F. At this evaporator temperature the valve was presumably fully opened - yet an appreciable pressure drop was sustained in establishing a vapor flow rate corresponding to 75 watts at 76°F. This could be reduced by designing the valve with a less tortuous vapor flow path and a larger flow area.

At this condition the pipe was outside of its control range; i.e., the valve was fully open. To bring it back within control the sink set point was lowered to 25°F. The temperature drop across the valve increased to 14°F, indicating the valve must have closed slightly, and the evaporator temperature fell to 74.5°F. These results suggest that the upper end of the control range (valve fully open) is about 75°F.

An important point to note is that, in responding to increases in power, the system exhibited no temperature overshoot. Thus, the thermal response of the control mechanism was fast in relation to the heat source as anticipated.

To test the response to a cooling transient the input power was then reduced to 10 watts. Simultaneously, the sink set point was raised to 35°F. to avoid freezing in the condenser as the valve closed. The response of the system was monotonic, with no evidence of a temperature undershoot. After 45 minutes, the condenser temperature had fallen to within 4°F. of the sink, indicating the valve was almost closed, while the evaporator was some 32°F. warmer at 71°F.

To see whether the valve would close further the power was lowered to 5 watts. In response, the condenser fell to within 2°F. of the sink. However, the evaporator temperature fell to 67°F; below its anticipated control range. It was apparent that the pipe was again outside of the control range, this time on the low side.

116

With the valve fully closed the evapcrator equilibrium temperature is established by heat leakage across the bulkhead. The sink temperature was then raised in steps to see if the evaporator temperature would increase, confirming this condition. The system was very slow to respond at such low power and after 45 minutes the power was increased to 20 watts to speed the process. In response the evaporator quickly rose to 71°F. and then slowly increased to 72°F., suggesting that the valve opened near the former value. Thus, the lower end of the control range appeared to be about 71°F. yielding a total range of 73 $\pm$ 2°F. This is in agreement with design calculations (see Sec. 5.5.4.1).

After the system had equilibrated, the evaporator temperature was 72°F. This compares to a similar value of 72°F. early in the test at a similar 20 watt input power, suggesting that the valve design is relatively free of hysteresis.

To summarize the results of this test, the following important conclusions can be drawn:

> o The heat pipe performed with the anticipated
>   4°F. control range at a nominal temperature
>   just above ambient, in agreement with theory.
>
> o The evaporator temperature was relatively in-
>   sensitive to variations in sink temperature as
>   long as the sink was below the evaporator control
>   range. The sensitivity which was observed at high
>   power and high sink temperature due to the valve
>   vapor pressure drop could be further reduced by
>   designing a valve with a larger flow area.
>
> o The system operated stably with the thermal
>   mass on the evaporator. No undershoots or
>   overshoots were observed. Nor did the system
>   exhibit any appreciable hysteresis.

5.7.3   Test Results - Capacity:

With proper operation of the control system established, several tests were performed to measure the heat transfer capacity of the system.

The first of these tests (Test 2) was directed at exploring the vapor flow capacity of the valve.

During Test 1, the heat pipe exceeded its control range at an input power of 75 watts and a condenser temperature of 67°F. Under these condi- tions (Table 5-4, time = 125 minutes) the pressure ratio across the valve was P_{ad}/P_{au} = 0.36 psia/0.44 psia = 0.818, where:

P_{ad} - Pressure in adiabatic sec   downstream
of the valve (condenser v.   pressure)

P_{au} - Pressure in adiabatic section upstream
of the valve (evaporator vapor pressure)

This valve is substantially above the sonic pressure ratio (P_{ad}/P_{au} = 0.545) indicating that the rise in evaporator vapor temperature above the control range was indeed due to the combination of high condenser temperature and high vapor pressure drop across the valve. Thus, in Test 2 the sink temperature was set low enough to assure sonic flow conditions across the valve. Under such circumstances the power at which the evapora- tor vapor temperature goes out of control represents the maximum flow ca- pacity of the fully opened valve.

Unfortunately, in preparing for this test the heat pipe was inad- vertently heated to a temperature slightly above 100°F. This had the effect of expanding the bellows beyond the point where the inverted cup bottomed against the valve body (see Fig. 5-8), causing the bellows to expand radial- ly and slightly stretching the pleats. The result was that the bellows was lengthened which was manifested as a decrease in the control range set point from 73 $\pm$ 2°F. to ~ 69 $\pm$ 2°F.

Test 2 was run by leveling the pipe, setting the condenser at 40°F. and continually lowering the sink temperature as power was increased so as to maintain the 40°F. nominal value at the condenser. This was the lowest feasible temperature for the condenser without running the risk of freezing while making the necessary adjustments to the sink temperature.

The results are shown on Fig. 5-16. Equilibrium values for the temperatures of the heat source (average of TC's 1 & 2), evaporator wall (TC 4), evaporator vapor (average of TC's 5,6,& 7), condenser vapor
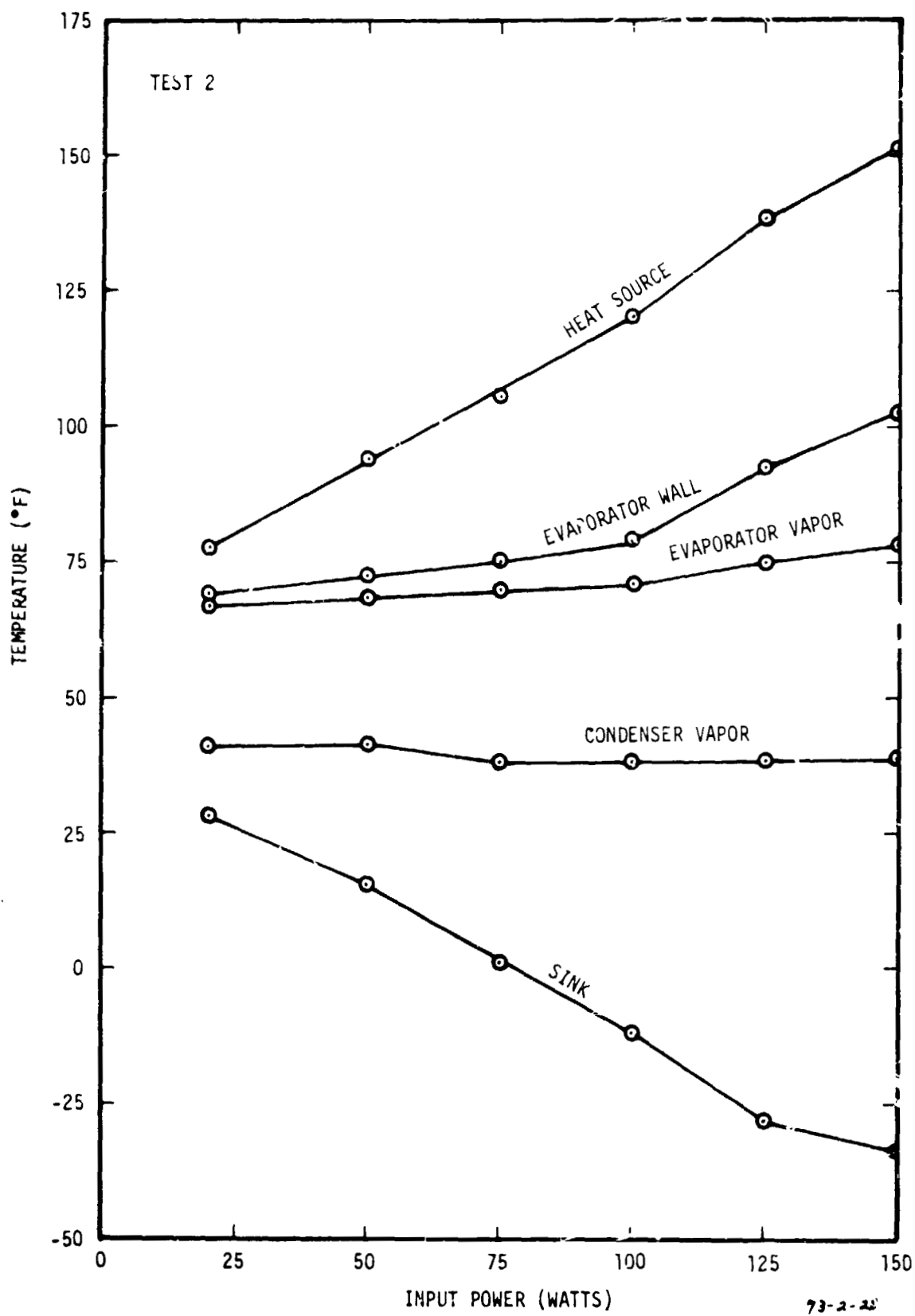
118

FIGURE 5-16.   Test 2 Results.

(average of TC's 8, 9 and 10) and sink (TC 12) are plotted as a function of input power. The figure clearly shows that the evaporator vapor temperature (controlled variable) is a linear function of input power in the range 67 to 71°F corresponding to input powers up to 100 watts. Above 100 watts the evaporator temperature rises more rapidly, reaching a value of 78°F at 150 watts.

For all conditions of Test 2 the pressure ratio across the valve was lower than critical. P_{ad}/P_{au} varied between 0.379 and 0.246 as the power was increased from 20 to 150 watts. Therefore, vapor flow through the valve was at sonic velocity for all conditions such that the mass flow was proportioned to the product of the upstream density and valve throat area. Within the range 20 to 100 watts the increased vapor flow rate was primarily accommodated by an increase in the valve flow area. However, above a vapor temperature of 71°F the valve was fully open. Thus for powers above 100 watts the increased vapor flow rate was accommodated only by an increase in vapor density, causing the change in slope of the evaporator vapor temperature curve. Within the range 100 to 150 watts the pipe was operating at the maximum valve capacity for each vapor temperature.

Figure 5-16 also points up a second limit observed during the test. When the power was raised from 100 to 125 watts the evaporator wall temperature rose disproportionately with respect to the evaporator vapor temperature. This indicated that the screen wicks around the walls (see Fig. 5-9) could no longer pump sufficient fluid and partially dried out. This might be regarded as a hydrodynamic limit although the axial flow system (the artery) did not fail and the pipe was able to operate stably.

Following completion of Test 2, a third test was run in an attempt to establish the capacity of the artery. The results of Test 2 indicated that the artery capacity was in excess of 150 watts. Since the heaters were rated at only 120 watts (at 115V) it was not feasible to establish the artery capacity by increasing the power. Thus, it was decided to maintain the power constant at 100 watts and elevate the evaporator end of the pipe until failure was achieved.

While fabricating the heat pipe the artery bubble point was independently measured at 25.75 psf in acetone at 75°F. This corresponds to 78.4 psf in water at 71°F which suggests that, under no load, the pipe could be tilted about 13 1/4 inches before the artery failed.

The test procedure was to set the input power at 100 watts and adjust the sink temperature such that the condenser vapor temperature was approximately 40°F. The evaporator was then elevated in steps and all temperatures recorded after the system equilibrated at each elevation. A summary of the test data is presented in Table 5-6.

Several interesting observations can be drawn from the data. At an elevation of 2 inches, TC 11 began to fall appreciably below those on the adiabatic section downstream of the valve (condenser vapor temperature). This was an indication of puddling at the end of the pipe due to a combination of excess fill and meniscus recession in the wicks. At 3 inches elevation TC 4 suddenly rose with respect to the evaporator vapor temperature indicating a circumferential wick dryout similar to that obtained at 125 watts with the pipe level in Test 2. Also, at this elevation TC 11 fell below the freezing temperature indicating the formation of ice at the puddle in the end of the condenser.

No further phenomena of interest occurred as the pipe elevation was increased to 4, 5, 6 and 7 inches. However, while operating at 7 inches elevation a power failure occurred in the laboratory. This loss of power caused the pipe to rapidly chill and, since the sink was at -20°F, the entire condenser froze. When the condenser froze the fluid could no longer be pumped to the evaporator and the pipe suffered a freezing limit failure, depriming the artery. This prematurely ended Test 3.

5.7.4 Failure of the Heat Pipe:

As a consequence of the premature termination of Test 3 due to a freezing limit failure, an attempt was made to repeat the test. This required repriming the artery - a task which proved to be impossible.

Many attempts were made to re-prime the artery using every means available. This included:

121

TABLE 5-6. MEASURED DATA - TEST 3

ELEVATION (INCHES)	HEATER BLOCK	EVAPORATOR		ADIABATIC SEC. UPSTREAM			ADIABATIC SEC. DOWNSTREAM			CONDENSER	SINK
	1	3	4	5	6	7	8	9	10	11	12
0	120.0	74.5	79.0	71.5	71.0	70.5	40.5	40.5	40.5	40.0	-16.0
1	120.0	74.5	79.0	71.5	71.0	70.5	41.0	41.0	41.0	39.5	-16.0
2	120.5	74.5	79.5	71.5	71.0	70.5	38.5	38.5	38.5	33.5	-19.0
3	120.0	74.0	85.0	71.5	71.0	70.5	36.0	36.0	36.0	14.0	-21.0
4	120.0	74.0	85.5	71.5	71.0	70.5	37.0	37.0	36.5	12.5	-20.0
5	120.0	74.0	85.5	71.0	70.5	70.5	36.5	36.5	36.5	9.0	-20.5
6	121.0	74.5	85.5	71.0	70.5	70.0	36.5	36.5	36.0	6.5	-20.0
7	121.0	74.5	86.5	71.0	70.5	70.0	38.0	37.5	37.5	6.0	-19.5

POWER LOSS CAUSED FREEZING. FOLLOWING ARE TEMPERATURES AT TIME WHEN TC'S 8, 9 AND 10 REACHED MINIMUM VALUE AFTER SINK COOLANT WAS SHUT OFF. (ARTERY HAD FAILED).

ELEVATION (INCHES)	HEATER BLOCK	EVAPORATOR		ADIABATIC SEC. UPSTREAM			ADIABATIC SEC. DOWNSTREAM			CONDENSER	SINK
7	117.5	92.0	101.5	66.5	65.5	65.5	8.5	8.5	8.5	-1.5	-6.0

TEMPERATURES (°F)

NOTES:
1. TC #2 USED FOR HI-LIMIT PROTECTIVE DEVICE. NOT RECORDED.
2. POWER = 100 WATTS.

o attempts with the pipe level and no load.

o attempts with the condenser elevated and no load.

o attempts with the heat pipe reversed; i.e., heating the condenser and cooling the evaporator.

o attempts to jar potential gas bubbles out of the artery with the condenser elevated.

o attempts to diffuse potential gas bubbles out of the artery by operating at low power.

o re-processing the pipe several times to achieve a gas free system.

Unfortunately, all attempts to reprime the artery failed. The pipe always burned out at less than 30 watts input power.

As a final attempt to recover the heat pipe it was re-processed with methanol instead of water as the working fluid. Methanol has better wetting properties than water and it was possible that it would prime the artery more readily. This was also un-successful.

At this point efforts to recover the pipe were terminated and the pipe was dissected in order to perform a failure analysis. The pipe was completely disassembled and examined. No physical degradation was apparent. The condenser end cap was then cut off to permit examination of the artery downstream of the valve - the region in which the water had frozen. Again, no visible damage was apparent.

At this point the pipe was placed level and methanol fed to the condenser end of the artery to see if it would prime through to the evaporator end. With the condenser side of the artery almost completely submerged in methanol, the liquid would not pass through to the evaporator. It was necessary to tip the condenser up before the liquid would flow through the bulkhead. It thus appeared that the system was damaged in the vicinity of the bulkhead in such a way as to interfere with capillary pumping through it.

A bubble point test was then performed on the artery from the condenser end. The bubbles emerged at the bulkhead on the

condenser side when the pressure reached 14.5 psf in acetone at 77°F. This compared with 25.75 psf when the pipe was fabricated, indicating a mechanical degradation of the artery at the bulkhead

The pipe was subsequently cut open at the weld on the condenser side of the 'ulkhead to permit examination of the artery in this region. It was found that the artery was torn at the point where it was welded to the tube representing the bulkhead artery (see Fig. 5-9). The tear was almost complete when examined. However, it is probable that the condition of the tear was altered during disassembly and it is not known exactly what conditions were originally. It appears, however, that the artery was torn at this location as a consequence of the freezing failure and that this caused the heat pipe to malfunction.

5.8   Summary and Conclusions:

A prototype vapor modulation heat pipe was designed, fabricated and tested. The heat pipe was constructed entirely of monel 400 and utilized water as the working fluid and methanol as a single (liquid) phase control fluid.

The control assembly performed well during testing, yielding a control range of 4°F and a relative insensitivity to sink temperature, in close agreement with theoretical predictions. Furthermore, the heat pipe operated stably, with no evidence of temperature overshoot, undershoot or hysteresis for the range of conditions tested.

The axial hydrodynamic capacity of the artery was not successfully measured before the heat pipe was damaged in a freezing failure. However, it clearly exceeded 150 watts with the pipe level and 100 watts with the evaporator elevated 6 inches. Actually, calculations indicate that, depending on the valve position and condenser temperature, the axial hydrodynamic capacity (artery failure) would have been in the range of 4-7 kilowatts.

However, the axial heat transfer capacity of the pipe was not controlled by a wicking limit but by the sonic limit for vapor flow through the valve. This was measured at 100 watts with the valve

fully open at 71°F, rising to 150 watts at 78°F.

Also measured was the capacity of the circumferential wicks. This was equal to 100-125 watts with the pipe level, yielding a maximum input heat flux of 4-5 watts/in^2.

The results of this effort indicate that the vapor flow modulation control scheme is a feasible and useful concept. As a first effort the prototype heat pipe was relatively successful. However, several design deficiencies showed up which should be improved in future versions. These were as follows:

1. The fully open flow area of the valve was too small, causing excessive vapor pressure drops and too low a sonic limit.

2. The artery was susceptible to damage when the condenser froze. This might have been alleviated by mounting it on a pedestal rather than up against the tube wall (Fig. 5-9).

3. The artery was difficult to prime even before it was damaged. This was due to two factors. First, the artery was made of two layers of screen which enhanced the probability of trapping a gas-stabilized bubble. A single layer artery would be preferable. Second, the artery cannot prime when the valve is closed and the evaporator is hotter than the condenser, since there is no vapor continuity across the bulkhead to allow pressure equilization. But, if the evaporator dried out there was poor thermal coupling between the evaporator wall and control fluid reservoir compared with that between the reservoir and bulkhead. Thus, it was not possible to prime the artery if the condenser (and bulkhead) was cool in relation to a dry evaporator because the valve would remain closed. This can be corrected by providing a conductive link between the evaporator wall and the control fluid reservoir. This will assure that the valve opens if the evaporator

125

wall temperature is higher than the low end of the
control range even if the evaporator is dry.

4. The valve system did not have sufficient over-
    temperature protection, causing the
    bellows to stretch when the temperature exceeded
    100°F. This can be simply corrected by providing
    more clearance between the actuating assembly and
    valve body.

These were the observed deficiencies. It is unfortunate
that the heat pipe was damaged before testing could be completed
since additional improvements might have been identified. It was
planned to test the heat pipe over its entire operating range as
defined by the freezing and blow-through limits. Instead, only
a small portion of this range was explored, as shown on Fig. 5-17.
In addition, no testing was done without the thermal mass on the
heat source so that the stability of the system under such conditions
is still unknown.

It is recommended that the heat pipe be repaired, reassembled,
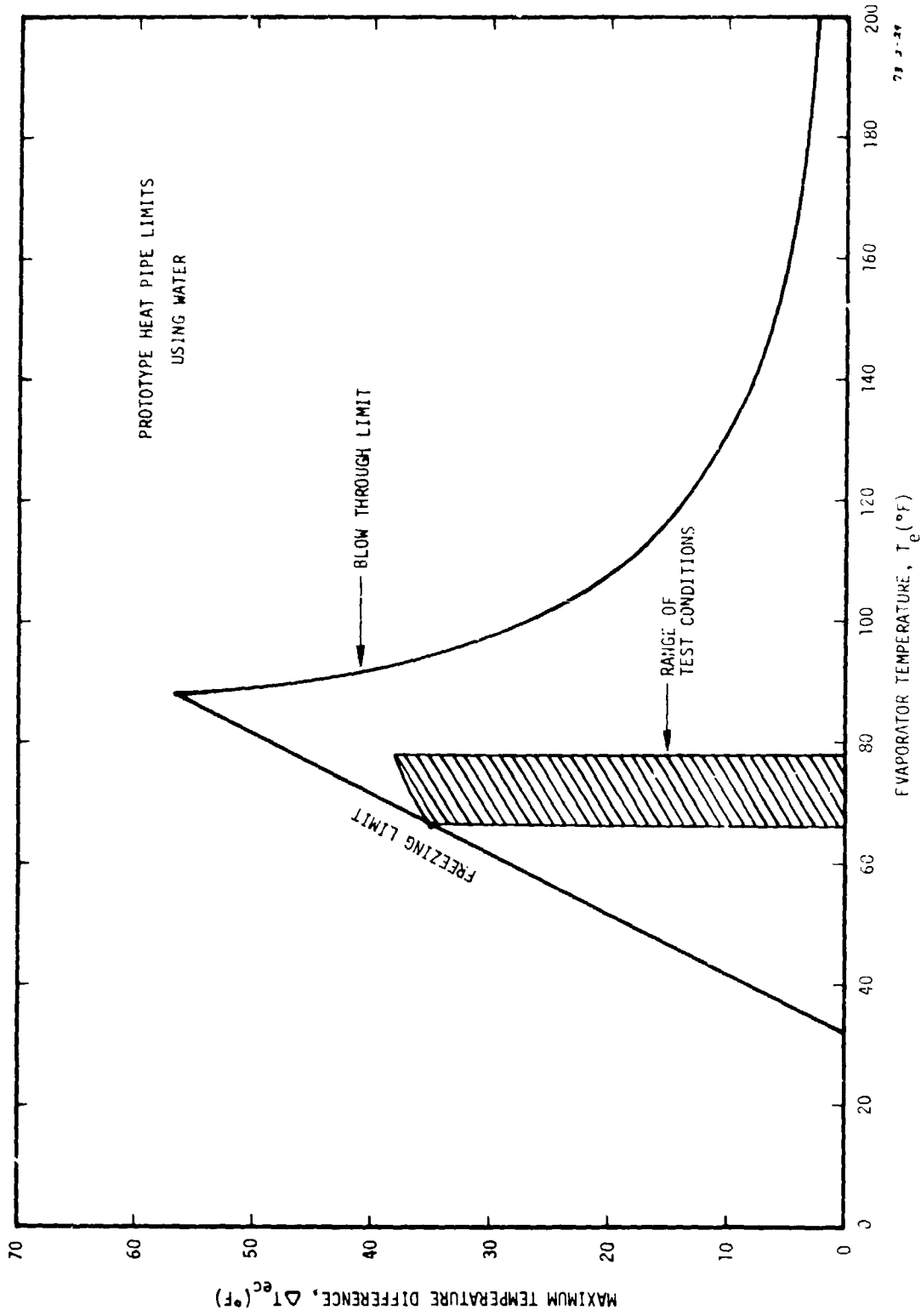and more fully tested before a second generation prototype is designed.

FIGURE 5-17. Operating Limits and Test Range - Prototype Vapor Modulation Heat Pipes.

6.0 REFERENCES

1. B. D. Marcus, "Theory and Design of Variable Conductance Heat Pipes: Hydrodynamics and Heat Transfer", Research Report No. 1, TRW Report No. 13111-6021-R0-00, April 1971.

2. B. D. Marcus, "Theory and Design of Variable Conductance Heat Pipes: Control Techniques", Research Report No. 2, TRW Report No. 13111-6027-R0-00, July 1971.

3. ' D. Marcus, "Theory and Design of Variable Conductance Heat Pipes", NASA CR-2018, April 1972.

4. B. D. Marcus and G. L. Fleischman, "Steady-State and Transient Performance of Hot Reservoir Gas-Controlled Heat Pipes", ASME Paper No. 70-HT/SpT-11, 1970.

5. D. K. Edwards and B. D. Marcus, "Heat and Mass Transfer in the Vicinity of the Vapor-Gas Front in a Gas Loaded Heat Pipe", ASME Jour. of Heat Transfer, Vol. 94, Ser. C, No. 2, pp 155-162, 1972.

6. D. K. Edwards, G. L. Fleischman and B. D. Marcus, "Theory and Design of Variable Conductance Heat Pipes: Steady State and Transient Performance", Research Report No. 3, NASA CR-114530, December 1972.

7. B. D. Marcus, D. K. Edwards and G. L. Fleischman, "Diffusion Freezeout in Gas-Loaded Heat Pipes", ASME Paper No. 72-WA/HT-33, 197^

8. J. P. Kirkpatrick and B. D. Marcus, "A Variable Conductance Heat Pipe Flight Experiment", Fundamentals of Spacecraft Thermal Design, Prog. Astronautics and Aeronautics, Vol. 29, John W. Lucas, Ed., p. 505, 1972.

9. J. P. Kirkpatrick and B. D. Marcus, "A Variable Conductance Heat Pipe/Radiator for the Lunar Surface Magnetometer", Thermal Control and Radiation, Prog. Astronautics and Aeronautics, Vol. 31, Chang-Lin Tien, Ed., p. 83, 1973.

10. B. D. Marcus, "Ames Heat Pipe Experiment (AHPE) Experiment Description Document", NASA CR-114413, January 1972.

11. D. K. Edwards, G. L. Fleischman and B. D. Marcus, "User's Manual for the TRW Gaspipe Program", NASA CR-114306, April 1971, and "User's Manual for the TRW Gaspipe 2 Program", NASA CR-114672, October 1973.

12. J. Schwartz, "Performance Map of the Water Heat Pipe and the Phenomenon of Noncondensible Gas Generation", presented at the ASME-AICHE Heat Transfer Conference, Minneapolis, MN, Aug. 3-6, 1969, ASME paper 69-HT-15.

13. S. W. Petrick, "Hydrogen Gas Generation in Water/Stainless-Steel Heat Pipes", presented at the ASME Winter Annual Meeting, New York, November 26-30, 1972, ASME paper 72-WA/HT-37.

14. Resistance of Huntington Alloys to Corrosion, Huntington Alloy Products Division, The International Nickel Company, Inc., Huntington, West Virginia.

15. H. H. Uhlign, Corrosion and Corrosion Control, Wiley, N.Y., (1963), p. 312.

16. M. Groll, H. Kreeb, W. D. Munzel, and P. Zimmerman, "Performance and Lifetests of Low Temperature Heat Pipes", presented at the 4th International Congress CHISA, Prague, Czechoslovakia, September 11-15, 1972.

17. U. R. Evans, The Corrosion and Oxidation of Metals, St. Martin's Press, Inc., N.Y., (1960).

18. C. H. Fellows, J. Amer. Water Wks. Ass. 21, 1373 (1929).

19. S. C. Datsko, Corrosion of Metals in High Temperature Water at 500F and 600F, Argonne National Laboratory Report No. ANL-5354 (1954).

20. B. Swerdling, R. Kosson, M. Urkowitz and J. Kirkpatrick, "Development of a Thermal Control Flight Experiment (ATFE)", Thermal Control and Radiation, Prog. Astronautics and Aeronautics, Vol. 31, Chang-Lin Tien, Ed., p. 35, 1973.

21. W. Bienert, "Study to Evaluate the Feasibility of a Feedback Controlled Variable Conductance Heat Pipe", NASA CR-73475, September 1970.

22. K. R. Schlitt, "Design and Testing of a Passive, Feedback-Controlled, Variable Conductance Heat Pipe", Proc. Int'l. Heat Pipe Conf., Stuttgart, Germany, 1973.

7.0   NOMENCLATURE

A, A_{eff}	-	Effective cross sectional area
B	-	Constant
C	-	Henry's constant
$\mathscr{D}$	-	Diffusivity
D	-	Diameter
F	-	Force
H	-	Henry number
K	-	Spring constant of bellows; Mass transfer coefficient
L	-	Length
M	-	Molecular weight
Nu	-	Nusselt number for heat transfer
Nu_m	-	Nusselt number for mass transfer
N_{tu}	-	Number of transfer units
$\mathscr{P}$	-	Perimeter of artery
P	-	Pressure
Q	-	Activation energy
$\dot{Q}$	-	Heat transfer rate
$\dot{Q}_o$	-	Normalizing heat transfer rate
R	-	Resistance
R_u	-	Universal gas constant
S	-	Parameter defined by Eq. (2-36b)
Sc	-	Schmidt number
T	-	Temperature

T_b	–	Boiling point at $P_o = 1$ atmosphere
TC	–	Thermocouple
T_z	–	Reference temperature $= \lambda M / R_u$
U	–	Coefficient of heat transfer
V	–	Velocity; Volume
X	–	Mole fraction

c	–	Molar concentration
c_p	–	Specific heat
h	–	Coefficient of heat transfer
k	–	Thermal conductivity; Boltzman's constant
$\dot{m}$	–	Mass flow rate
n	–	Moles of gas
r	–	Radial coordinate; meniscus radius of curvature
t	–	Time
v^*	–	Mole average velocity
x	–	Mole fraction - liquid side
y	–	Mole fraction - vapor side
z	–	Axial coordinate

β	–	Volumetric coefficient of thermal expansion
δ_a	–	Artery wall sheath thickness
$\zeta,\ \mathcal{L}$	–	Parameters defined by Eq. (1-34)

λ	-	Latent heat of vaporization
μ	-	Viscosity
ν	-	Kinematic viscosity
ξ	-	Bubble nucleation parameter
ρ	-	Density
σ	-	Surface tension
τ	-	Tortuosity
ϕ	-	Porosity

Subscripts (except as noted above):

a	-	Artery; Adiabatic section
ad	-	Adiabatic section; Adiabatic section downstream of valve
au	-	Adiabatic section upstream of valve
b	-	Bubble
bc	-	Bubble cap
c	-	Condenser
cr	-	Critical
d	-	Double
e	-	Evaporator
g	-	Gas
h	-	Heat
i	-	Internal; Interval
in	-	Into
ℓ	-	Liquid; Less volatile
L	-	Axial position
m	-	Mass; More volatile

mix	-	Mixture
oa	-	Overall
p	-	Pore
s	-	Surface
sat	-	Saturation
sh	-	Sheath
v	-	vapor
w	-	Back up wick
x	-	Fxcess
1, 2	-	Region1; Region 2